TKK Dissertations 159
Espoo 2009

SYSTEMATIC COARSE-GRAINING USING STRUCTURAL INFORMATION: APPLICATIONS TO LIPID MEMBRANES

Doctoral Dissertation

Teemu Murtola

Helsinki University of Technology
Faculty of Information and Natural Sciences
Department of Applied Physics

TKK Dissertations 159
Espoo 2009

SYSTEMATIC COARSE-GRAINING USING STRUCTURAL INFORMATION: APPLICATIONS TO LIPID MEMBRANES

Doctoral Dissertation

Teemu Murtola

Dissertation for the degree of Doctor of Science in Technology to be presented with due permission of the Faculty of Information and Natural Sciences for public examination and debate in Auditorium E at Helsinki University of Technology (Espoo, Finland) on the 16th of May, 2009, at 13 o'clock.

Helsinki University of Technology
Faculty of Information and Natural Sciences
Department of Applied Physics

Teknillinen korkeakoulu
Informaatio- ja luonnontieteiden tiedekunta
Teknillisen fysiikan laitos

Distribution:
Helsinki University of Technology
Faculty of Information and Natural Sciences
Department of Applied Physics
P.O. Box 1100
FI - 02015 TKK
FINLAND
URL: http://tfy.tkk.fi/
Tel. +358-9-451 5804
Fax +358-9-451 3116
E-mail: teemu.murtola@tkk.fi

ISBN 978-951-22-9854-9
ISBN 978-951-22-9855-6 (PDF)
ISSN 1795-2239
ISSN 1795-4584 (PDF)
URL: http://lib.tkk.fi/Diss/2009/isbn9789512298556/

TKK-DISS-2589

Picaset Oy
Helsinki 2009

ABSTRACT OF DOCTORAL DISSERTATION	HELSINKI UNIVERSITY OF TECHNOLOGY P. O. BOX 1000, FI-02015 TKK http://www.tkk.fi

Author Teemu Murtola

Name of the dissertation

Systematic coarse-graining using structural information: applications to lipid membranes

Manuscript submitted	6.2.2009	Manuscript revised	14.4.2009
Date of the defence	16.5.2009 at 13 o'clock, TKK main building, Otakaari 1, auditorium E		
☐ Monograph		☒ Article dissertation (summary + original articles)	
Faculty	Faculty of Information and Natural Sciences		
Department	Department of Applied Physics		
Field of research	Computational biophysics		
Opponent(s)	Dr. Alexander de Vries		
Supervisor	Prof. Tapio Ala-Nissilä		
Instructor	Prof. Ilpo Vattulainen		

Abstract

Within last 20 years, advances in computational power and methodology have made computer simulations an integral part of studies of biomolecular systems. Simulations on all-atom level are routinely used to study, e.g., microscopic details of lipid aggregates and proteins. However, many phenomena are still outside the reach of all-atom simulations, and coarser models are needed. Detailed information from all-atom models can provide input data for parameterizing coarse-grained (CG) models. Techniques for such parameterization are called systematic coarse-graining methods, and can be based, e.g., on matching forces or structural information between the two resolutions.

The main part of this dissertation employs inverse Monte Carlo (IMC) for constructing CG models for a lipid membrane containing dipalmitoylphosphatidylcholine (DPPC) and cholesterol. Three 2D models are constructed at different levels of resolution, in each case matching the radial distribution functions (RDFs) of the CG model to those from atom-scale simulations. The main results are the presence of cholesterol-rich and cholesterol-poor domains at intermediate cholesterol concentrations and the presence of strong tail density fluctuations at low cholesterol concentrations. The former agrees with the experimental studies of the system, while the latter was confirmed through atom-scale simulations. Accurate quantitative studies were restricted by transferability problems in all the CG models; hence, focus is on comparing the different models and critical discussion of the RDF inversion as a basis for coarse-graining. The IMC method is also improved by increasing its tolerance to statistical noise, as well as through inclusion of a virial pressure constraint and generalization to models where particles have internal degrees of freedom.

The dissertation also discusses the analysis of individual lipid conformations from atom-scale simulations using self-organizing maps (SOMs), as well as the use of SOMs in coarse-graining. Atomistic simulations provide a vast amount of data, and direct analysis may be difficult. SOM, an unsupervised machine learning method, is studied as an alternative to more traditional analysis. Focus is on determining good parameters for the method and on qualitative analysis based on the good visualization properties of SOM. The internal dynamics of the molecules are also analyzed using SOMs for visualization. A bilayer of palmitoyllinoleoyl-PC (PLPC) is used as a model system.

Keywords	coarse-graining, computer simulation, statistical physics, self-organizing maps, cholesterol		
ISBN (printed)	978-951-22-9854-9	ISSN (printed)	1795-2239
ISBN (pdf)	978-951-22-9855-6	ISSN (pdf)	1795-4584
Language	English	Number of pages	82 p. + app. 71 p.
Publisher	Department of Applied Physics, Helsinki University of Technology		
Print distribution	Department of Applied Physics, Helsinki University of Technology		

☒ The dissertation can be read at http://lib.tkk.fi/Diss/2009/isbn9789512298556/

VÄITÖSKIRJAN TIIVISTELMÄ	TEKNILLINEN KORKEAKOULU PL 1000, 02015 TKK http://www.tkk.fi

Tekijä Teemu Murtola

Väitöskirjan nimi

Rakenteellisten suureiden käyttäminen järjestelmällisessä karkeistuksessa: sovelluskohteena lipidikaksoiskerrokset

Käsikirjoituksen päivämäärä	6.2.2009	Korjatun käsikirjoituksen päivämäärä	14.4.2009

Väitöstilaisuuden ajankohta 16.5.2009 klo 13, Teknillisen korkeakoulun päärakennus, Otakaari 1, luentosali E

☐ Monografia ☒ Yhdistelmäväitöskirja (yhteenveto + erillisartikkelit)

Tiedekunta	Informaatio- ja luonnontieteiden tiedekunta
Laitos	Teknillisen fysiikan laitos
Tutkimusala	Laskennallinen biofysiikka
Vastaväittäjä(t)	Dr. Alexander de Vries
Työn valvoja	Prof. Tapio Ala-Nissilä
Työn ohjaaja	Prof. Ilpo Vattulainen

Tiivistelmä

Edistysaskeleet tietokoneiden laskentatehossa ja käytetyissä menetelmissä viimeisten 20 vuoden aikana ovat mahdollistaneet tietokonesimulaatioiden nousun keskeiseksi työkaluksi biologisten molekyylien tutkimuksessa. Atomitason simulaatioita käytetään yleisesti esimerkiksi lipidien ja proteiinien yksityiskohtaiseen tutkimiseen. Monet ilmiöt ovat kuitenkin atomitason simulaatioiden ulottumattomissa ja niiden tutkimiseen tarvitaan karkeampia malleja. Atomitason simulaatioista saatavaa yksityiskohtaista dataa voidaan käyttää tällaisten karkeistettujen mallien muodostamiseen. Tätä kutsutaan järjestelmälliseksi karkeistamiseksi, ja menetelmät voivat pohjautua esimerkiksi voimien tai rakenteellisen informaation sovittamiseen eri mallien välillä.

Pääosa tästä väitöskirjasta muodostuu käänteisen Monte Carlo -menetelmän soveltamisesta lipidikaksoiskerrosten karkeistukseen. Erityisesti tarkastellaan DPPC-lipidiä ja kolesterolia sisältävää kaksoiskerrosta. Työssä tarkastellaan kolmea erilaista kaksiulotteista mallia, jotka on luotu sovittamalla parikorrelaatiofunktiot atomitason simulaatioista saatuihin. Tärkeimmät tulokset ovat kolesterolirikkaiden ja -köyhien alueiden muodostuminen tietyissä kolesterolikonsentraatioissa sekä vahvat tiheysvaihtelut alhaisissa kolesterolikonsentraatioissa. Ensimmäinen tulos on sopusoinnussa kokeiden kanssa, ja jälkimmäinen vahvistettiin tässä työssä atomitason simulaatioilla. Työn mallit eivät sovellu tarkkaan kvantitatiiviseen analyysiin vuorovaikutusten vahvan konsentraatioriippuvuuden takia. Tämän takia työssä keskityttiin eri mallien vertailuun ja käytetyn menetelmän soveltuvuuden tutkimiseen. Työssä myös kehitettiin käytettyä menetelmää sietämään paremmin tilastollista kohinaa, lisättiin menetelmään rajoitusehto paineelle sekä yleistettiin menetelmä tilanteeseen, jossa mallissa on sisäisiä vapausasteita.

Väitöskirjassa tarkastellaan myös atomitason tuottamien lipidikonformaatioiden analyysiä itseorganisoituvilla kartoilla ja saadun informaation soveltamista karkeistukseen. Konformaatioiden tutkiminen suoraan on usein vaikeaa niiden suuren määrän takia. Itseorganisoituvat kartat perustuvat valvomattomaan koneoppimiseen ja antavat vaihtoehdon perinteisemmälle analyysille. Työssä keskitytään menetelmän parametrien optimointiin ja konformaatioiden kvalitatiiviseen analyysiin käyttäen karttoja havainnollistamiseen. Mallisysteeminä käytetään PLPC-lipideistä muodostuvaa kaksoiskerrosta.

Asiasanat	karkeistus, tietokonesimulaatio, tilastollinen fysiikka, itseorganisoituvat kartat, kolesteroli		
ISBN (painettu)	978-951-22-9854-9	ISSN (painettu)	1795-2239
ISBN (pdf)	978-951-22-9855-6	ISSN (pdf)	1795-4584
Kieli	englanti	Sivumäärä	82 s. + liit. 71 s.
Julkaisija	Teknillisen fysiikan laitos, Teknillinen korkeakoulu		
Painetun väitöskirjan jakelu	Teknillisen fysiikan laitos, Teknillinen korkeakoulu		

☒ Luettavissa verkossa osoitteessa http://lib.tkk.fi/Diss/2009/isbn9789512298556/

Preface

The work reported in this Thesis has been carried out at the Helsinki University of Technology, in the Laboratory of Physics, now part of the Department of Applied Physics. The Biological Physics and Soft Matter (BIO) research group, where the research was carried out, is part of the Computational Nanoscience (COMP) Center of Excellence supported by the Academy of Finland.

My sincere gratitude goes to Prof. Ilpo Vattulainen, the leader of the BIO group, who has gathered together an excellent group of people and created a relaxed atmosphere for doing research. Many discussions with him, both on scientific matters and related to life in general, have been useful and have helped me improve as a scientist. I am equally grateful to Dr. Emma Falck for her constant support, encouragement, and guidance when I started working in the group. Prof. Mikko Karttunen has also been helpful in guiding the research. My work would have been substantially more difficult without the many discussions with these people. I would also like to thank Prof. Tapio Ala-Nissilä for supervising my dissertation, as well as Prof. Risto Nieminen for creating the excellent working conditions at COMP. Other co-authors are acknowledged for providing much of the data used in the work, as well as their help in general. Other colleagues, both in the BIO group and in Tapio's group, also deserve to be thanked for the atmosphere and social life in the lab. I would also like to thank Prof. Klaus Schulten for providing me an opportunity to visit his group in Urbana-Champaign, and all the group members there for providing me invaluable experience about working abroad.

Financial support by the National Graduate School in Nanoscience, the National Graduate School in Materials Science, the Academy of Finland, the Finnish Academy of Science and Letters, and the Finnish Foundation for Technology Promotion are gratefully acknowledged. I would also like to thank the computing resources provided by the Finnish IT Center for Science (CSC) and the HorseShoe supercluster at the University of Southern Denmark.

Finally, I wish to thank my family, friends, and in particular Riikka for being there for me.

Espoo, April 2009

Teemu Murtola

Contents

List of Publications

This Thesis consists of this overview and the following publications:

[I] T. Murtola, E. Falck, M. Patra, M. Karttunen, and I. Vattulainen. 2004. Coarse-grained model for phospholipid / cholesterol bilayer. *J. Chem. Phys.*, 121:9156–9165.

[II] T. Murtola, E. Falck, M. Karttunen, and I. Vattulainen. 2007. Coarse-grained model for phospholipid/cholesterol bilayer employing inverse Monte Carlo with thermodynamic constraints. *J. Chem. Phys.*, 126:075101.

[III] T. Murtola, M. Karttunen, and I. Vattulainen. 2009. Systematic coarse-graining from structure using internal states: Application to phospholipid/cholesterol bilayer. Helsinki Institute of Physics preprint HIP–2009–08/TH.

[IV] T. Murtola, T. Róg, E. Falck, M. Karttunen, and I. Vattulainen. 2006. Transient ordered domains in single-component phospholipid bilayers. *Phys. Rev. Lett.*, 97: 238102.

[V] T. Murtola, M. Kupiainen, E. Falck, and I. Vattulainen. 2007. Conformational analysis of lipid molecules by self-organizing maps. *J. Chem. Phys.*, 126:054707.

The author has played an active role in all stages of the research reported in this Thesis. He has developed the computer programs for the coarse-graining studies in Papers [I]–[III] based on an earlier program, and developed several non-standard analysis tools for the other publications. He has designed the improvements to the inverse Monte Carlo method reported in Papers [II] and [III]. He has participated in planning the analyses in all the publications, and independently performed most of the work in Paper [III]. All the calculations and analyses in Papers [I]–[IV], with the exception of molecular dynamics simulations, have been performed by the author. For Paper [V], the author has planned and performed the analyses for the application part. The author has written the first draft of all the publications.

During the work described in this Thesis, the author has also made a significant contribution to several publications not included in the Thesis:

- T. Murtola, I. Vattulainen, and E. Falck. 2008. Insights into activation and RNA binding of *trp* RNA-binding attenuation protein (TRAP) through all-atom simulations. *Proteins: Struct. Funct. Bio.*, 71:1995–2001.

- T. Murtola, I. Vattulainen, and M. Karttunen. 2008. Systematic approach to coarse-graining of molecular descriptions and interactions with applications to lipid membranes. In G. A. Voth (editor), *Coarse-graining of condensed phase and biomolecular systems*. CRC Press, Boca Raton, FL.

- T. Murtola, A. Bunker, I. Vattulainen, M. Deserno, and M. Karttunen. 2009. Multiscale modeling of emergent materials: biological and soft matter. *Phys. Chem. Chem. Phys.*, 11:1869–1892.

- T. Murtola, T. A. Vuorela, S.-J. Marrink, M. Karttunen, M. T. Hyvönen, I. Vattulainen. 2009. Lipid–apolipoprotein B-100 interactions in low-density lipoproteins. (in preparation)

Overview

This Thesis deals with computational modeling of biological systems. Many phenomena in these systems occur on time and length scales that are beyond the reach of traditional, detailed simulation techniques. This Thesis focuses on coarse-graining techniques and methodology that can be used to reach larger scales while still retaining (at least some of) the accuracy of detailed simulations. The analysis of the large amounts of data produced by detailed simulations is also studied. The methods are developed and applied in the context of lipid membranes, but have general applicability in other areas.

Chapter 1 describes the biological background of the systems studied, as well as gives an overview of experimental and computational approaches for studying biological systems. Chapter 2 proceeds to discuss the simulation methods used in this work in detail. Chapter 3 then discusses the theoretical and practical aspects of constructing coarse-grained models, with focus on the inverse Monte Carlo method used in this Thesis. This chapter also describes the improvements made to the inverse Monte Carlo method as part of the work.

Chapters 4 and 5 present an overview of the computational results of this Thesis. Chapter 4 is based on Papers [I]–[IV], and discusses simple two-dimensional coarse-grained models for lipid bilayers composed of phospholipids and cholesterol, complemented by atomistic simulations. Chapter 5 is based on Paper [V], and discusses the use of self-organizing maps, an unsupervised machine learning method, in the analysis of simulation data and possible applications in coarse-graining. Finally, a brief summary, together with possible directions for future research, is given in Chapter 6.

Chapter 1

Background

The focus of this Thesis is on the development of computational methods for simulating biological systems. This Chapter gives an overview of biological membranes, which have been used as model systems in this Thesis. Section 1.1 gives an overview of membranes in cells, and Section 1.2 then focuses on lipids, a class of compounds that are an essential component of all biological membranes. This is followed by a brief general discussion of the relevant time and length scales in such systems in Section 1.3. Section 1.4 briefly discusses experimental techniques used to study membranes. Finally, computational approaches and their relationship to experiments and theory is discussed in Section 1.5.

1.1 Cells and Membranes

Cells are basic building blocks of all living organisms [3]. Single cells are typically of the order of 1–30 μm in diameter, with bacteria and other simple organisms on the lower end of the scale and more complex eucaryotic (animal and plant) cells having sizes from 10 μm up.

The internal structure of cells is complex (Fig. 1.1), and different kinds of *membranes* play a central role in structuring them. A *plasma membrane* surrounds the cell, and different compartments and organelles within the cell are also separated by membranes. Further, certain organelles, such as the endoplasmic reticulum and the Golgi device, consist mostly of folded membranes.

Membranes play various roles in cells. First, and probably the most obvious, is their role as barriers that keep substances where they belong. They also take part in active and passive transport of substances in and out of the cell and organelles, helping, e.g., in maintaining ion concentration gradients across the plasma membrane. The large surface area of membranes also makes them important reaction centers for different biochemical reactions.

The structure of a plasma membrane is shown schematically in Fig. 1.2. There is a *lipid bilayer* that holds the membrane together and into which other membrane components are attached. It is composed of a wide variety of different lipids, and will be discussed in more detail in Section 1.2. The active roles of membranes are carried out mostly by *proteins* attached to the lipid bilayer. They function, e.g., as passive, regulated channels for different types of substances, or as active pumps that transport ions against a concentration gradient. The third major class of substances present at the membrane

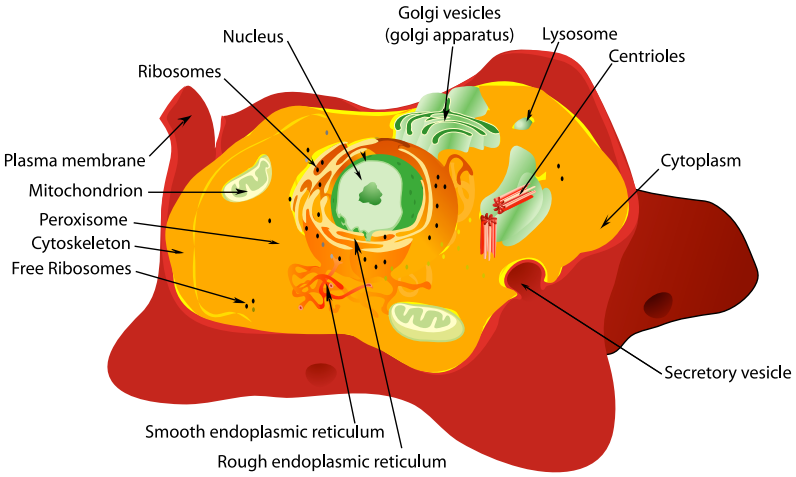

Figure 1.1: Structure of a typical animal cell. [1]

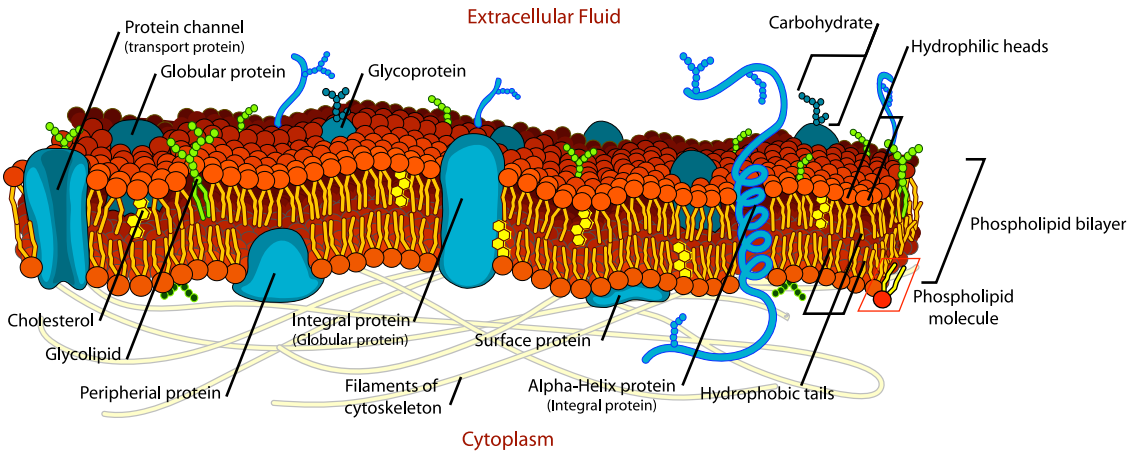

Figure 1.2: Structure of eucaryotic plasma membranes. [2]

is *carbohydrates*. They are attached to lipids or proteins, and take part, e.g., in recognition processes between cells. The different components do not function independently; instead, there is complex interplay between them. For example, the lipid bilayer contains hundreds of components, and it has been proposed that they can form domains called *lipid rafts* that take part in cellular functions [177], e.g., through protein sorting.

1.2 Lipids and Lipid Bilayers

Lipids are a broad class of naturally occurring molecules that are fat-soluble [127]. Most lipids are *amphiphilic*, i.e., they contain both water-soluble and water-insoluble (hydrophobic) parts. When placed in a water solution in sufficient concentrations, they tend to aggregate to minimize contact between hydrophobic regions and water [87]. Depending on the shape of the molecules and other factors, several different kinds of self-assembled structures can form, as shown in Fig. 1.3. The possible phases range from

[1] Image adapted from `http://commons.wikimedia.org/wiki/File:Animal_cell_structure_en.svg`.
[2] Image from `http://commons.wikimedia.org/wiki/File:Cell_membrane_detailed_diagram_en.svg`.

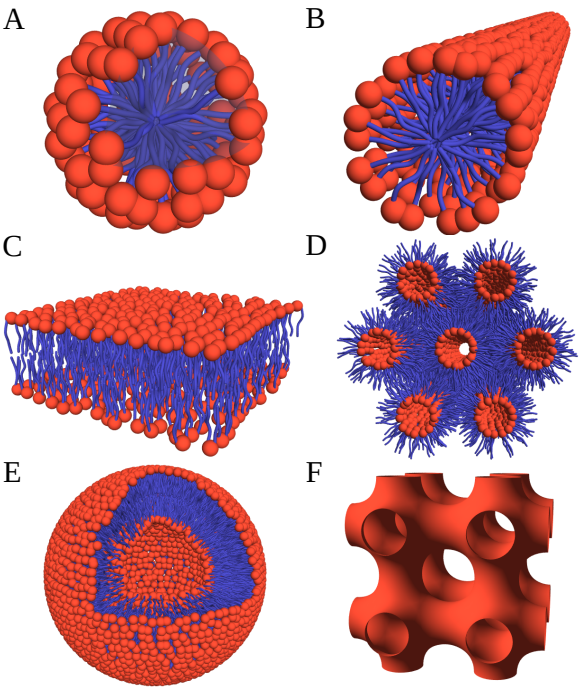

Figure 1.3: Examples of phases formed by lipids in water solution. Polar headgroups are shown in red, hydrophobic tails in blue, and water is not shown.
(A) A *spherical micelle*.
(B) A *cylindrical micelle*.
(C) A *bilayer*.
(D) An *inverted hexagonal phase*.
Bilayers can bend to form, e.g., *vesicles* (E), and *bicubic phases* (F) are also possible.

spherical and cylindrical micelles through bilayers and vesicles to inverted phases.

The bilayer phase (Fig. 1.3C) is the most relevant for biological systems: a bilayer of lipids joins together and supports the other components in all membranes (see Fig. 1.2). In fact, the whole plasma membrane can be seen as a large and complex vesicle, and smaller vesicles act in various roles in transport of substances and signaling. Micellar structures and larger lipid droplets that have a lipid monolayer on the surface and hydrophobic lipids inside can also be found in cells as storage components.

Most membrane lipids have a phosphate atom in the headgroup, and are classified as *phospholipids* [127]. They are typically based on glycerol, having the phosphate attached to one hydroxyl group and hydrocarbon tails esterified to the other two (see Fig. 1.4A). Different headgroups can be attached to the phosphate, the most common being choline (resulting in PC lipids), ethanolamine (PE), inositol (PI), glycerol (PG), and serine (PS). Several of these are shown in Fig. 1.4. Similarly, there is large variability in the fatty acids that form the tails. Most common chain lengths are even number of carbons between 16 and 22, and the number of double bonds ranges from zero to six. Some lipids are based on sphingosine, which provides one of the tails, and the other tail and the headgroup are attached as shown in Fig. 1.4B. For these *sphingomyelins*, the headgroup is most commonly PC.

There is one major exception to the "head and two tails" structure for lipids commonly present in plasma membranes (mitochondrial membranes also contain, e.g., cardiolipin, which has typically four tails). This is *cholesterol* [12, 143], shown in Fig. 1.4C. It has only a single hydroxyl group as the hydrophilic head and a short flexible tail, both attached to a planar sterol ring structure. In bilayers, the ring structure orients along the membrane normal between the lipid tails, and hence restricts the movement of nearby tails. This leads to higher ordering of the nearby tails compared to the fluid phase. Ordered tails take less space, and hence the bilayer condenses, i.e., the area per lipid decreases. However, cholesterol prefers a laterally disordered phase, i.e., it lowers the melting point of

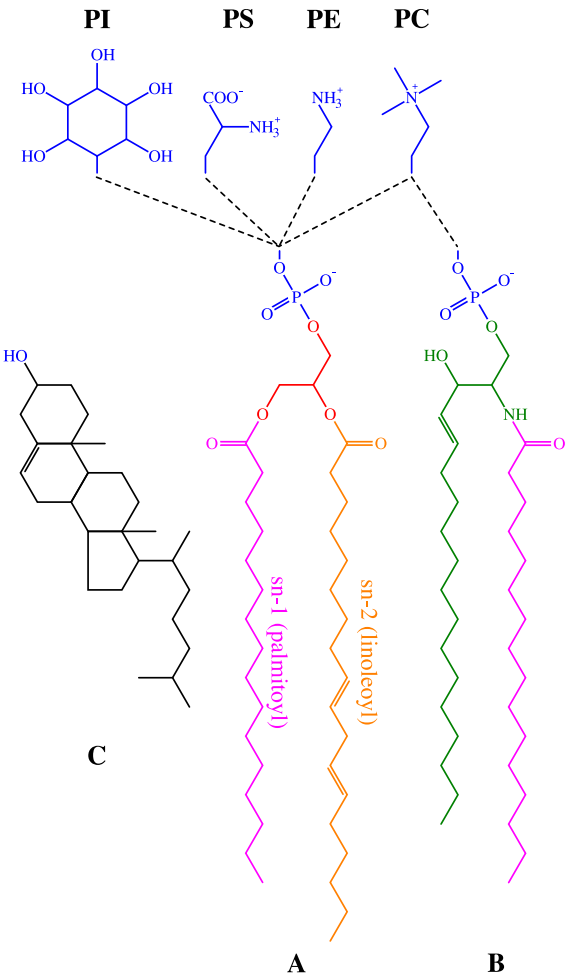

Figure 1.4: Chemical structure of common phospholipids (A and B) and cholesterol (C).

(A) *Phospholipids based on glycerol* can have various headgroups (blue) (glycerol shown in red), and different fatty acids can be esterified as the two tails. The *sn*–1 tail (purple) is typically saturated, while the *sn*–2 tail (orange) usually contains one or more double bonds.

(B) *Sphingomyelins* are based on sphingosine (green), to which the headgroup and one fatty acid is attached. The headgroup is typically PC, and the tail is saturated.

(C) *Cholesterol* has a rigid sterol ring structure to which a short tail and a single single hydroxyl group are attached.

the chains. Cholesterol also increases the bending rigidity of the bilayer, decreases the permeability, and increases the mechanical stability.

Real biological membranes often contain hundreds of different types of lipids [3, 127]. This variety remains largely unexplained, although some differences have a clear role. For example, increasing the unsaturation of the tails makes the bilayer more fluid, and helps to maintain a fluid phase also in lower temperatures. Different headgroups have different sizes, and PG, PS, and PI headgroups also carry a negative charge. These have an effect, e.g., on the intrinsic curvature of the membrane, and hence on the phase behavior. Many membranes are also asymmetric, with different lipid compositions in the different leaflets of the bilayer. For example, the outer leaflet of the plasma membrane is rich in PC and sphingomyelin, while the cytoplasmic side contains more PE and PS.

Because of the large number of entities, it is difficult to study the full complexity of even the lipid component of real membranes. In order to isolate and understand the important effects of certain components, studies on *model systems* are used. These systems are constructed to reproduce certain features of the underlying system at a manageable level of complexity. For example, instead of the complex mixture of lipids present in real membranes, the effects of different lipids are studied in mixtures of a few components that are chosen to represent the major components present in real membranes [54].

A mixture of dipalmitoyl-PC (DPPC) and cholesterol is a widely studied model system, which has also been used in Papers [I]–[III]. Paper [IV] also deals with the same

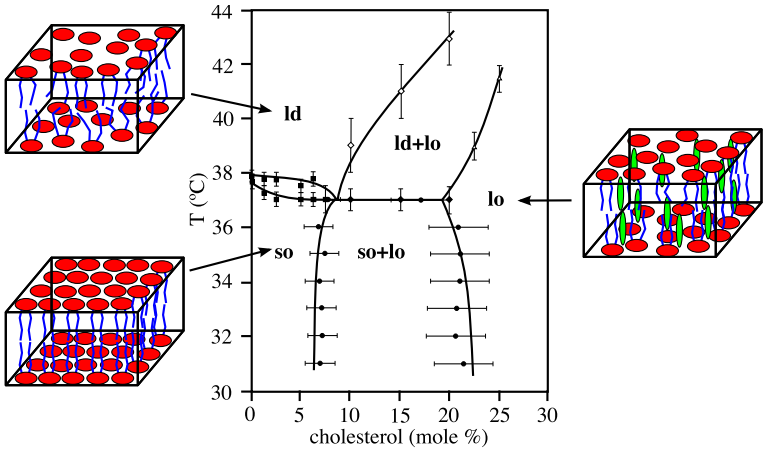

Figure 1.5: Experimental phase diagram of DPPC/cholesterol mixture (data from [197]). Three different phases appear (notation according to [76], see text for details): (i) *solid-ordered* (**so**) phase is gel-like with low area per lipid and high translational and conformational order, (ii) *liquid-disordered* (**ld**) phase has low translational and conformational order, (iii) *liquid-ordered* (**lo**) phase has liquid-like translational order, but high conformational order. In the *main phase transition* (**so** $\leftrightarrow$ **ld** in pure DPPC) both types of order are coupled, i.e., the transition takes place simultaneously for both of them.

phospholipid in the absence of cholesterol. Let us now briefly discuss this system as an example of the complexity that even simple lipid systems can possess.

The phase diagram of DPPC/cholesterol was first determined by Vist and Davis [197] (Fig. 1.5), and it has been studied by various other techniques afterwards (see, e.g., Ref. [32] and references therein). The system has also been studied theoretically (see Ref. [147] for a review), and the generic phase diagram can be reproduced already with simple phenomenological models that contain translational and conformational degrees of freedom [76, 134, 135]. Here, translational order refers to the packing of the lipids in the plane of the bilayer. Conformational order refers to the internal ordering of the tails, high order meaning straighter chains. At low cholesterol concentrations, there are two different phases, commonly referred to as solid-ordered (**so**) and liquid-disordered (**ld**). The transition between them is common to all single-component lipid systems, and is called the *main phase transition*. Both types of order change phase simultaneously, i.e., they are coupled. When cholesterol is added in larger amounts, both phases transform into a new phase. This liquid-ordered (**lo**) phase is translationally liquid-like, but the tails are highly ordered, and hence the area per lipid is lower than in the **ld** phase. Hence, cholesterol decouples the two types of order. At intermediate densities, wide coexistence regions appear. However, the nature of the system within this region has remained elusive: direct observation, e.g., through microscopy is not possible, and different indirect techniques place the boundaries at different locations [32].

1.3 Time and Length Scales in Biological Systems

It is clear from the preceding discussion that a wide range of length scales is important in biological systems. Individual lipids are in the Å–nm range and individual proteins in

the nm–10 nm range. These components, together with water and other small molecules, continue to form larger and larger aggregates up to the size of cells (μm–mm) and organisms (μm–meters). Similarly, time scales cover a wide range, starting from fs-scale motions of individual atoms and ps-scale for rearrangement of bonds in small molecules such as lipids, and ranging up to seconds necessary for large-scale phase separation. It is clear that no single method, either experimental or computational, is enough to study the whole complexity of biological systems. Instead, different methods are needed for studying phenomena at different scales, and a combination of methods is needed to understand biological systems in detail.

1.4 Experimental Methods

Several different experimental methods can be used to study lipid membranes and biological systems. The most common techniques are outlined in this section. The presentation does not try to cover all possible techniques, but instead focuses on the basic principles and on the kinds of information that can be measured.

Perhaps the most direct approach is *microscopy* of model vesicles or complete cells. The contrast between different phases in membranes is typically increased by fluorescent probes. For example, macroscopic phase separation and fluctuations in model membranes can be studied [72], and the partitioning of different proteins in cells followed. The resolution of ordinary microscopy is limited by the diffraction limit to hundreds of nanometers, while advanced fluorescence techniques can improve the resolution to tens of nanometers [66]. Better resolution can be achieved with electron microscopy or atomic force microscopy [60], but these are difficult to use for living cells.

Many fluorescent probes are bulky and may have an effect on the observed behavior. *Scattering techniques* such as X-ray scattering can be used to determine the structure of periodic structures such as stacks of bilayers or protein crystals without any probes, but careful interpretation of the data is required [133]. Microscopic details of fluid systems can be obtained as averaged profiles, and quantities such as area per lipid determined [133]. The scattering profiles can be compared to different models to select the most feasible ones.

Different *spectroscopic techniques* such as NMR can also be used to obtain information on, e.g., the ordering, relaxation times, and diffusion [100]. Most of these techniques also require probes, but NMR, for example, uses only isotopic labeling, which should not have any major effect. Relationship to microscopic quantities is often indirect and requires careful interpretation. The same holds for *thermodynamic* techniques such as calorimetry, which provide information on phase boundaries and different thermodynamic quantities, which are macroscopic in nature.

1.5 Modeling and Simulations

There are very few if any experimental techniques to directly measure the nanoscale structure or behavior of biological systems in detail. One of the central roles of computational and theoretical techniques is to fill this gap. Simulations can be seen as *computer experiments*, in which the researcher has unlimited control over the conditions and can measure

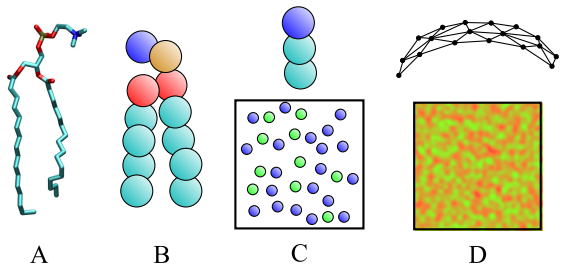

Figure 1.6: Lipid models at different resolutions. (A) *United-atom model* where aliphatic hydrogens are not represented explicitly. (B) *Semi-atomistic/superatom model* where each bead describes a few heavy atoms. (C) *Coarser particle-based models* where chemical identity is often lost and focus is on generic behavior. (D) *Continuum models* where fields are used to describe a bilayer as an elastic manifold (upper) and/or to describe local structure (lower). High-detail models missing from the figure: *quantum mechanical models* where (valence) electrons are explicitly described, *all-atom models* where all hydrogens are present.

arbitrary quantities (as long as they depend only on the degrees of freedom of the model). They can also be used to fit models to indirect experimental data such as scattering or spectroscopic data to understand the nanoscale origin of the observed behavior.

Computational and theoretical approaches are based on *models* that try to capture the essential features of a given system [13]. Figure 1.6 shows examples of models for lipids at different levels of detail. The most detailed model shown (Fig. 1.6A) is a united-atom model, where atoms are described classically, but aliphatic hydrogens are treated as parts of the corresponding carbon atoms. More detailed models, not shown in the figure, include quantum mechanical (QM) models needed to describe chemical reactions and all-atom models that describe all hydrogens explicitly. Moving to coarser models, Fig. 1.6B shows a semi-atomistic model which still retains most of the chemical detail [116, 137]. The particles in this model can be thought as superatoms that describe the center-of-mass positions of a group of atoms. Figure 1.6C shows two different models that contain only a minimal set of features while still retaining a particle-based description. The upper describes the amphiphilic nature of the molecules in a minimal way [24, 35, 132], while the lower focuses on lateral organization [134, 135] (the latter kind of models were also studied in Papers [I]–[III]). Finally, Fig. 1.6D shows two continuum models that describe the bilayer either as an elastic manifold [10, 139] or a field describing the local order or density [53, 147, 173]. Such descriptions can also be coupled in a single model [9].

Initial models are often constructed based on theoretical considerations and physical intuition, with some parameters possibly fitted to experimental values. If the model is simple enough, its behavior can be studied using analytical techniques, but for complex systems, the equations are often too complex for such treatment. Instead, the equations can be solved numerically using simulations. Irrespective of the way the model is studied, the results can be compared to experimental values or results from other models, which ultimately should lead to better understanding of the system. If the results from a model seem inadequate, the comparison can also be used to pinpoint the most probable cause and the model can be refined.

There are two basic approaches for constructing models. The first, which could be called a *top-down* approach, aims at minimalistic models to identify the most essential features of the system [129]. If a simple model can explain the general features of the system, we can identify the features included in the model as central. Such a model can also be used to understand the relative importance of different factors. For example, simple theoretical models have been very successful in understanding the features required

to reproduce phase transitions in lipid bilayers [123, 128, 134, 135, 136].

The other, *bottom-up* approach aims at as a detailed model as possible which can still be simulated at large enough scales to study the phenomena of interest. In such models, the aim is to use basic physical principles to select the degrees of freedom and the interactions with a minimum amount of fitting. Theoretical considerations and/or experimental data can be used in parameterization. After the model has been constructed and parameterized, it is *validated* for a particular system using experimental data that has not been directly used in the parameterization. Once confident enough in the validity of the model, one can use the model to study other features, which cannot be directly measured. Atom-scale simulations, discussed in more detail in the next chapter, generally fall into this category.

The main limitation of computational studies, in particular with the second approach, is available computer power. Although the power available has increased considerably during the last decade, it is still not possible to study, e.g., formation of domains in multicomponent lipid bilayers using atomistic simulations [147] (semi-atomistic simulations are currently approaching this limit [160]). Another limiting factor is the descriptive power of the models employed. These two factors are connected, because although better models can be developed, they are often computationally more expensive, limiting the timescale. Hence, a compromise between accuracy and the computational complexity of a model is always required.

It is also possible to parameterize more approximate, *coarse-grained* (CG) models using results from more detailed models [198]. The main goal is to retain the accuracy of the detailed model as well as possible while reducing the computational cost of the model through, e.g., simplifying the interactions and/or reducing the degrees of freedom. The reverse process, going from a CG model back to the detailed model, is *fine-graining*, the main ingredient being transforming the CG structures back to detailed ones. This can be used to enhance sampling of the detailed model: after the CG model has been simulated, representative configurations are mapped back to the detailed model and the properties studied in more detail [92, 184]. It is also possible to do this in a more rigorous way using *resolution exchange* schemes [103, 104].

A more ambitious goal is to link together models at *multiple resolutions* in a single simulation, with the goal that the detailed model is only used where it is needed, and the rest of the system is modeled in less detail. Mixed QM and classical simulations can already be used to simulate, e.g., enzymatic reactions [13, 172]: the active site is modeled quantum mechanically, while the rest of the enzyme is treated using classical models. Recently, several different schemes for interfacing classical atom-scale and coarser models have also been developed [34, 156]. These methods aim at *adaptive resolution*, i.e., that the particles can freely exchange between the regions of different resolutions.

An umbrella term for the above techniques, from coarse- and fine-graining to multiple and adaptive resolution simulations, is *multiscale modeling*. The basic principle is to use models at different resolutions to understand a system. For example, information from more detailed models can be carried on to semi-atomistic and even continuum models to predict larger-scale properties. Systematic techniques for constructing CG models are also important to obtain a good match between different models. This is important for smooth behavior of adaptive and multiple resolution models at the interface between the different resolutions [158] and for effectiveness of resolution exchange simulations [103, 104].

Chapter 2

Computational Methods

A variety of simulation techniques have been developed for studying models at different levels of detail. The most detailed *ab initio* simulations model electrons explicitly [183]. These methods are computationally very expensive, and only tens or hundreds of atoms can be treated over short (picosecond) timescales. Their main use in biological systems is in modeling chemical reactions such as enzymatic processes. However, more approximate methods are needed for most biological systems.

The workhorse of biomolecular simulations is classical molecular dynamics (MD) technique [186], which is also the simulation method used in Papers [IV] and [V]. The target data for parameterizing the CG models in Papers [I]–[III] were also obtained from MD simulations. In this method, atoms (or other particles) follow the classical equations of motion, and forces are typically approximated using relatively simple functional forms. This method will be presented in detail in Section 2.1. With modern supercomputers, classical atomistic MD simulations can treat tens or hundreds of thousands of atoms, and the time scales range from tens of nanoseconds to microseconds. The atomistic description can also be abandoned and several atoms treated as one interaction center in semi-atomistic CG models. This can extend the accessible scales by two to three orders of magnitude, with some loss in accuracy and detail.

Another technique that is commonly used, in particular with simpler models, is Monte Carlo (MC) sampling, where random numbers are used extensively to sample the configurational space of the system [183]. This method is discussed in more detail in Section 2.2. In this Thesis, MC simulations have been used for simulating the CG models in Papers [I]–[III]. It is often not possible to associate meaningful dynamics with MC simulations, but as the focus in these papers is on static quantities, this is not a problem. Further, writing meaningful equations of motion for the simple models studied in these papers is very difficult (see Section 3.6), making MC simulations a preferred choice.

For coarser models, other techniques can also be applied. The degrees of freedom in these models can be particles or fields, and the main difference from the above two approaches is in the equations of motion. For example, the equations of motion can include stochastic terms to describe fluctuations, or be designed for efficient numerical computation. Dissipative particle dynamics [13, 61] and stochastic rotation dynamics [114, 115] provide examples of particle-based techniques, while field-based methods can be used to model, e.g., elastic properties of membranes [10] or organization the plane of the bilayer [9, 53, 147, 173]. Some of these techniques are also discussed briefly in Section 3.5 in the context of coarse-graining applications.

2.1 Classical Molecular Dynamics

2.1.1 Basics

In the classical MD method, the movement of particles, typically atoms, is described by Hamilton's equations of motion [56]:

$$\frac{\partial H}{\partial \boldsymbol{p}} = \dot{\boldsymbol{q}}, \tag{2.1a}$$

$$\frac{\partial H}{\partial \boldsymbol{q}} = -\dot{\boldsymbol{p}}. \tag{2.1b}$$

Here, $H(\boldsymbol{p}, \boldsymbol{q})$ is the Hamiltonian of the system, $\boldsymbol{q}$ are the generalized coordinates of the particles, and $\boldsymbol{p}$ are the corresponding momenta. Typically, the Hamiltonian can be written as

$$H(\boldsymbol{p}, \boldsymbol{q}) = \sum_i \frac{p_i^2}{2m_i} + V(\boldsymbol{q}), \tag{2.2}$$

where the first term is the kinetic energy and V is the potential energy of the system. In this case, the movement of the particles is determined by the potential energy function $V(\boldsymbol{q})$ and the initial positions and velocities of the particles. The details of the method are discussed in the next sections: Section 2.1.2 discusses the form of the potential energy function V and Section 2.1.3 the selection of parameters for the potentials. Section 2.1.4 discusses simulations at constant temperature and/or constant pressure, and Section 2.1.5 discusses implementation issues such as numerical integration of Eqs. (2.1), boundary conditions, and efficient calculation of short- and long-range forces.

2.1.2 Force Fields

The main factor affecting both the speed and accuracy of MD simulations is the potential energy function $V(\boldsymbol{q})$. The derivatives of V with respect to the particle positions define the forces acting on the particles, and hence, a particular choice of V is often referred to as a *force field*. In principle, QM calculations could give $V(\boldsymbol{q})$ as a function of all the particle positions, but such a calculation is not feasible for more than a few particles. Hence, in practice, the function is approximated by a sum of semi-empirical, easily computable functions. The parameters in the functions are fitted to correctly reproduce quantities from experiments (densities, thermodynamic quantities etc.) and QM calculations (energies in bond angles, partial charges etc.).

In biomolecular simulations, the force field is typically written as

$$V = V_{bonds} + V_{es} + V_{vdW}, \tag{2.3}$$

where V_{bonds} describes chemical bonds and angles, and V_{es} and V_{vdW} describe electrostatic and van der Waals contributions to the non-bonded interactions, respectively.

The bonded term is written as a sum of contributions from bond length and angle

vibration and dihedral potentials, e.g., as follows [192]:

$$\begin{aligned} V_{bonds} = & \sum_{bonds} \frac{1}{2} k^b_{ij} (r_{ij} - r^0_{ij})^2 + \sum_{angles} \frac{1}{2} k^\theta_{ijk} (\theta_{ijk} - \theta^0_{ijk})^2 \\ & + \sum_{dihedrals} k^\phi_{ijkl} \cos(n_{ijkl} \phi_{ijkl} - \phi^0_{ijkl}) \\ & + \sum_{impropers} \frac{1}{2} k^\xi_{ijkl} (\xi_{ijkl} - \xi^0_{ijkl})^2. \end{aligned} \tag{2.4}$$

The first (second) term uses harmonic potentials with force constants k^b_{ij} (k^θ_{ijk}) to keep bond lengths (angles) around their reference values r^0_{ij} (θ^0_{ijk}). The sums run over all pairs ij or triplets ijk of particles connected by bonds. The third term describes rotation about bonds with k^ϕ_{ijkl} determining the stiffness, n_{ijkl} the multiplicity, and ϕ^0_{ijkl} the reference angle. More complex cases with multiple minima of unequal depth, e.g., in hydrocarbon chains, can be treated with several terms for a single angle [55, 112], or a different functional form can be used [192]. The last term describes so-called improper dihedrals that are used to force planarity of certain groups of particles, as well as preventing changes in the chirality of molecules. The functional forms in Eq. (2.4) are not the only possibilities: some force fields use different functions to achieve more efficient computation of the forces [192] or additional terms for more accurate description [113]. One should note that writing the bonded potential in the form (2.4) disallows changes in the bonds during the simulation, excluding the possibility to study chemical reactions.

The non-bonded electrostatic term is the standard Coulombic interaction

$$V_{es} = \sum_{i,j} \frac{q_i q_j}{4\pi\varepsilon_0 r_{ij}}, \tag{2.5}$$

where q_i are the partial charges on the atoms. For the van der Waals term, the Lennard-Jones (LJ) interaction is typically used:

$$V_{vdW} = \sum_{i,j} 4\epsilon_{ij} \left(\left(\frac{\sigma_{ij}}{r_{ij}} \right)^{12} - \left(\frac{\sigma_{ij}}{r_{ij}} \right)^{6} \right). \tag{2.6}$$

The second term includes dipole–dipole, dipole–induced dipole, and induced dipole–induced dipole interactions. All these are attractive on average and have a common r^{-6} dependence [77]. The first term is a computationally effective implementation of repulsion at short interatomic distances, resulting from electronic overlap. The parameters ϵ_{ij} and σ_{ij} determine the depth of the attractive minimum and the distance at which the potential crosses zero, respectively (the minimum is located at $r_{ij} = \sqrt[6]{2}\sigma_{ij}$).

2.1.3 Force Field Parameters

The force field function defined by Eqs. (2.3)–(2.6) has quite a few parameters that need to be determined in order to completely specify the force field: the force constants k and the equilibrium lengths/angles for all the different bond terms in Eq. (2.4), the partial charges q_i, and the Lennard-Jones parameters ϵ_{ij} and σ_{ij}. These parameters are typically determined semi-empirically, i.e., the parameters are adjusted until selected experimental

properties such as densities, heats of vaporization, and/or solvation free energies are reproduced. The bonded potentials and the partial charges can also be parameterized based on *ab initio* calculations of isolated molecules; however, in particular the partial charges determined this way are often subject to further optimization because also the environment has an effect on the electronic structure. Due to the way the optimization is done, the force field is an entity, and different force fields should be mixed with care if at all [187]. Also, although the total forces from the force field are typically adequate, the individual terms in the force field may or may not describe the underlying interactions accurately.

The force fields commonly in use for biological systems are AMBER [36, 199, 200], GROMOS [145, 167], CHARMM [25, 55, 57, 112, 113], and OPLS [89, 90]. The first three have their origins with similar-named simulation programs, while OPLS focused on improvement of non-bonded potentials, using AMBER for the other parameters. The development of force fields for water is also an active research area (see, e.g., [62, 195] and references therein), but the above force fields have been parameterized to work together with older water models such as SPC [14] or TIP3P [88].

The first MD simulation of a phospholipid bilayer with explicit water was performed by Egberts *et al.* [42], with the force field based on GROMOS87 with the hydrocarbon angles taken from Ryckaert and Bellemans [162]. However, they performed several *ad hoc* adjustments to the parameters to reproduce the correct phase. A more systematic parameterization approach was taken by Berger *et al.* [17], who used the bonded interactions from Egberts's work, but took LJ parameters from OPLS and adjusted hydrocarbon parameters based on simulations of pentadecane. Partial charges were taken from a study by Chiu *et al.* [33]. This combination of parameters is one of the most widely used for lipids [187], and it is termed the *Berger lipids*. This force field was also used for the atomistic simulations discussed in this Thesis. The other commonly used force field for lipids, in particular in combination with proteins, is CHARMM [55].

The Berger parameterization does not include unsaturated chains; later studies have used either GROMOS87 parameters or a more detailed set calculated by Bachar *et al.* [11] for double bonds in the lipid tails. In Paper [V], the latter parameters were used. Finally, cholesterol parameterization by Höltje *et al.* [71], which is based on GROMOS87, has been used for the simulations containing cholesterol in this Thesis. Combining GROMOS87 with Berger lipids may result in problems due to too strong attraction between GROMOS87 and Berger atoms [187]. However, this should not be a major concern for the studies in this Thesis as the focus has been on the methodology of developing CG models.

2.1.4 Thermostats and Barostats

The exact solution to Eqs. (2.1) conserves the Hamiltonian H, i.e., the total energy of the system is constant [56]. However, this is often not the most accurate description of the underlying system: in reality, most systems can exchange energy with their environment, and hence a simulation at a constant temperature would be more appropriate. Such conditions are achieved through the use of a *thermostat*, a slight modification of the equations of motion such that the correct temperature is achieved [183]. One should note that because the equations of motion are altered, all thermostats have an effect on the dynamics of the system. In most situations, this effect is neglected, but it is important to realize that in certain situations and/or with certain thermostats it can become significant. This is the

case, e.g., if the system contains flows [178], or if the coupling of the thermostat and the system is very strong.

One popular approach, termed the *Berendsen thermostat*, rescales the velocities at each step such that the temperature tends to the target temperature T_0 according to the equation [15]

$$\frac{\mathrm{d}T}{\mathrm{d}t} = \frac{T_0 - T}{\tau_T}, \tag{2.7}$$

where T is the current temperature and τ_T gives the strength of the coupling. This approach is simple, but it does not produce a well-defined ensemble [183]. Recently, a velocity rescaling scheme that gives the correct ensemble has also been proposed [26].

Perhaps the most popular approach for obtaining the full canonical ensemble is to use the *Nosé-Hoover thermostat* [74, 142], where an additional friction parameter ξ is added to the equations of motion:

$$\dot{\boldsymbol{p}} = \boldsymbol{F} - \xi \boldsymbol{p}. \tag{2.8}$$

The friction parameter obeys the differential equation

$$\dot{\xi} = \frac{T - T_0}{Q}, \tag{2.9}$$

where Q is a fictional mass that determines the strength of the coupling. A chain of such thermostats can also be applied to reduce oscillations and to achieve the correct ensemble for systems where the traditional Nosé-Hoover fails [119]. A more recent development is the *Nosé-Poincare thermostat* [23], which preserves the Hamiltonian structure of the equations of motion, allowing more stable integration.

Other approaches are also possible. A common approach, in particular with coarse-grained models, is to add dissipative and randomly fluctuating forces to the equations of motion. Such approaches include dissipative particle dynamics [13, 61] and using the Langevin equation [4, 183]. These equations and their physical interpretation are discussed more closely in Section 3.6, here it suffices to note that these approaches can also be seen as thermostats [178].

Volume and pressure form a set of variables similar to energy and temperature, and in many situations, a constant pressure simulation would be more appropriate than a constant volume one. This can be achieved with *barostats*, which are similar in idea to thermostats, but control the pressure tensor $\boldsymbol{P}$ instead of the temperature. Again, a simple box rescaling scheme, the *Berendsen barostat* [15], is often used for its simplicity, but it does not produce correct fluctuations. An extended ensemble method, similar to Nosé-Hoover, is called the *Parrinello-Rahman barostat* [150], and is often used if the volume fluctuations are important. Because $\boldsymbol{P}$ is a tensor and not a scalar, the coupling can be implemented separately for any combination of system dimensions. In particular, bilayer simulations often use semi-isotropic coupling where the system size along the membrane normal is allowed to vary independently from the other two, which are coupled.

2.1.5 Practical Implementation

The previous sections have outlined the basic equations underlying MD simulations. When implementing a simulation program, several other issues need to be considered

as well to make the simulation represent the underlying system as well as possible with as little computational effort as possible.

First, the MD systems are always finite, and typically much smaller than those observed in reality. Hence, the boundaries of the MD system need to be treated carefully or they may affect the results significantly. The most common choice is to use *periodic boundary conditions* (PBC) where particles leaving one side of the simulation box enter from the other side, and particles also interact across the boundaries [4]. In effect, this setup corresponds to simulating a system that repeats itself in all directions infinitely. The thickness of the solvent layer between periodic copies of the solute, e.g., a lipid bilayer or a protein, should be large enough that the copies do not significantly influence each other. Although one has to be careful when applying PBC, the problems associated with them are typically smaller than with other types of boundary conditions of similar complexity such as simulating in vacuum or in a static external potential.

Second, the equations of motion need to be solved numerically using an *integrator*. Hamilton's equations (2.1) conserve the value of the Hamiltonian, i.e., the total energy, and this is a desirable property also for the numerical solution. There is a class of numerical integrators which guarantee long-term conservation of energy of Hamiltonian systems, as well as certain geometric properties in phase space; these *symplectic* integrators can be shown to conserve a perturbed Hamiltonian exactly, the perturbation becoming small as the time step is reduced [183]. Commonly used integrators [183], such as velocity-Verlet and leapfrog, belong to this class.

The time step of the integration is limited by the shortest oscillations present in the system: if the time step is too large, the displacement during a single step can result in very large forces during the next time step, leading eventually to instability. For a typical force field, the fastest oscillations are associated with bonds involving hydrogens (and bonds in general), limiting the time step to 1 fs or so. Even with more advanced treatment of such bonds, e.g., with constraint algorithms such as SHAKE [163], RATTLE [5], SETTLE [124] or LINCS [68, 69], the time step is still limited to a few fs.

Finally, the non-bonded interactions in Eqs. (2.5) and (2.6) involve sums over all pairs of atoms. The straightforward implementation requires evaluation of $\mathcal{O}(N^2)$ terms, which rapidly becomes unfeasible with larger system sizes. For short-range forces such as the Lennard-Jones interactions [Eq. (2.6)], the forces beyond some cutoff distance can typically be neglected (for standard force fields, this distance is typically of the order of 1 nm). This reduces the number of terms to $\mathcal{O}(N)$. However, for long-range forces, such as electrostatic interactions, this method is not adequate (for a homogeneously charged system, the force contribution from charges at any given distance is finite). Instead, the full sum in Eq. (2.5) must be evaluated, also taking into account the periodic images in the case of PBC. The sum is conditionally convergent and can be evaluated with Ewald summation methods, where the interaction is divided into a short-ranged part and a long-ranged part, and these are evaluated separately [183]. The short-ranged part can be evaluated using a cut-off, while the long-ranged part can be evaluated in reciprocal space using, e.g., Fourier transforms. The most commonly used method is the particle-mesh Ewald (PME) [37, 50]. For larger simulations, the reaction field approximation [144] can be used to reduce the computational complexity: outside the electrostatic cutoff, the system is treated as a homogeneous, polarizable medium, and an appropriate correction is added to the electrostatic potential.

Although the basic idea of MD is simple, efficient technical implementation of all

the above techniques is not an easy task, and it becomes even more complicated with the introduction of parallel computing. However, the computation is very similar for any biomolecular MD simulation, and there are several software packages to perform such simulations. A few of the most popular packages are GROMACS [16, 70, 99, 193], NAMD [153], and CHARMM [25]. All of them are capable of large, parallel simulations, but there are some differences in efficiency and features.

2.2 Monte Carlo Simulations

2.2.1 Basics

Generally, the term Monte Carlo (MC) simulations refers to any technique that uses random numbers extensively as a part of the algorithm [183]. In physics, the meaning is often more limited, and the term refers to a class of techniques that randomly sample the phase space of the system and use the samples to evaluate ensemble averages. Here, we will focus on the latter class of methods, but very similar techniques can also be applied in other fields.

In basic MC simulations [4, 183], the goal is to sample configurations of a system according to the Boltzmann distribution: in a system with a constant number of particles in a constant volume and temperature, the probability of observing a configuration $\boldsymbol{q}$ follows the Boltzmann distribution [151]

$$P(\boldsymbol{q}) \propto e^{-\beta H(\boldsymbol{q})}, \tag{2.10}$$

where $\boldsymbol{q}$ are the degrees of freedom of the system, $\beta = 1/k_{\mathrm{B}}T$ is the inverse thermal energy, and $H(\boldsymbol{q})$ is the Hamiltonian of the system. An MC simulation starts from an initial configuration, and proceeds by randomly generated trial moves (changes to $\boldsymbol{q}$) that are either accepted or rejected. The probabilities for generating and accepting different moves are chosen such that the generated configurations are distributed according to the Boltzmann factor. However, the target probability distribution can be arbitrary; this, and the flexibility in choosing the trial moves, gives MC simulations a wide field of applicability. The main difficulty is often in generating good trial moves.

2.2.2 Importance Sampling

The main goal of MC simulations is to sample numerical integrals of the form

$$I = \int f(\boldsymbol{q})\rho(\boldsymbol{q})\mathrm{d}\boldsymbol{q}, \tag{2.11}$$

where $\boldsymbol{q}$ are the degrees of freedom of the system and $\rho(\boldsymbol{q})$ is a probability distribution, typically given by the Boltzmann factor. Typically, the integral is high-dimensional, making it impossible to use a numerical quadrature such as Simpson's rule to evaluate the integral with reasonable accuracy. Namely, the error of a numerical quadrature scales as N^{-k}, where N is the number of evaluation points along one dimension and k a small integer, and hence as $M^{-k/d}$, where $M = N^d$ is the total number of evaluations and d is the number of dimensions [183]. Hence, if $d \gg 1$, it is often impossible to evaluate

the integral to any reasonable accuracy. The problem becomes even more difficult if the integrand is close to zero in large regions, as is typically the case with the Boltzmann factor.

In a stochastic approach, the integral is evaluated by randomly generating M samples $\{\boldsymbol{q}_i\}_{i=1}^{M}$ from the probability distribution $\rho(\boldsymbol{q})$, and then evaluating

$$I \approx \hat{I} = \frac{1}{M} \sum_{i=1}^{M} f(\boldsymbol{q}_i). \tag{2.12}$$

If the samples are independent, the variance of the sum (without the normalization) scales as M^1, and hence the error of the integration scales as $M^{-1/2}$ independent of the dimensionality of the integral.

The stochastic sampling approach is termed *importance sampling*, because only the regions that contribute significantly to the integral are sampled. It should be noted that the probability density $\rho(\boldsymbol{q})$ does not need to be proportional to the target distribution; if it is not, the difference can be included in the function $f(\boldsymbol{q})$. Such an approach is called *reweighing* or *biased sampling*, and it can be useful, e.g., if the original $f(\boldsymbol{q})$ has values that differ significantly from zero only in regions where $\rho(\boldsymbol{q})$ is small. Because the error in the integration is proportional to the variance of f within the integration domain, the error is reduced if the probability distribution is chosen such that the reweighed f is close to a constant [183].

2.2.3 Markov Chain Monte Carlo

To take advantage of importance sampling, one needs to be able to generate random numbers from an arbitrary probability distribution function; however, basic computer implementations of random number generators only generate uniformly distributed numbers (simple mappings can be used to transform these to, e.g., Gaussian random numbers). If the cumulative distribution function is known, and can be inverted, it is simple to map a set of uniformly distributed random numbers to the desired distribution. However, this is often not the case for high-dimensional, complicated functions such as the Boltzmann distribution, and one has to resort to other methods. The common approach is to use *Markov chains*, which can generate random numbers from an arbitrary distribution [183].

A Markov chain is a discrete-time stochastic process that has a discrete set of states [41]. At a given step t, it is at a certain state i, and has transition probabilities p_{ij} of being in a state j at the next step $t+1$. The transition probabilities depend only on the initial state, and not on the history of how the process arrived at that state. For the present discussion, two properties of Markov chains are interesting: periodicity and ergodicity. A *periodic* chain has a finite probability of returning to the initial state only at steps $t = am$, $a, m \in \mathbb{N}$, $m > 1$, while for an *ergodic* chain, there is a finite probability for moving between any pair of states in a finite number of steps. It can be proven that if a Markov chain is not periodic and it is ergodic, there exists a unique limiting distribution $\boldsymbol{\pi}$ such that as $t \to \infty$, the probability of being in state i approaches the limiting distribution π_i regardless of the initial state. Hence, if we can generate a chain that has $\rho(\boldsymbol{q})$ as its limiting distribution, we can use the chain to create a sequence of states that will be distributed according to $\rho(\boldsymbol{q})$ after an initial equilibration period.

Because the limiting distribution $\boldsymbol{\pi}$ should not be changed during a step, it holds that $P^T\boldsymbol{\pi} = \boldsymbol{\pi}$, where P is the matrix of the transition probabilities p_{ij}. This gives

$$\pi_i = \sum_j p_{ji}\pi_j, \tag{2.13}$$

resulting in equations that the transition probabilities should satisfy in order for the chain to have the desired limiting distribution. There are S^2 transition probabilities, where S is the number of states, but only S conditions, so several different chains can be used to arrive at the same limiting distribution. One commonly used construction for such a chain is described in the next section.

It should be noted that when Markov chains are used to generate the samples, the samples are no longer independent. This affects the error estimates: if we introduce a correlation time τ after which the states of the Markov chain are independent to a sufficient degree, we can then estimate that there are M/τ independent samples, and hence the error scales as $(M/\tau)^{-1/2}$ [183].

2.2.4 Detailed Balance and Metropolis Criterion

Equation (2.13) gives necessary conditions for the transition probabilities to satisfy, but often, it is useful to impose a much more stringent criterion of *detailed balance* [183]:

$$\pi_i p_{ij} = \pi_j p_{ji}. \tag{2.14}$$

This implies that the transition probabilities between two states, weighted with the probabilities of the initial states, are the same in both directions. Equation (2.13) easily follows from Eq. (2.14).

For computer simulations, it is useful to divide the transition probability into two parts

$$p_{ij} = \omega_{ij} a_{ij}, \tag{2.15}$$

where ω_{ij} is a *trial probability* and a_{ij} is an *acceptance probability*. ω_{ij} describes the probability of generating a trial move from state i to j, and a_{ij} then gives the probability of accepting the new state. If the new state is not accepted, the chain stays in the old state. The detailed balance criterion (2.14) now becomes

$$\frac{a_{ij}}{a_{ji}} = \frac{\pi_j \omega_{ji}}{\pi_i \omega_{ij}}. \tag{2.16}$$

One common choice for the acceptance probability is the Metropolis criterion [122]

$$a_{ij} = \min\{1, \frac{\pi_j \omega_{ji}}{\pi_i \omega_{ij}}\}, \tag{2.17}$$

which has been also used in the simulations in this Thesis. If the trial probabilities are symmetric, i.e., $\omega_{ij} = \omega_{ji}$, the condition reduces further to include only the ratio of the probabilities of the two states. If the probability distribution $\boldsymbol{\pi}$ is the Boltzmann distribution, the ratio of the probabilities simplifies to $\exp\{-\beta\Delta E\}$, where ΔE is the energy difference of the two states.

2.2.5 Discussion

For simulations on atomic scales, MD is the method of choice in most cases because of its simplicity: there is no need to devise and optimize the trial moves. For simpler models, however, MC simulations are widely used. The main reason is flexibility: one does not need to be limited to models where forces are easily available (for example, if the model contains discrete degrees of freedom, or the particle number is not fixed), and sampling can be speeded up by, e.g., biased sampling or by clever choice of global or even unphysical trial moves. Most biasing methods can also be applied in MD simulations, although implementation of more complex schemes is more involved because forces are needed. Biasing methods also alter the dynamics in MD, requiring special techniques if correct dynamic information is needed [31, 38].

In contrast to MD, MC simulations have no equations of motion; they are replaced by random trial moves. In principle, it is possible to associate dynamics with the moves, e.g., by considering each trial move as a time step and matching the time scale to some known correlation function. Such an approach can be made more quantitative by employing a kinetic MC scheme where the rates of the different types of processes are also used in selecting the trial moves. However, for most models it is more correct to think of the configurations generated by an MC simulation only as static snapshots that sample the Boltzmann distribution.

MC simulations rely heavily on random numbers, but a large number of truly random numbers is difficult to generate in computers. Correlations and non-uniform distribution in the generated numbers can significantly alter the results, and hence, a high-quality pseudo-random number generator must be used in such simulations. Further, the generator should preferably be tested in the context of similar simulation techniques. The random number generator used in this work is a Mersenne Twister generator by Matsumoto and Nishimura [120].

Chapter 3

Coarse-graining

As discussed in the previous chapter, atomistic classical MD is the most widely used simulation technique in biomolecular studies. However, many interesting phenomena occur on much larger scales than those that can be simulated even with the most powerful supercomputers in atomistic detail (see Chapter 1), examples being phase behavior and large-scale structural changes [118].

The main factors limiting the accessible time and length scales are the number of particles in the system, leading to expensive evaluation of the forces, and a large difference between the timestep and the slowest relaxations in the system. Simplifying the representation of the system, i.e., constructing a CG model, can help in overcoming both these issues. A simpler representation generally has less particles, and if the force field retains a similar form, most importantly the pairwise nature of the forces, the force evaluation becomes less expensive. Also, CG interactions are typically smoother, allowing longer time steps and simplifying the energy landscape, which leads to shorter relaxation times in terms of simulation steps. Naturally, the speedup comes at a price: details on small length and time scales are lost, and it is not clear how well the CG model is able to reproduce the behavior of the underlying atomistic system. To minimize such problems, systematic approaches for constructing the CG models from available data are needed. Data from atomistic simulations of a system provide a good starting point for constructing a model, but other approaches based on experimental quantities are also possible. However, experimental information is often not as detailed, and hence more assumptions and approximations are needed. In this chapter, the focus is on the use of detailed data from atomistic simulations, but some approaches where experimental information is used are also mentioned.

The basis of systematic coarse-graining lies in statistical mechanics; the basic quantities and equations used in describing liquid systems are reviewed in Section 3.1, and the theoretical background of coarse-graining is outlined in Section 3.2. Section 3.3 then moves on to discuss the theoretical basis for constructing effective interactions based on structural information. Practical methods for obtaining the interactions are also introduced. Section 3.4 presents in more detail the inverse Monte Carlo (IMC) method that has been used in Papers [I]–[III], including development of the method that has been done as part of this Thesis. Other approaches for constructing CG models are discussed in Section 3.5, and finally the dynamics of CG models are briefly discussed in Section 3.6. For clarity, we assume throughout this chapter all the particles in the system to be identical, but the results are easily generalized to mixtures.

3.1 Statistical Mechanics of Liquids

A major goal in the classical theory of liquids is to study relationships between the interactions, structure, and thermodynamics of liquid systems [65]. Here, we focus on the quantities used to describe the structure of a liquid, as well as equations that link them to the microscopic interactions. With the coarse-graining applications in mind, we will focus on systems with pairwise interactions, i.e., whose Hamiltonian is

$$H(\boldsymbol{q}) = \sum_{i<j} V(x_i, x_j), \tag{3.1}$$

where x_i contains the coordinates of particle i. We further assume that the system is homogeneous and isotropic, i.e., V only depends on the relative positions of the particles. However, results that do not explicitly refer to the potential V are generally valid for any Hamiltonian.

3.1.1 Particle Density Functions

The instantaneous density of a system consisting of pointlike particles is

$$\rho(y) = \sum_i \delta(x_i - y). \tag{3.2}$$

The *n-particle density* $\rho^{(n)}$ can then be defined by

$$\rho^{(n)}(y_1, \ldots, y_n) = \frac{1}{n!}\langle {\prod_{i=1}^{n}}' \rho(y_i)\rangle = \frac{1}{n!}\frac{1}{Z}\int {\prod_{i=1}^{n}}' \rho(y_i)\exp[-\beta H(\boldsymbol{q})]\mathrm{d}\boldsymbol{q}, \tag{3.3}$$

where

$$Z = \int \exp[-\beta H(\boldsymbol{q})]\mathrm{d}\boldsymbol{q} \tag{3.4}$$

is the (configurational) partition function of the system. $\rho^{(n)}(y_1, \ldots, y_n)$ gives the probability of finding a particle at y_n provided that there are particles at $y_1, \ldots, y_{n-1}$. The prime in the product stands for omission of terms that contain the same x_i in two different delta functions when the product is expanded. This removes delta function contributions at points where $y_i = y_j$ for one or more pairs $i \neq j$. Often, the $\rho^{(n)}$ with the delta functions removed is termed the *n-particle correlation function*, but here we will neglect this distinction for simplicity.

$\rho^{(1)}$ and $\rho^{(2)}$ are commonly used to characterize the structure of fluid-like systems. $\rho^{(1)}(x)$ is just the density at x, and if the system is assumed homogeneous, it equals ρ, the average density of the system. Similarly, for a translationally invariant system $\rho^{(2)}(x, x')$ only depends on the relative position $(x - x')$, and if the system is also rotation invariant, $\rho^{(2)}$ only depends on $r = \|x - x'\|$. In such a case, it is convenient to define the *radial distribution function* (RDF) $g(r)$ as

$$g(r) = \frac{V}{N_p S(r)}\int \rho^{(2)}(x, x')\delta(\|x - x'\| - r)\mathrm{d}x\,\mathrm{d}x', \tag{3.5}$$

where N_p is the number of particle pairs, $S(r)$ is the surface area of a sphere of radius r, and V is the volume of the system. The prefactor normalizes $g(r)$ such that for an ideal gas (no correlations), $g(r) = 1$. Because of the normalization, $g(r) \to 1$ as $r \to \infty$ for a fluid with no long-range order.

3.1.2 Static Structure Factors

In addition to the RDF, another important structural quantity is the *static structure factor* $S(\boldsymbol{k})$, defined as

$$S(\boldsymbol{k}) = \frac{1}{N}\langle|\hat{\rho}(\boldsymbol{k})|^2\rangle = \frac{1}{N}\langle\hat{\rho}(\boldsymbol{k})\hat{\rho}(-\boldsymbol{k})\rangle = \frac{1}{N}\langle\sum_{i,j} e^{-i\boldsymbol{k}\cdot(\boldsymbol{r}_i-\boldsymbol{r}_j)}\rangle, \tag{3.6}$$

where $\hat{\rho}(\boldsymbol{k})$ is the (spatial) Fourier transform of the instantaneous density ρ [Eq. (3.2)]. From the definition, it is clear that for a homogeneous system, $S(\boldsymbol{k})$ is directly related to the Fourier transform of the two-particle density $\rho^{(2)}(x - x')$. The importance of $S(\boldsymbol{k})$ stems from the fact that it gives the intensity of the scattered wave in scattering experiments, and hence provides a route to experimentally determine the RDF. Also, the small $\boldsymbol{k}$ region provides a more convenient characterization of large-scale structure than RDFs.

3.1.3 Integral Equations

A classical approach to the relationship between the interactions and the structure of a fluid is to use *integral equations*. In the context of coarse-graining, perhaps the one most commonly used is the Ornstein-Zernike (OZ) equation [65]

$$h(r_{12}) = c(r_{12}) + \rho\int c(r_{13})h(r_{23})\mathrm{d}\boldsymbol{r}_3, \tag{3.7}$$

where $h(r) = g(r) - 1$ is the *total correlation function* and $c(r)$ is called the *direct correlation function*. The OZ equation splits the total correlation function $h(r)$ into a direct part [$c(r)$ by definition], and an indirect part that includes all correlation effects mediated by other particles. The idea behind this splitting is that $c(r)$ should be more directly related to the microscopic interactions than $h(r)$, because the latter also includes many-body effects in higher densities.

Another integral equation is the Yvon-Born-Green (YBG) equation [65]

$$\left(k_{\mathrm{B}}T\frac{\partial}{\partial\boldsymbol{r}_1} + \frac{\partial V(r_{12})}{\partial r}\right)\rho^{(2)}(\boldsymbol{r}_1,\boldsymbol{r}_2) = -\int\frac{\partial V(r_{13})}{\partial r}\rho^{(3)}(\boldsymbol{r}_1,\boldsymbol{r}_2,\boldsymbol{r}_3)\mathrm{d}\boldsymbol{r}_3, \tag{3.8}$$

which relates the two-particle density to the pair interaction $V(r)$ and the three-particle density. It is essentially a statement of equilibrium: it links the average total force between a pair of particles at $\boldsymbol{r}_1$ and $\boldsymbol{r}_2$ to the slope of the two-particle density at that point.

The above equations need a *closure relation* in order to provide an explicit link between the structure and the interactions. For the OZ equation, a closure that relates the direct correlation function to the pair interaction is needed, while the YBG equation needs an expression for $\rho^{(3)}$ in terms of the lower-order densities. However, these closures always include approximations. This can lead to severe problems in higher densities, e.g., in the form of unphysical or multiple solutions [161, 205].

3.1.4 Thermodynamics

Analytically, the thermodynamics of a liquid can be obtained from the partition function Z [Eq. (3.4)]: the excess free energy of the system (in addition to an ideal gas contribution) is given by [151]

$$F = -k_{\mathrm{B}}T\ln Z. \tag{3.9}$$

This can be differentiated to obtain, e.g., the pressure. However, calculating free energies of complex systems from simulations is difficult, as only free energy differences of very similar systems can be calculated reliably. Methods for such calculations are beyond the scope of the present discussion; see, e.g., Refs. [194] and [95] for reviews.

The derivatives of the free energy can also be evaluated directly from simulation. For the pressure, there are two common routes [65]: the *virial* and the *compressibility* routes. In the first, the pressure is evaluated through the virial equation

$$dPV = 2\langle E_{\text{kin}}\rangle + \left\langle \sum_{i<j} r_{ij} f_{ij} \right\rangle = 2\langle E_{\text{kin}}\rangle - \frac{1}{2}\int r\rho^{(2)}(\boldsymbol{r})\frac{\partial V(r)}{\partial r}\mathrm{d}\boldsymbol{r}, \tag{3.10}$$

where d is the dimensionality of the system, E_{kin} is the kinetic energy and $f_{ij} = -\frac{\partial V(r_{ij})}{\partial r}$ is the interparticle force. The second gives the isothermal compressibility κ_T in terms of the RDF of the liquid as

$$\rho k_{\text{B}} T \kappa_T = \frac{\langle N^2\rangle - \langle N\rangle^2}{\langle N\rangle} = 1 + \rho\int [g(r) - 1]\mathrm{d}\boldsymbol{r}, \tag{3.11}$$

which can then be integrated over densities to yield the pressure. Eq. (3.10) is only valid for pairwise interactions, while the latter equation is independent of the Hamiltonian of the system (as long as the Hamiltonian is not explicitly density-dependent). The two approaches are equivalent for a simple liquid, but the situation changes in coarse-graining [102]: the interactions in the system become density-dependent, and several different interpretations are then possible [181] (see Section 3.2).

3.1.5 Derivatives of Pair Densities

For the discussion in Section 3.2, it is useful to note a few links between the two-particle density $\rho^{(2)}$, the pair potential V, and the free energy F of a system. Namely, the free energy F [Eq. (3.9)] can be viewed as a functional of V, and its functional derivative is

$$\begin{aligned}\frac{\delta F}{\delta V(\boldsymbol{y})} &= -\frac{1}{\beta Z}\frac{\delta Z}{\delta V(\boldsymbol{y})} = \frac{1}{Z}\int \frac{\delta H(\boldsymbol{q})}{\delta V(\boldsymbol{y})}\exp[-\beta H(\boldsymbol{q})]\mathrm{d}\boldsymbol{q} \\ &= \langle\frac{\delta H(\boldsymbol{q})}{\delta V(\boldsymbol{y})}\rangle = \langle\sum_{i<j}\delta(x_i - y)\delta(x_j - y')\rangle = \rho^{(2)}(y, y'),\end{aligned} \tag{3.12}$$

where we have combined the two parameters of V into a single $\boldsymbol{y} = (y, y')$ to simplify the notation. Similarly, we can calculate the functional derivative of $\rho^{(2)}(\boldsymbol{y})$ with respect to V:

$$\begin{aligned}&\frac{\delta\rho_V^{(2)}(\boldsymbol{y})}{\delta V(\boldsymbol{y}')} = \frac{\delta}{\delta V(\boldsymbol{y}')}\frac{1}{Z}\int\frac{\delta H(\boldsymbol{x})}{\delta V(\boldsymbol{y})}\exp[-\beta H(\boldsymbol{x})]\mathrm{d}\boldsymbol{x} \\ &= -\rho_V^{(2)}(\boldsymbol{y})\frac{1}{Z}\frac{\delta Z}{\delta V(\boldsymbol{y}')} - \frac{\beta}{Z}\int\frac{\delta H(\boldsymbol{x})}{\delta V(\boldsymbol{y})}\frac{\delta H(\boldsymbol{x})}{\delta V(\boldsymbol{y}')}\exp[-\beta H(\boldsymbol{x})]\mathrm{d}\boldsymbol{x} \\ &= \beta\rho_V^{(2)}(\boldsymbol{y})\rho_V^{(2)}(\boldsymbol{y}') - \beta\langle\frac{\delta H(\boldsymbol{x})}{\delta V(\boldsymbol{y})}\frac{\delta H(\boldsymbol{x})}{\delta V(\boldsymbol{y}')}\rangle = -\beta\mathrm{Cov}\left[\frac{\delta H(\boldsymbol{x})}{\delta V(\boldsymbol{y})}, \frac{\delta H(\boldsymbol{x})}{\delta V(\boldsymbol{y}')}\right],\end{aligned} \tag{3.13}$$

where $\mathrm{Cov}(x, y) = \langle xy\rangle - \langle x\rangle\langle y\rangle$ is the covariance of x and y.

3.2 Theory of Coarse-Graining

A central concept in the study of static properties of an ensemble of particles is the Boltzmann factor, which gives the (relative) probability for observing a particular configuration $\boldsymbol{Q}$ of particles [151]:

$$P(\boldsymbol{Q}) \propto e^{-\beta H(\boldsymbol{Q})}. \tag{3.14}$$

Let us now focus on a smaller, coarse-grained set of coordinates $\boldsymbol{q}$, which are related to $\boldsymbol{Q}$ by a mapping function M: $\boldsymbol{q} = M(\boldsymbol{Q})$ (the presentation here follows loosely that in Ref. [141]). Eq. (3.14) now gives

$$P(\boldsymbol{q}) \propto \int e^{-\beta H(\boldsymbol{Q})} \delta(\boldsymbol{q} - M(\boldsymbol{Q})) \mathrm{d}\boldsymbol{Q} \propto \int_{\boldsymbol{Q} \in M^{-1}(\boldsymbol{q})} e^{-\beta H(\boldsymbol{Q})} \mathrm{d}\boldsymbol{Q}, \tag{3.15}$$

where the last form explicitly shows that the integration is over all microstates $\boldsymbol{Q}$ consistent with $\boldsymbol{q}$. Here, we have assumed that the mapping M is linear; otherwise, the Jacobian of M may depend on $\boldsymbol{q}$ and should be included in the analysis. In analogy with Eq. (3.14), we can now define an *effective Hamiltonian* $H_{\text{eff}}(\boldsymbol{q})$ as

$$P(\boldsymbol{q}) \propto e^{-\beta H_{\text{eff}}(\boldsymbol{q})} = \int_{\boldsymbol{Q} \in M^{-1}(\boldsymbol{q})} e^{-\beta H(\boldsymbol{Q})} \mathrm{d}\boldsymbol{Q}. \tag{3.16}$$

If $H_{\text{eff}}(\boldsymbol{q})$ was known exactly, it could be used to sample the configurations of the CG system such that all averages of quantities that depend only on the CG coordinates $\boldsymbol{q}$ would be exact. In practice, this is not possible. First, $\boldsymbol{q}$ is typically high-dimensional, which makes it impossible to even store the values of H_{eff}, e.g., on a grid of points. Second, it is often not enough to know the H_{eff} for a given set of $\boldsymbol{q}$, but instead, one would like a form that generalizes to a larger system. This way, one could determine the effective Hamiltonian using a smaller system, and then use the result to study a larger one.

For the above reasons, the effective Hamiltonian needs to be approximated. One can always write H_{eff} as a sum of terms involving increasing number of particles:

$$H_{\text{eff}}(\boldsymbol{q}) = w_0 + \sum_i w_1(x_i) + \sum_{i<j} w_2(x_i, x_j) + \dots. \tag{3.17}$$

The first term is a constant, the second term describes a single-particle field, the third term describes pairwise interactions etc. In principle, the sum can range up to an N-body term that includes all the degrees of freedom. To make the sum unique, one often requires that (3.17) should hold for all N with the *same* functions w_n.

If we now assume that the sum (3.17) can be *approximated* by a truncated sum of the form

$$H_{\text{eff}}(\boldsymbol{q}) \approx V_0 + \sum_i V_1(x_i) + \sum_{i<j} V_2(x_i, x_j), \tag{3.18}$$

we can overcome both of the problems: the Hamiltonian is now written as a sum of low-dimensional functions, and the sum can also be generalized to a larger system by simply adding terms that include interactions involving the new particles. Using higher-order terms in the approximation is also possible, but often too costly computationally. Further, the system is typically assumed homogeneous and isotropic. After these assumptions,

the task of determining the effective Hamiltonian is reduced to finding a function $V_2(r)$ such that Eq. (3.16) is as accurate as possible. Because such a pair interaction typically includes contributions from the original higher-order interactions w_n implicitly, it is called an *effective interaction* or an *effective potential*.

Eq. (3.16) defines $H_{\text{eff}}(\boldsymbol{q})$ as the free energy of a configuration $\boldsymbol{q}$. Thus, it can be misleading to call a CG interaction an effective potential, because it also contains entropic contributions. However, this is a common nomenclature, and is also followed here. When performing any analysis of a CG system, one must carefully consider how the (often unknown) dependence on the thermodynamic variables may affect the results [2, 102, 181].

Because H_{eff} is a free energy, effective potentials derived at one thermodynamic state point (temperature, density, etc.) are strictly valid at only this state point, and in principle, distinct interactions should be derived for each state point. In practice, this is often not desirable or even possible, because estimating H_{eff} even at a single state point can be computationally expensive. This is the case in particular if the input data comes from atomistic simulations of the system. Because of these limitations, *transferability* of the potentials, i.e., the applicability of the potentials at nearby state points, is an issue of interest. Further, it is typically impossible to obtain an effective interaction that could reproduce all quantities of interest [102]. This issue of *representability* should always be kept in mind when interpreting results from CG models. Also, a connected issue is that the meaning of several quantities can change between the models at different resolution. For example, the value of H_{eff} no longer represents the internal energy. Similarly, if the water is coarse-grained out of a water–ion solution, the virial pressure in the CG model becomes the osmotic pressure [2, 106]. The approximation (3.18) induces additional problems, as the state dependence of the effective pair potentials may or may not accurately estimate that of the exact H_{eff}. Transferability and representability problems are also connected, since poor transferability means, in effect, large derivatives of the potentials wrt. thermodynamic variables, and these derivatives are an important factor in representability problems [102]. One should also note that although the constant term and the effective one-particle field in Eq. (3.18) do not depend on the positions in a homogeneous system, they *can* depend on the thermodynamic state, which can also affect the treatment [181].

In principle, Eq. (3.16) can be written for any mapping function M, but the accuracy of the truncation and the isotropic assumption depend heavily on the mapping. This is easy to understand from a simple example: if the underlying system consists of hard rods, and $\boldsymbol{q}$ consists of the centers of these rods, using only pairwise isotropic interactions clearly leads to losing important features of the underlying system. A more realistic example comes from polymer physics [52]: when constructing a model for polyisoprene, the form of the required bonded potential depends heavily on where the bead centers are placed. This is because the chain contains both single and double bonds, and if the beads are connected by double bonds, which are more rigid, also the distance between the beads is better constrained. Hence, a simple harmonic potential can be used to represent the bonded potential in this case, while placing the bead centers on the double bonds requires a more complicated potential.

The above examples clearly highlight the importance of proper selection of the degrees of freedom for CG models. Often, this choice is done based on intuitive or heuristic arguments based on the experience of the modeler. In many cases this works, but for more

complex models, tools for finding possibilities and evaluating the choices are desirable. This issue is discussed in more detail in Chapter 5 and links the trajectory analysis using self-organizing maps (Paper [V]) loosely to the coarse-graining framework.

3.3 Effective Interactions from Structure

Even with the assumption of pairwise interactions, direct use of Eq. (3.16) in optimizing the form of the interactions is usually not feasible, because it leads to complicated equations [180] and/or requires extensive sampling of a high-dimensional probability distribution function. In practice, some derived quantity, not H_{eff} itself, is used as the optimization target. Common choices include RDFs [52] and derivatives of the Hamiltonian with respect to positions [141], i.e., forces.

Recently, Shell has suggested using relative entropy as a generic framework for constructing CG models [169]. This is an interesting approach, because it approaches H_{eff} in a more direct way: the relative entropy arises naturally when maximizing the likelihood that the model reproduces the probability distribution of the original system [169]. For a model with only pairwise interactions, it actually follows that the optimal model that minimizes the relative entropy is the one that reproduces the two-particle densities, justifying the use of RDFs. It has also been shown that under the constraint that given RDFs are reproduced, the model that has the highest entropy is one with pairwise interactions [106].

For clarity and simplicity, let us now focus on a situation where each pair of particles interacts with the same pair interaction V, i.e., the Hamiltonian is given by Eq. (3.1) (we drop the subscript eff from now on). However, all discussion is easily generalized to multicomponent systems even if not explicitly stated.

3.3.1 Uniqueness and Existence of Pair Interactions

The question of uniqueness of interactions determined from RDFs was first addressed by Henderson in 1974 [67]: he proved that for a system at a fixed thermodynamic state, the pair potential that reproduces a given RDF is unique. Although less often cited in this context, an existence proof also exists: Chayes *et al.* proved in 1984 that such a potential always exists, provided that the RDF is a two-particle reduction of a physical N-particle probability distribution (physical here means that it satisfies certain finiteness conditions) [29, 30]. Chayes *et al.* proved the existence (and uniqueness) for a very general situation where, in addition to the pair potential to be fitted, there is a *fixed* N-particle interaction $W(x_1, \ldots, x_N)$, which again only needs to satisfy certain finiteness conditions. Any such W can be complemented by a pairwise interaction to reproduce the given RDFs.

To be precise, Chayes *et al.* did not explicitly prove the existence of the pair potential for the canonical ensemble which we are here interested in. In [29], they treated the inverse problem for the single-particle density in both canonical and grand-canonical ensembles, also for multicomponent systems, while [30] gave a more general proof for a single-component system in the grand-canonical case, also for higher-order densities. However, an explicit proof seems little more than a straightforward combination of the techniques in the two papers. Although the full generality of the results in [30] may be difficult to achieve in the canonical ensemble, for CG applications it is typically enough to

restrict oneself to cases where $W = 0$ (or to W that satisfy the more restrictive conditions in [29]); problems in the proof are only expected in cases where W contains interactions that are of hard-core nature [29, 30].

The existence can be proved by constructing a functional

$$\mathcal{F}[v] = \frac{\exp[-\beta \int V(x,x')\rho^{(2)}(x,x')\mathrm{d}x\mathrm{d}x']}{\int \exp[-\beta W(\boldsymbol{x}) - \beta \sum_{i<j} V(x_i,x_j)]\mathrm{d}\boldsymbol{x}}, \tag{3.19}$$

where $\rho^{(2)}$ is the target two-particle density, and then showing that there is a V that maximizes $\mathcal{F}$, and that this V gives the correct RDF. The details of the mathematically rigorous proof are lengthy, and are skipped here. The basic idea is to show that $\mathcal{F}$ is bounded from above and then take a maximizing sequence. It can then be shown that the maximizing sequence (actually, a new sequence is constructed to deal with the fixed interaction) is bounded, and hence has a weakly convergent subsequence. Such a subsequence can be shown to converge strongly, which allows one to define a candidate V. Finally, one needs to prove that V is in the proper function space, that it maximizes $\mathcal{F}$, and that it reproduces the correct RDF. For rigorous mathematical details, the reader is referred to [29, 30], and here we only focus on less rigorous discussion of the functional $\mathcal{F}$ in the case $W = 0$.

For physical intuition, it is more useful to study the logarithm of $\mathcal{F}$ instead of $\mathcal{F}$ directly (since $\ln$ is monotonic, the logarithm is maximized exactly when $\mathcal{F}$ is):

$$F[V] = \ln \mathcal{F}[V] = -\ln \int \exp[-\beta H_g(\boldsymbol{x})]\mathrm{d}\boldsymbol{x} = -\ln Z_g[v], \tag{3.20}$$

$$H_g(\boldsymbol{x}) = \sum_{i<j} V(x_i,x_j) - \int V(x,x')\rho^{(2)}(x,x')\mathrm{d}x\mathrm{d}x'. \tag{3.21}$$

Eq. (3.20) allows us to interpret F as the total free energy of a system with the Hamiltonian H_g from Eq. (3.21). The second term in H_g is just a constant for a given V, and hence contributes only an additive constant to $F[V]$. However, this constant is important when considering different V: the correct V maximizes the free energy F. This maximization property can be understood based on the analysis by Shell [169]: the F defined by (3.20) differs from the negative of the relative entropy between the model and the original system only by a constant.

Formal calculation of the functional derivative of $F(V)$ with respect to V gives [29]

$$\begin{aligned} \frac{\delta F}{\delta V(\boldsymbol{y})} &= -\frac{\delta}{\delta V(\boldsymbol{y})} \ln Z - \beta \frac{\delta}{\delta V(\boldsymbol{y})} \int V(x,x')\rho^{(2)}(x,x')\mathrm{d}x\mathrm{d}x' \\ &= \beta(\rho_V^{(2)}(\boldsymbol{y}) - \rho^{(2)}(\boldsymbol{y})), \end{aligned} \tag{3.22}$$

where Eq. (3.12) has been used and $\rho_V^{(2)}$ denotes the two-particle density resulting from the pair potential V. Eq. (3.22) motivates the original choice of the functional $\mathcal{F}$ in Eq. (3.19): at an extremum of F, and hence $\mathcal{F}$, $\rho_V^{(2)} = \rho^{(2)}$. Similarly, the second functional derivative can be evaluated as

$$\frac{\delta^2 F}{\delta V(\boldsymbol{y})\delta V(\boldsymbol{y}')} = \beta \frac{\delta \rho_V^{(2)}(\boldsymbol{y})}{\delta V(\boldsymbol{y}')} = -\beta^2 \mathrm{Cov}\left[\frac{\delta H(\boldsymbol{x})}{\delta V(\boldsymbol{y})}, \frac{\delta H(\boldsymbol{x})}{\delta V(\boldsymbol{y}')}\right], \tag{3.23}$$

where Eq. (3.13) has been used. The covariance matrix $C_{ij} = \mathrm{Cov}(x_i, x_j)$ of a set of variables is always a positive (semi)definite, and hence $F[V]$ is convex downwards. Formally, the uniqueness of the maximum follows from the convexity, and hence Eqs. (3.22)

and (3.23) give a heuristic justification for the existence and uniqueness proofs using the functional $\mathcal{F}$. The convexity also guarantees that $F[V]$ has a single maximum, i.e., that it cannot have local maxima. This property is important in discussing algorithms for actually finding the maximizing V.

Contrary to the existence, the proof of uniqueness is simple. Here, we follow the idea of Henderson [67], and essentially the same argument was used by Chayes *et al.* in their proof of uniqueness [29]. The starting point is a basic thermodynamic inequality (which follows from Jensen's inequality used in Ref. [29]):

$$F_2 - F_1 \leq \langle H_2 - H_1 \rangle_1, \tag{3.24}$$

where the subscripts denote two different systems with Hamiltonians H_1 and H_2 and Helmholtz free energies F_1 and F_2, and $\langle \cdot \rangle_1$ denotes an ensemble average in system 1. For two systems with only pairwise interactions, i.e., $H_{1,2} = \sum_{i<j} V_{1,2}(x_i, x_j)$, the expectation value on the right-hand side can be written as

$$\langle H_2 - H_1 \rangle_1 = \int [V_2(\boldsymbol{x}) - V_1(\boldsymbol{x})] \rho_1^{(2)}(\boldsymbol{x}) \mathrm{d}\boldsymbol{x}, \tag{3.25}$$

where $\rho_1^{(2)}(\boldsymbol{r})$ is the two-particle density of the first system. Exchanging the subscripts 1 and 2 we get a second equation, and summing the resulting inequalities gives

$$\int [V_2(\boldsymbol{x}) - V_1(\boldsymbol{x})][\rho_2^{(2)}(\boldsymbol{x}) - \rho_1^{(2)}(\boldsymbol{x})] \mathrm{d}\boldsymbol{x} \leq 0. \tag{3.26}$$

The equality holds if and only if it holds in Eq. (3.24), i.e., if the Hamiltonians differ by no more than a constant. Hence, if $\rho_1^{(2)} = \rho_2^{(2)}$, i.e., the equality holds, the Hamiltonians can only differ by a constant, and the pair potential is unique.

The form of Eq. (3.26) also gives some indication of how the pair potential and the RDF are related: if the RDFs differ only around one point, then the pair potentials must also differ around the same point, and direction of the difference is the opposite. However, it is not possible to say how the pair potentials change elsewhere, or anything about the magnitude of the change.

The existence and uniqueness theorems above have been formulated with the functions $V(x, x')$ and $\rho^{(2)}(x, x')$, i.e., without any assumptions about the homogeneity or isotropicity of the system. However, when implementing the inversion in practice, the system is typically assumed homogeneous and isotropic *a priori*, and hence both functions are assumed to only depend on $\|x - x'\|$. The assumption of homogeneity is necessary to enable generalization of the potential to a larger system, and isotropicity is often assumed to simplify the representation of the potential and to reduce the number of parameters that need to be determined. Another assumption necessary in practice is that the potential $V(r)$ is constant beyond some cutoff $r > r_{cut}$. This is necessary both because of computational efficiency and because $\rho^{(2)}(r)$ can only be calculated up to some cutoff because of the limited system size. In the integral equation framework, the RDF can be treated also beyond the cutoff, but a potential cutoff is still necessary [19].

If the underlying system is not homogeneous and/or isotropic, e.g., because of insufficient sampling of the atomistic model, the approximations can result in problems during the inversion. Most notably, the form $V(x, x')$ is general enough to contain an arbitrary

single-particle field $U(x)$, while this field is assumed zero when the potential is treated as homogeneous. This may have subtle effect on the interactions if an RDF averaged from an inhomogeneous $\rho^{(2)}(x, x')$ is represented with homogeneous and isotropic potentials.

To minimize effects of system size on the effective interactions, the inversion should be carried out in a system that is identical in size to the one where the target RDFs were determined [105]. This way, the finite system size affects both sets of RDFs equally, and the finite size effects should cancel to at least to some degree. This is also in agreement with the existence proof, because there the phase space over which the target RDFs are calculated is the same as in which the existence is proved. However, if the cutoff of the interactions is close to the system size, it may happen that the determined interactions do not generalize to a larger system. This was observed in Papers [II] and [III], where a direct inversion of the RDFs resulted in very inhomogeneous density distributions in larger systems. The source of the problems was not identified with certainty, but it was speculated that insufficient sampling in the underlying MD simulations may be to blame. To obtain effective interactions that worked in larger systems, constraints were imposed during the inversion process, as discussed in more detail in Sections 3.4 and 4.3.

Some further discussion of the RDF inversion problem is in place for the situation where (some of) the particles have *internal states*. This is the case for the models in Paper [III], where two discrete states are used to describe the ordering of lipid tails (see Chapter 4). To be precise, each internal state is treated as a separate particle kind, and the particles can switch between the kinds during the MC simulation. For clarity, we will refer to particle types when all internal states are considered as a single type, and particle kinds, when each internal state is separated.

The existence and uniqueness proofs make no explicit reference to the form of the phase space, and are hence valid also when the coordinates x_i contain discrete states in addition to the particle positions. In this description, the pair potential $V(x, x')$ and $\rho^{(2)}$ for the particles with internal states actually contains several distinct pair potentials (which are functions of positions only), each corresponding to a particular combination of internal states. Hence, an equivalent description can be achieved by having a separate potential and two-particle density for each combination of internal states. However, the number of each particle kind is no longer constant, which should be handled properly. In particular, it is the $\rho^{(2)}$, and not the RDF, which is the fundamental target quantity: $\rho^{(2)}$ contains information on the occurrence probabilities of different particle kinds, which is (partially) lost when the RDF is normalized with the average number of pairs.

The approximations introduced for simulations, in particular the finite cutoff, also need to be treated carefully. Namely, since the number of a particular pair kind is no longer constant, adding a constant to one of the potentials changes the system (if one or both of the involved particle types have multiple states). Hence, if we insist to set all potentials to zero beyond the cutoff, we need to introduce additional parameters in order to be able to represent the full range of Hamiltonians required for the existence of the solution. A full calculation was carried out in Paper [III], with the result that the Hamiltonian should have the form

$$H = \sum_{i<j} V_{ij}(x_i, x_j) + \sum_{k=1}^{N_s} E_k n_k + \sum_{k=1}^{N_s} \sum_{l=k}^{N_s} E_{kl} \delta n_k \delta n_l \tag{3.27}$$

to guarantee both existence and uniqueness of the solution. Here, n_k are the numbers of

particles of each kind, N_s is the number of *independent* n_k, E_k and E_{kl} are parameters to be determined, and $\delta n_k = n_k - n_k^{ave}$ with arbitrary constants n_k^{ave}.

Eq. (3.27) shows that in addition to the pair potentials, we need to include internal energies of the states (the first sum) as well as energy terms that control the fluctuations in the particle kind numbers (the second sum) in order to represent the full class of Hamiltonians required for the existence of a solution.

Despite the theoretical need for the second-order terms, they were observed to cause several difficulties in Paper [III]. (i) For some cases, accurately determining the parameters E_{kl} can be quite difficult. (ii) The Hamiltonian (3.27) is not extensive, and it is difficult to generalize it to larger systems: if the number of particles increases by a factor of M, n_k^{ave} should also be multiplied by M, but for E_{kl} the value can either remain the same or be divided by M. The latter makes the Hamiltonian extensive, but changes the energetics of flipping a single state, thus possibly also affecting $\langle n_k \rangle$. The former results in problems if $E_{kl} < 0$, as the states far away from the $\langle n_k \rangle$ can become energetically favorable. (iii) It is not clear how the n_k^{ave} should be treated when transferring the interactions to another concentration, as they can contain direct information from the state point. For these reasons, Paper [III] used a set of interactions with $E_{kl} \geq 0$ for studies of larger systems and further restricted $E_{kl} = 0$ for transferability studies, and the full Hamiltonian (3.27) was only used for studying the inversion problem itself.

3.3.2 Practical Methods

The fact that the solution to the inverse problem always exists and is unique is commonly used to justify taking the RDFs as the target quantities for the determination of pair potentials [189]. Also, it is possible to determine the RDFs from experiments, although it is often better to use the structure factors as the target if possible [189].

Despite the existence, constructing the pair potential is not always an easy task. In principle, any kind of optimization technique could be used, but the issue is complicated by the fact that evaluation of the RDF for a given pair potential requires, e.g., an MC simulation. Hence, the number of function evaluations is the limiting factor in the optimization. Further, the evaluation of any derivatives is even more costly. If some functional form is assumed for the interaction, the parameters can then be optimized with optimization techniques such as simplex [52] or Monte Carlo methods [2]. However, only a limited number of parameters can be used, and this can lead to problems in reproducing the RDF in more complex systems.

To achieve a better match, the interaction should be allowed to have any functional form. This can be achieved with tabulated potentials, where the value within each bin can be changed individually. Such potentials, however, include a huge number of parameters (the value at each bin is an independent parameter), and physics needs to be employed to effectively optimize the potentials.

For dilute systems, the potential of mean force, $V(r) = -k_\mathrm{B}T \ln g(r)$, gives a reasonable potential, becoming exact in the limit of infinite dilution. At intermediate densities, the OZ equation (3.7) has been used [19, 20, 109, 176]. However, the fact that an approximate closure is needed, makes the approach break down for dense systems, and thus iterative methods are needed [176]. There have also been attempts to circumvent the need for a closure: a reverse Monte Carlo (RMC) approach was used to generate configurations consistent with the given $g(r)$ and the resulting three-particle density was used in

the YBG equation (3.8) to determine the potential [190]. However, this approach is undermined by the fact that $g(r)$ is in general not enough to uniquely fix the three-particle density; this is only true if the system has only pairwise interactions, but since the RMC approach does not include the potentials explicitly, it is very difficult to impose such a restriction [86].

Perhaps the simplest iterative technique for approximating the pair potential is iterative Boltzmann inversion (IB) [165, 166, 179]. One starts with an initial guess for the pair potential, e.g., with the potential of mean force $v^0(r) = -k_{\mathrm{B}}T \ln g(r)$, and then calculates the corresponding RDF $g^0(r)$. An improved potential is then obtained from

$$v^{i+1}(r) = v^i(r) + k_{\mathrm{B}}T \ln \left(\frac{g^i(r)}{g(r)} \right), \tag{3.28}$$

and the iteration is continued until desired accuracy has been reached. Soper has argued that the method converges, based on a calculation using Eq. (3.26) [179]. This method has been applied, e.g., in polymer physics [27, 52, 130, 159] and to construct CG models for adaptive resolution simulations [158]. Shelley *et al.* have also parameterized some interactions in their semi-atomistic lipid model using IB [170].

Another iterative method for inverting the RDFs is the inverse Monte Carlo (IMC) method [105]. It is based on a linear approximation for the changes of the RDFs in terms of changes in the potentials, and in contrast to IB, it also takes into account correlations between the changes in the RDFs. The method is presented in detail in the next Section. Here, let us only briefly note several applications where the IMC approach has been used: Lyubartsev and co-workers, the original developers of the method, have applied the method to study ion solutions [105, 106, 110], ion-DNA interactions [107], to determine the effective interactions for water from *ab initio* simulations and experiments [108], and to modeling of lipids [111]. Kremer and co-workers have also used the approach in some of their adaptive resolution work to match models at different resolutions [121].

There are also other iterative approaches, which either try to improve the accuracy of the above ones, or use the static structure factors directly as the target values. An interested reader is referred to Ref. [189]. However, IB and IMC are by far the most commonly used [189].

In their series of publication on polymer–colloid mixtures, Bolhuis *et al.* have stressed the importance of accurate inversion and careful treatment to obtain the correct thermodynamics from RDF inversion [18, 19, 20, 21]. By construction, the effective interactions should reproduce the thermodynamics through the compressibility route [Eq. (3.11)], but the virial route generally disagrees [102], unless a suitable single-particle field is included and the explicit density dependence taken into account [181].

3.4 Inverse Monte Carlo

3.4.1 Basic Formulation

Let us consider a system with only a single type of particles interacting through a pair potential $V(r)$. To formulate the IMC method, we explicitly use a grid approximation for $V(r)$:

$$V(r) = V_b, \quad r \in [r_b - \frac{1}{2}h, r_b + \frac{1}{2}h], \quad r_b = (b + \frac{1}{2})h, \tag{3.29}$$

where h is the size of an individual bin and the bin index b runs upwards from zero. The Hamiltonian (3.1) can then be written as

$$H = \sum_b S_b V_b, \tag{3.30}$$

where S_b is the number of particle pairs within bin b, and the sum runs over all bins. $\langle S_b \rangle$ then represents a grid approximation to the RDF:

$$\langle S_b \rangle = \frac{N_p S(r_b) h}{V} g(r_b), \tag{3.31}$$

where the prefactor is just the normalization factor of the RDF [Eq. (3.5)].

The traditional way of deriving the IMC method [105, 110] is to consider small changes in the potential and write a linear approximation for the changes in $\langle S_b \rangle$ as

$$\Delta \langle S_b \rangle = \sum_c \frac{\partial \langle S_b \rangle}{\partial V_c} \Delta V_c + \mathcal{O}(\Delta V_c^2) \tag{3.32}$$

and evaluate the derivatives similarly to the calculation in Eq. (3.23). The result is

$$\frac{\partial \langle S_b \rangle}{\partial v_c} = \frac{\partial}{\partial v_c} \frac{\int S_b e^{-\beta H} \mathrm{d}\boldsymbol{q}}{\int e^{-\beta H} \mathrm{d}\boldsymbol{q}} = -\frac{\langle S_b S_c \rangle - \langle S_b \rangle \langle S_c \rangle}{k_\mathrm{B} T}. \tag{3.33}$$

Assume now that we have a trial potential $V^0(r)$ that corresponds to an RDF $g^0(r)$. Neglecting the higher-order terms in Eq. (3.32) results in a linear equation for Δv_c, i.e., the changes in the potential, in terms of the desired changes in $\langle S_b \rangle$, i.e., in the RDF. This equation can then be iterated as in IB. In practice, at each iteration one has to solve a matrix equation of the form

$$A\boldsymbol{x} = \boldsymbol{b}, \tag{3.34}$$

where the matrix A contains the derivatives from Eq. (3.33), $\boldsymbol{x}$ are the changes in the potential values, and $\boldsymbol{b}$ contain the desired changes in the RDFs.

The same set of equations can also be arrived in a different way. Namely, we know that the correct potential maximizes Eq. (3.20). If we apply Newton's method to maximize this functional, we get

$$V^{i+1}(\boldsymbol{y}) = V^i(\boldsymbol{y}) - \left[\frac{\delta^2 F}{\delta V(\boldsymbol{y}) \delta V(\boldsymbol{y}')} \right]^{-1} \frac{\delta F}{\delta V(\boldsymbol{y}')}. \tag{3.35}$$

Using the derivatives from Eqs. (3.22) and (3.23) gives

$$V^{i+1}(\boldsymbol{y}) = V^i(\boldsymbol{y}) + \beta \left[\beta^2 \mathrm{Cov} \left(\frac{\delta H(\boldsymbol{x})}{\delta V(\boldsymbol{y})}, \frac{\delta H(\boldsymbol{x})}{\delta V(\boldsymbol{y}')} \right) \right]^{-1} (\rho_V^{(2)}(\boldsymbol{y}) - \rho^{(2)}(\boldsymbol{y})), \tag{3.36}$$

which reduces exactly to (3.34) when the Hamiltonian (3.30) is used. The identification with Newton's method allows us to say something about the convergence properties of IMC: if the covariance matrix and the RDFs can be calculated exactly, the method converges quadratically, i.e., very fast, when we are sufficiently close to the actual solution [155]. However, much less is known of the behavior of Newton's method further away

from the solution, and in fact, the behavior can be quite erratic [155]. Nevertheless, the direction given by Newton's method is always an ascent direction for the functional F, i.e., if we take small enough steps in the direction given by IMC, F increases at every step, and eventually it will reach a maximum. Because F is convex, it is not possible to get stuck in a local maximum, and hence IMC should, in principle, always converge to the correct solution if the step size is kept sufficiently small. Additional consideration is required to study the effect of statistical inaccuracies in the derivatives; in this Thesis, only the practical aspects of minimizing their effect is discussed in 3.4.5.

IMC can be easily generalized to multiple pair interactions, because the form of the Hamiltonian [Eq. (3.30)] does not change. However, calculating the derivatives using Eq. (3.33) requires the knowledge of the four-particle density $\langle S_b S_c \rangle$ for all pairs of bins, and its calculation scales as $\mathcal{O}(N_b^2)$, where N_b is the total number of bins in all the potentials. This quickly becomes prohibitive and places some limits on the number of interactions that can be handled. The solution of the matrix equation (3.34) actually scales as $\mathcal{O}(N_b^3)$, but the cost is negligible compared to the MC simulation for all the cases studied in this Thesis, i.e., up to $N_b \approx 2000$.

3.4.2 Including Bonded Interactions

If the model contains *bonded interactions*, as the models constructed in Papers [II] and [III], the IMC equations need to be modified slightly. This is because a constant can be added to any bonded interaction without changing the RDFs at all. Because of this, the solution of Eq. (3.34) is no longer unique (the matrix A has a zero eigenvalue corresponding to an addition of such a constant). However, there is a simple solution: we can choose to add a constraint such that the changes of the bonded potential in different bins should sum to zero. The most straightforward implementation is simple: if $\boldsymbol{v}$ is a normalized eigenvector of A with a zero eigenvalue ($A\boldsymbol{v} = 0$, $\|\boldsymbol{v}\| = 1$), then the solution to the problem $\tilde{A}\boldsymbol{x} = \tilde{\boldsymbol{b}}$, $\tilde{A} = A + \boldsymbol{v}\boldsymbol{v}^T$, $\tilde{\boldsymbol{b}} = \boldsymbol{b} - (\boldsymbol{v} \cdot \boldsymbol{b})\boldsymbol{v}$ satisfies both $A\boldsymbol{x} = \boldsymbol{b}$ and $\boldsymbol{v} \cdot \boldsymbol{x} = 0$. For each bonded potential, there is such a vector $\boldsymbol{v}$ that correspond to the addition of a constant, and Eq. (3.34) is easily modified.

3.4.3 Including Discrete Degrees of Freedom

Let us now discuss the case that there are also *internal states* in the model, as in Paper [III] (see also the end of Section 3.3.1). The Hamiltonian (3.27) is linear in the new parameters E_k and E_{kl}; hence, we can include E_k and E_{kl} in the optimization through a calculation similar to Eq. (3.33). The set of target values now includes also $\langle n_k \rangle$ and $\langle \delta n_k \delta n_l \rangle$. Any value can be chosen for the n_k^{ave}, but setting it to the target $\langle n_k \rangle$ minimizes the magnitude of the derivative terms and improves stability.

Another possibility to determine the potentials is to optimize the RDFs and the parameters E_k and E_{kl} separately. In this approach, the target pair counts are calculated at each iteration from the target $g(r)$ by scaling with the number of particle pairs observed *during that iteration*. In contrast, in the full Newton-type approach, the target pair counts are calculated directly from the target $\rho^{(2)}(r)$, and remain the same for every iteration. After the potential change is determined, the E_k are adjusted using a linearization similar to (3.32) to counter any changes in $\langle n_k \rangle$ caused by the potential changes. The changes to E_k

and E_{kl} are then calculated using a separate equation that depends only on the expectation values and fluctuations of n_k (see Paper [III] for the equations and their derivation).

With the second approach, there are then several possibilities to treat the derivative matrix: (i) use (3.33) directly, (ii) make an *ad hoc* modification to factor out the structural part of the change (e.g., through the replacement $S_\alpha \rightarrow S_\alpha \langle N_\alpha \rangle / N_\alpha$, where N_α is the total number of particle pairs of type α), or (iii) calculate the derivative for $\langle S_b \rangle / \langle N_b \rangle$. All of the approaches have their disadvantages: (i) restricts the values of E_k near the initial values, (ii) cannot be easily justified theoretically, while (iii) leads to a non-symmetric matrix and to stability problems. An interested reader is referred to Paper [III] for more details.

Paper [III] discusses the potentials determined with the different approaches. The full Newton-type approach was shown to be the most accurate one for reproducing the two-particle densities. The potentials determined from the second approach using (ii) or (iii) also gave very similar results to those from the full Newton-type approach. However, none of these interactions worked well when the system size was increased from the one in which they were determined. Instead, the potentials resulted very inhomogeneous density distributions in larger systems. The only potentials that worked were those from the second approach using (i). They worked well if E_{kl} were set to zero, and also worked if E_{kl} was not restricted to zero as long as the value was not scaled when increasing the system size (see end of Section 3.3.1).

The main reason for the problems in generalizing to larger systems seemed to be negative values of E_{kl}: neither of the options discussed in the end of Section 3.3.1 work for this case, and in the larger systems $\langle n_k \rangle$ deviate significantly from those in the small system. When the values of E_k are restricted as is the case with (i), E_{kl} are positive, and no problems are encountered. However, this cannot be done with the full Newton-type approach: if the energy terms are not exactly right, the method tries to compensate for this by changing the long-range part of the potentials, which only works for a specific system size. Hence, although a workable set of interactions was determined, including the internal states in the iteration was found to be difficult. Studies on simpler model systems where sufficient sampling in the underlying MD simulations can be guaranteed should yield insight into the process.

3.4.4 Virial Pressure Constraint

In Paper [II], it was observed that unconstrained RDF inversion resulted in interactions that did not generalize to larger systems. The virial pressure [Eq. (3.10)] was identified as a good indicator for identifying such interactions: if the virial pressure is close to zero or negative in a small system, the interactions most likely do not generalize to a larger system. Hence, to solve the problem, we chose to implement a constraint in the IMC iteration such that the virial pressure is fixed to a given value. In general, the pressure defined by the virial equation (3.10) for the CG model is not the same as the pressure in the detailed model, because the effective interactions can be volume dependent [2, 102, 181]. Nevertheless, several authors have used the pressure of the original system as an additional target quantity for constructing the effective interactions to better reproduce the thermodynamics of the original system [80, 159]. Bolhuis *et al.* have also noted that minor changes in the potentials can have large effects on the thermodynamics, while the RDFs change only minimally [19, 20].

To implement the constraint, we need to replace Eq. (3.34) with a minimization problem, because the solution is unique. During each iteration, we now solve

$$\min_{\boldsymbol{x}} \|A\boldsymbol{x} - \boldsymbol{b}\| \tag{3.37}$$

with a constraint

$$\frac{1}{Vd}\sum_b r_b \left[\Delta f_b(\boldsymbol{x})\langle S_b\rangle + f_b\Delta\langle S_b\rangle\right] = \Delta P, \tag{3.38}$$

where ΔP is the deviation of the pressure from the desired value, and the left-hand side is a linearization of the virial equation (3.10). The second term in the sum can be evaluated directly using the target changes in the RDFs ($\boldsymbol{b}$), while the first term depends on the potential changes ($\boldsymbol{x}$) through the changes in the forces $\Delta f_b(\boldsymbol{x})$. The constraint (3.38) can easily be implemented using a Lagrange multiplier and makes it possible to fix the pressure within a few percents of the prescribed value, the main limitation being the accuracy of the linearization. In practice, quite a wide range of pressures can be set as the target without significant changes in the RDFs, showing that the RDFs are very insensitive to certain types of changes in the potential, in agreement with studies of Bolhuis *et al.* [19, 20]. However, if the pressure constraint is released, the IMC immediately results in changes in the potential such that some "intrinsic" pressure is favored. This shows that although the changes in the RDFs seem minor, they are still sufficient to tell apart the different potentials. This is in contrast to IB, in which the pressure converges slowly [85].

Because of the volume dependence of the effective interactions, the target pressure for the constraint cannot be set to be the same as in the atomistic simulation. Instead, other quantities need to be used to select the value. In Paper [II], we determined the proper value by qualitatively matching the area compressibility of the model with the experimental values. We also checked that qualitative conclusions do no depend on the exact value of the imposed surface tension. Paper [III] used the same pressure values to facilitate comparison.

3.4.5 Convergence and Regularization

If the difference to the target RDFs is large, the linear assumption (3.32) is not valid. In reality, the effect of a change is closer to exponential, which is the basis of the IB equation (3.28). Hence, IMC greatly underestimates the effect of the potential change, leading to instability of the iteration. Also, if there is too much noise, either in the derivative matrix A or in the RDFs ($\boldsymbol{b}$), this is transferred to the potentials, again destabilizing the iteration. To reduce such problems, different kinds of *regularization* techniques can be employed. This can help in improving the convergence and decreasing the computational time, because if the iteration tolerates more noise, shorter simulations can be used in sampling the RDFs and the four-particle densities required for (3.33).

If the linearization accuracy is a problem, it is possible to multiply $\boldsymbol{b}$ (or equivalently, $\boldsymbol{x}$ after the solution), with a regularization factor $r \in (0, 1)$ to stabilize the iteration at the cost of increasing the required number of steps [110]. For the noise, the simplest solution is to use local smoothing for the target and the computed RDFs, as well as for the changes in the potentials ($\boldsymbol{x}$), as is commonly done in IB [179]. However, this does not reduce noise in the derivative matrix.

The minimization formulation (3.37) allows more sophisticated regularization. In particular, the tolerance for noise in A and the RDFs can be improved by adding a penalty for potential changes that have large local fluctuations. This was implemented in Paper [II]. A typical regularization procedure for minimization problems is to add one or more terms of the form $a\|R\boldsymbol{x}\|^2$ to the function being minimized. Here, $a > 0$ is a regularization parameter and R is a regularization operator, chosen to penalize for certain types of solutions. To restrict local fluctuations, a convenient choice for R is the numerical second derivative operator. It is also possible to use a diagonal matrix to restrict the magnitude of the potential changes.

The best values for the regularization parameters r and a, as well as the form of R, can be selected by trial and error, and they can also be changed during the iteration. Although this adds some manual labor to the construction of the potentials, it can speed up the calculation considerably. This is because with proper regularization, even a short MC run is enough to see the differences in the RDFs on a general level in the initial stages of the iteration, and better sampling is only needed when the RDFs are close to the target ones.

The main disadvantage of introducing regularization is that it may distort the solution. However, this risk can be minimized by making the regularization weaker towards the end of the iteration, and also by selecting regularization terms that only penalize for certain changes, not for certain types of potentials.

3.4.6 Choice of Initial Potentials

The choice of the initial potential can also have a significant effect on the speed of convergence and stability of the IMC iteration. The most common choice is to use the potential of mean force $V(r) = -k_{\mathrm{B}}T \ln g(r)$, but since it is an approximation, it may result in a system whose RDFs are quite far from the target ones. Although strong enough regularization usually allows one to keep the iteration stable until one gets close enough to the target RDFs, this can be a cumbersome and time-consuming process. The problems become more apparent for multicomponent systems: if the modification of the potential at some step results in a phase separation of the system, the changes in the RDFs can be very large, and the iteration becomes unstable. Similar problems can occur in systems with internal states if one state suddenly becomes more favorable as a result of a slightly incorrect change in the potential. Such incorrect potentials are more likely to occur during the iteration if the initial potential is far off the target.

One possible approach for obtaining better initial potentials is to use potentials from a similar problem that is easier to solve. This approach was used by Elezgaray and Laguerre [43]: they first optimized the potentials based on simulations of different pairs of molecular fragments in water, and used these as the initial potentials when matching the structure of a lipid bilayer simulation. A similar approach was also used in Paper [III], where the interactions were first determined without the internal states.

It is also possible to use interactions obtained with another technique as the initial potentials for the iterative inversion. The other technique should then be computationally light and provide a better estimate than the potential of mean force. Possibilities include integral equation approaches discussed in 3.3.2, as well as other systematic approaches such as force matching (see next section). In addition to reducing the labor and the computational time required for the inversion, such an approach can also give insight into the differences of different coarse-graining approaches.

3.5 Other Approaches

Inversion of the RDFs is a popular approach for constructing effective interactions, but it is by no means the only one. Putting differences in the computational complexity of different approaches aside, even in light of the issue of representability there is no single approach that is optimal in all situations. Instead, different approaches can complement each other and give additional insight into the problem.

One rigorous approach is to match the forces, i.e., derivative of Eq. (3.16) with respect to $\boldsymbol{q}$, between the models at different levels. This *force matching* (FM) approach was first proposed by Ercolessi and Adams [44], and has been recently developed further by Izvekov and Voth [80, 83]. The central idea of the approach is to represent the potentials as splines and perform a least-squares fit to the forces computed from the atomistic level [83]. To obtain better thermodynamic properties, the virial of the system can be included into the least-squares fit [80]. The advantage of this approach over RDF-based techniques is that it is computationally inexpensive once the atomic-scale configurations and forces are available: only a linear least-squares problem needs to be constructed and solved. The approach has been applied to various systems: constructing simple water models from more detailed ones [78, 83], modeling of lipid bilayers [79, 81] and monosaccharides [101], protein folding [185, 203], and also a mixed resolution model with an atomistic membrane protein and a CG lipid bilayer [174]. An approach where the model resolution is not decreased, but the interactions are simplified, has also been proposed [84], and applied to obtain effective short-range electrostatic interactions for water and water solutions.

Noid *et al.* have also analyzed the FM approach theoretically [140, 141]. Perhaps the most interesting result is that for a homogeneous and isotropic system, the effective pairwise potential given by the FM method actually solves the YBG equation (3.8) with the two- and three-particle densities of the detailed model [140]. In general, a pairwise interaction cannot reproduce both the two- and three-particle densities; hence, the FM approach gives an estimate that in some sense incorporates both the two- and three-particle correlations, but neither of them exactly.

Toth has proposed a *potential matching* method that is similar in spirit to the FM method, with the difference that the total potential of each configuration is taken as the target for the least-squares fit [188]. This approach cannot be directly justified as an approximation method for H_{eff}, because the CG Hamiltonian is a free energy and should also contain entropic contributions, and thus its value should not equal the microscopic energy. Nevertheless, comparison of this approach with other possibilities could possibly be used to estimate the enthalpic and entropic contributions to H_{eff}, improving the transferability to different temperatures.

Several different *semi-atomistic CG models* for lipid systems have been reported in the literature. Although a few of these have been derived from atomistic simulations using RDF inversion [43, 111] or FM [79, 81], they have not been widely applied. Models whose parameters have been derived similarly to atomistic force fields by fitting to experimental quantities have been more popular. The most popular of these is the MARTINI model [116, 117, 125], which has been parameterized through densities and partition coefficients between different solvents. A major factor in boosting the applications of the model is its free availability and compatibility with the GROMACS MD software, and the model has been applied to a wide variety of problems including large-scale dynamics

and phase behavior of lipid systems (see Ref. [118] for a review) and membrane proteins [28, 152, 191, 201]. Models derived from the MARTINI model have also been applied to protein modeling [22, 175]. A more detailed model has been derived by Orsi *et al.* [146], and their model can reproduce several features of atomistic simulations quantitatively. Finally, in a somewhat earlier work, Klein and co-workers have combined the semi-empirical parameters with RDF inversion used for some interactions, and applied this model to several problems [137, 170, 171].

Some researchers have also constructed even simpler models, which abandon the chemical details and focus on general behavior. Several studies within the framework of dissipative particle dynamics [13, 61] (see next section) fall into this category. Many solvent-free descriptions also fall into this category [24, 35], as their goal is often to study the behavior of elastic sheets that possibly also include some hydrophilic and hydrophobic regions. For details and applications of both approaches, see, e.g., Ref. [132] and references therein.

It is also possible to abandon the particle description completely, and describe the system using *field-theoretical models*. Also here, the parameters can be fitted to data from atomistic simulations. Shi and Voth have applied this approach to model phase separation in DPPC/DPPE mixtures [173], while Pandit and co-workers have focused on modeling the effect of cholesterol in membranes [93, 147, 148, 149]. Both these models used a 2D field description for the local order, but Pandit and co-workers still used a particle-based description for cholesterol. Ayton *et al.* have constructed models where the elasticity of the membrane is described using continuum models [10], and the description has been coupled to the local composition [9] and atomistic simulations [8].

3.6 Dynamics

So far, the focus has been on the static properties of CG models. Although this Thesis focuses solely on static properties, let us now briefly discuss CG dynamics for completeness.

In principle, the Mori-Zwanzig projection operator formalism [126, 204] provides a framework for rigorously treating the dynamics in a similar way to the static properties. In general, it is very difficult to evaluate the dissipative and fluctuating terms resulting from application of the formalism, which can depend on all the degrees of freedom. In the limiting case of weak coupling between the different sets of variables, the equations reduce to the Langevin equation [1]

$$m\dot{\boldsymbol{v}}_i = \boldsymbol{F}(\boldsymbol{q}) - \eta m_i \boldsymbol{v}_i + \boldsymbol{F}^r(t), \tag{3.39}$$

where $\boldsymbol{F}(\boldsymbol{q})$ is the force from the conservative potentials, η is a friction coefficient and $\boldsymbol{F}^r(t)$ is a Gaussian random force that has the properties

$$\langle \boldsymbol{F}^r(t) \rangle = 0, \tag{3.40}$$

$$\langle F_i^r(t) F_j^r(t') \rangle = 2mkT\eta\delta_{ij}\delta(t-t'). \tag{3.41}$$

In the second equation, the factor $2mkT\eta$ ensures that the system samples conformations from temperature T [183], i.e., that the energy lost in the dissipative process is put back in through the random forces. Since this value couples the magnitude of the fluctuating

force $\boldsymbol{F}^r$ to the strength of dissipation η, it is known as a fluctuation-dissipation theorem. The equations of different particles couple only through the conservative forces, and can easily be solved numerically [47]. The dissipative and random forces can be thought of as friction and thermal motion caused by the degrees of freedom that have been integrated out.

Although relatively simple to solve, the Langevin equation has a major shortcoming in describing large systems over long time scales: each particle experiences dissipative and random forces independently from all other particles, and hence momentum is not conserved. Because of this, hydrodynamics is not properly described [40].

A method similar in spirit to Langevin equation but with local momentum conservation can be devised by making the dissipative and random forces act on each pair of particles. This leads to so-called dissipative particle dynamics [48, 49, 61], where the equations of motion are of the form

$$m\dot{\boldsymbol{v}}_i = \boldsymbol{F}(\boldsymbol{q}) - \sum_j \omega_D(r_{ij})(\boldsymbol{v}_{ij} \cdot \boldsymbol{e}_{ij})\boldsymbol{e}_{ij} + \sum_j \omega_R(r_{ij})\xi_{ij}\boldsymbol{e}_{ij}, \tag{3.42}$$

where ξ_{ij} are symmetric Gaussian random variables with zero mean and unit variance, and r_{ij}, $\boldsymbol{v}_{ij}$ and $\boldsymbol{e}_{ij}$ are the distance, relative velocity, and unit vector between particles i and j. The functions $\omega_D(r)$ and $\omega_R(r)$ describe the magnitude of the dissipation and random forces as a function of the pairwise distance, and they should satisfy the fluctuation-dissipation relation

$$2kT\omega_D(r) = [\omega_R(r)]^2 \tag{3.43}$$

in order to reproduce the correct ensemble [48].

The parameter η in Eq. (3.39) and the functions ω in (3.42) can also be obtained systematically from atomistic simulation data by fitting to correlation functions [45, 46, 82, 121]. This allows more accurate modeling of dynamic phenomena, although it can also slow down the sampling of the positional degrees of freedom (see below). Also, in schemes where multiple resolutions are included in a single simulation, it is important to have the same dynamic behavior in both resolutions to avoid complications in the interface region [91, 156, 157, 158], at least if accurate dynamics are of interest.

In practice, one often uses ordinary MD, i.e., Newton's equations, for moderately coarse-grained models such as the MARTINI model [116, 117]. This way, it is possible to take advantage of the efficient software developed for MD simulations, and it also reduces the number of parameters in the model. The philosophy of such models is then to focus on time scales that are much longer than the microscopic timescales that are integrated out in the coarse-graining process. It is reasonable to assume that the relative timescales of different events are qualitatively correct at long enough time scales, because they are mainly determined by energy barriers. The speedup gained by neglecting the dissipative forces also improves the sampling of the positional degrees of freedom.

For heavily coarse-grained models, such as those in Papers [I]–[III], it is very difficult to obtain meaningful equations of motion. We have experimented with the Langevin and generalized Langevin equations for these systems with the effective interactions from IMC, but these approaches turned out to be too approximate to obtain meaningful dynamics. For this reason, the main use of such models is in the study of static properties.

Chapter 4

Modeling of Phospholipid / Cholesterol Mixtures

4.1 Motivation

Mixtures of cholesterol with different lipids are widely studied as a model system for cellular membranes [54]. Already two-component mixtures show interesting and non-trivial phase behavior, and DPPC/cholesterol mixtures is one of the most widely studied of these (see Chapter 1). The length and time scales required to study the phase behavior of such systems are beyond the reach of atom-scale simulations, although the MARTINI model has been recently used to study phase separation in ternary mixtures at near-atomic resolution [160]. However, the microscopic interactions ultimately determine the phase behavior, making it conceivable that a systematically constructed CG model, based on the atom-scale data, could be used to study the phase behavior. Simple phenomenological models have also been successful in explaining the phase behavior of single-component phospholipid membranes [39, 128, 134, 154] as well as phospholipid/cholesterol mixtures [76, 123, 135, 136].

This chapter discusses the CG models constructed in Papers [I]–[III] for bilayers composed of DPPC and cholesterol, as well as atomic scale analysis motivated by the findings (Paper [IV]). The CG models are similar in spirit to the phenomenological models mentioned above, but now constructed systematically using the IMC method (Section 3.4). Hence, one purpose was to investigate how well can parameters for such models be obtained from atomistic simulations. Also, the level of coarse-graining is very high, making it possible to study the limits of the employed CG approach.

The different CG models are briefly reviewed in Section 4.2, and the construction of the model is discussed in Section 4.3, together with associated problems. Results from large-scale simulations using the models are then discussed in Section 4.4. Finally, large-scale atomistic MD simulation results from Paper [IV] are discussed in Section 4.5, confirming an unexpected behavior seen in the CG model for pure DPPC.

4.2 Overview of Different Models

All the three models in Papers [I]–[III] were constructed using the same principles, varying only in the level of detail. A schematic description of the models is shown in Fig. 4.1.

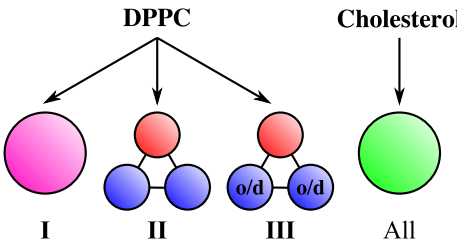

Figure 4.1: CG scheme in Papers [I]–[III] (see text for details). The particles describe the 2D COM positions of a set of atoms in the plane of the bilayer. Cholesterol is always described by a single particle, and one or three particles are used for DPPC. Paper [III] adds an internal degree of freedom to the tail particles: o=ordered, d=disordered.

All the models describe a single monolayer of the bilayer as a flat two-dimensional fluid. Hence, membrane undulations and interactions between the monolayers are neglected, although the latter are implicitly included in the effective interactions. Also, we assume that the lateral structure can be adequately described by just a few particles per molecule interacting through isotropic pair interactions. The particles represent the center-of-mass (COM) positions of (parts of) the molecules. The effective interactions were determined through inversion of the RDFs using the IMC method, creating a model that accurately reproduces the structure of the atomistic MD simulations. The underlying simulations were performed in several different cholesterol concentrations (0, 5, 13, 20, 30, and 50 mole-% of cholesterol) [51], and separate interactions were determined for each concentration. The 50% concentration was studied only in Paper [I], where it phase separated.

Paper [I] started with the simplest possible model: each molecule was described by a single particle. Hence, there were two types of particles (DPPC and cholesterol) and three different pair interactions.

Paper [II] added a more detailed description of the molecular structure of DPPC: each DPPC was described by three particles instead of one, one for the headgroup and one for each tail. This development added bonded interactions to the model; each pair of particles within the same molecule was connected together by a bond potential, which was parameterized using IMC. In total, the model contained seven non-bonded interactions (head–head, head–tail1, head–tail2, head–chol, tail–tail, tail–chol, chol–chol) and three bonded ones. The interactions within the hydrophobic region of the membrane, i.e., tail–tail and tail–chol pairs, were treated with a single potential each, although the two tails of DPPC are not completely equivalent in terms of molecular structure.

Finally, Paper [III] added ordering of the chains to the models. In the spirit of the models by Nielsen *et al.* [134, 135], each tail had an internal degree of freedom with two possible states: ordered and disordered. The pair interactions then need to be complemented with internal energy terms to ensure that the RDFs (and state occurrence probabilities) can be reproduced (see Section 3.3). There are two of these terms, and the coefficients were denoted as ΔE and E_{fluct}. The bonded interactions were treated as in Paper [II]. When considering models with non-zero E_{fluct}, non-bonded interactions were also calculated between bonded pairs, i.e., no exclusions were used. The remaining contributions to the bonded interactions were assumed to be independent of the internal states. In total, the models contained ten non-bonded interactions, three bonded interactions, and two internal energy terms.

To calculate the RDFs for the last model, it is necessary to have a definition for when an atomistic tail is ordered and when it is not. For this purpose, we have used the S_{zz} order parameter, which is a commonly used measure for lipid chain order. It is also closely related to deuterium order parameters [168], which can be measured using NMR.

Here, we used the following definition: if S_{zz} for a chain conformation was larger than 0.6, it was treated as ordered. We defined S_{zz} for a chain as an average over all the carbons:

$$S_{zz} = \frac{1}{N_c - 2} \sum_{i=2}^{N_c - 1} \left(\frac{3}{2} \langle \cos^2 \theta_i \rangle - \frac{1}{2} \right). \tag{4.1}$$

Here, $N_c = 16$ is the number of carbons in the tail and θ_i is the orientation of the tail with respect to the membrane normal at the i'th carbon. The cutoff value 0.6 was essentially an arbitrary choice, limited by practical considerations (see Paper [III]).

4.3 Model Construction

The process of model construction is the same for all the models: (i) The target two-particle densities are calculated from the MD simulations, as are the areas per molecule. (ii) The target RDFs are smoothed using a spline-fitting algorithm [182] to remove noise. (iii) IMC iteration is carried out to invert the RDFs, using the PMF as the initial guess. (iv) The potentials are smoothed using the same spline-fitting algorithm together with power-law fits in regions where the target RDFs are zero. (v) It is checked that the system behaves reasonably also in a larger system.

In Paper [I], the above procedure worked well without any modifications to the original IMC algorithm. The resulting set of interactions is shown in Fig. 4.2.

In Paper [II], problems were seen in step (v) with a basic IMC algorithm. This led to the implementation of the constraint for the virial pressure discussed in detail in Section 3.4.4. With the virial pressure constrained, the model generalized well to a larger system in all concentrations. The final set of interactions is shown in Fig. 4.3. We also observed that the exact value of the virial pressure does not have any major effect on the RDFs or the qualitative behavior, as long as it is within reasonable limits.

Several problems were encountered in Paper [III], both in steps (iii) and (v). First, the initial stages of the iteration were very unstable when the PMF was used as the initial potential. This was cured by first optimizing the potentials without the internal states, i.e., treating the states as identical, and using the obtained potentials as the initial guess for further optimization. Also, the virial pressure again got negative values without a constraint, and hence the same constraints were applied as in Paper [II]. Next, different implementations of IMC were compared (see Section 3.4.3), and seen to produce very different interactions, in particular in higher cholesterol concentrations. Further, several of these

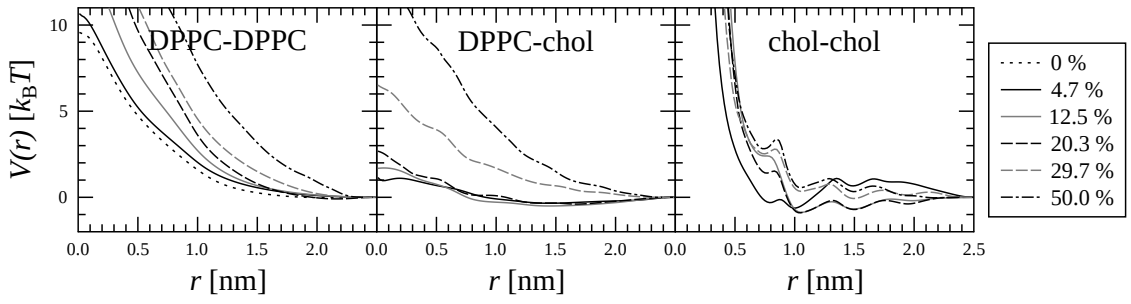

Figure 4.2: Effective pairwise interactions from [I]. Adapted from [I].

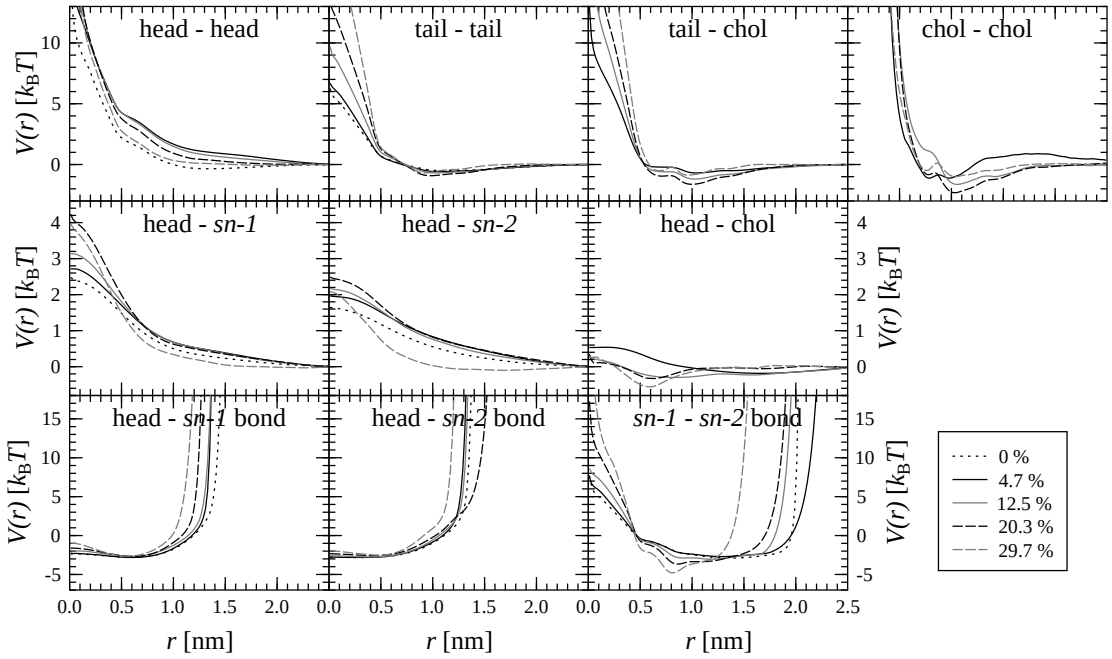

Figure 4.3: Effective pairwise interactions from [II]. Reproduced from [II].

interactions did not generalize to larger systems than in which they were determined. It proved difficult to construct a set of potentials that would be consistently determined over all the concentrations while still generalizing to larger systems and reproducing the RDFs as well as possible. It was speculated that insufficient sampling in the underlying simulations might be the cause for these problems. In the end, the last requirement (RDF reproduction) was slightly relaxed, and one set of potentials was chosen for studies of large-scale behavior. This set of interactions is shown in Fig. 4.4.

When comparing the interactions between the models, we observe that the strength of the interactions and the level of detail are similar, although at higher cholesterol concentrations the interactions in [I] seem to have a slightly longer range. For the more detailed models, many of the interactions in the tail region acquire a small hard-core region. This demonstrates a general feature of coarse-grained potentials [94]: with decreasing level of detail, they become softer, because it is often possible to have the COM positions overlap without any overlap of the underlying particles. Similarly, the concentration dependence becomes weaker when the level of detail is increased from [I] to [II]. Interestingly, this does not happen when tail ordering is included in [III], contrary to *a priori* expectations. Also, the concentration dependence in the cholesterol–cholesterol interactions, the only one for which direct comparison is possible, seems very similar in all the models.

4.4 Simulations with Coarse-Grained Models

This section summarizes the behavior of the constructed CG models at large length scales. The linear sizes of the studied systems for the CG simulations were larger than the atomistic simulations by a factor 24 (Paper [I]) or 16 (other models). For transferability studies, systems with the size halved were used, because qualitative trends could be seen there as

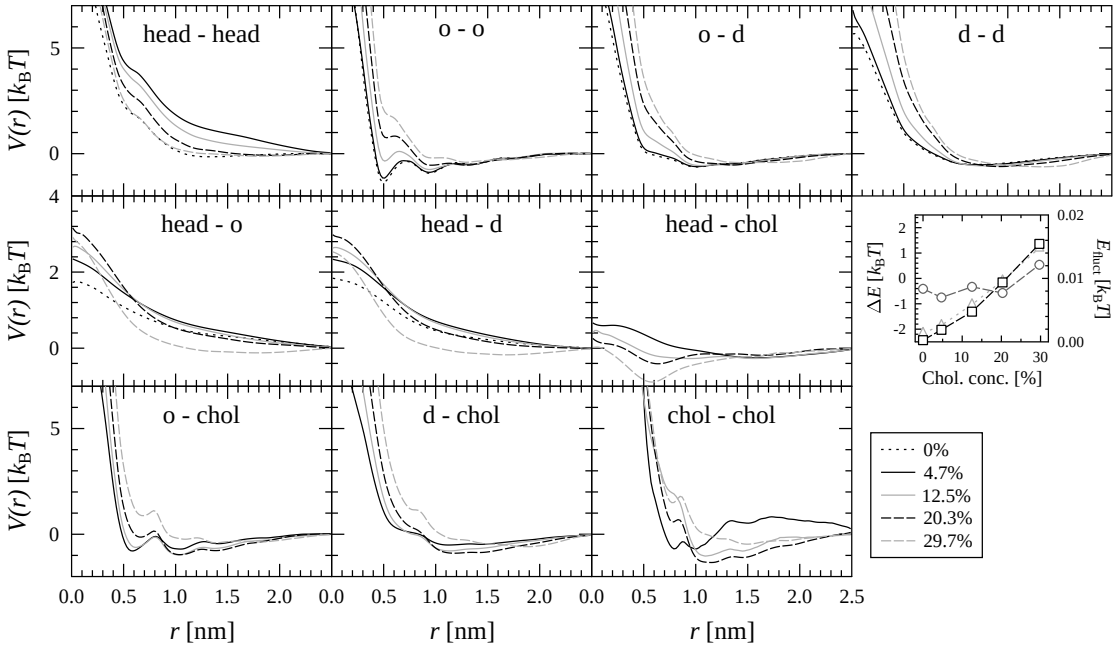

Figure 4.4: Effective pairwise interactions from [III]. Ordered and disordered tails are marked with *o* and *d*, respectively. The small figure shows the energy difference between the ordered and disordered states (ΔE, squares) and the magnitude of the fluctuation energy term (E_{fluct}, circles). The triangles show the internal energy values $\Delta E = k_{\text{B}}T \ln(\langle n_o \rangle / \langle n_d \rangle)$, which were used as like a constraint in the IMC iteration. Bonded interactions are not shown for brevity. Reproduced from [III].

well. For Paper [III], only a representative set of interactions that generalized well to a larger system are discussed (other interactions that did generalize gave similar results).

In Paper [I], the sampling efficiency of the simplest model was estimated some 10^8 times faster than the atomistic simulation; the increase in the number of particles and in the particle density makes the more complex models approximately 10 times slower. Reasonable statistics for the CG models, good enough for qualitative conclusions, could be obtained within a few days on a desktop computer.

The main results are shown in Fig. 4.5, which contains the total static structure factors for all the models at all the cholesterol concentrations. The following sections focus on different aspects of the results, and discuss the reasons for the observed behavior.

4.4.1 Organization of Cholesterol

The large-scale ($k \to 0$) behavior is similar in all three models: the system is inhomogeneous at 13% and 20% concentrations, but homogeneous for the others (see, however, the next section). Analysis of partial structure factors showed that in all cases, the main source of the inhomogeneity is in cholesterol density variations, with the other structure factors magnifying this effect in [II] and [III]. This is in qualitative agreement with the experimentally observed coexistence region at these concentrations. More detailed studies, e.g., on the phase behavior of the CG models, is not possible because of transferability problems (see Section 4.4.3). Nevertheless, the fact that all the models give similar results

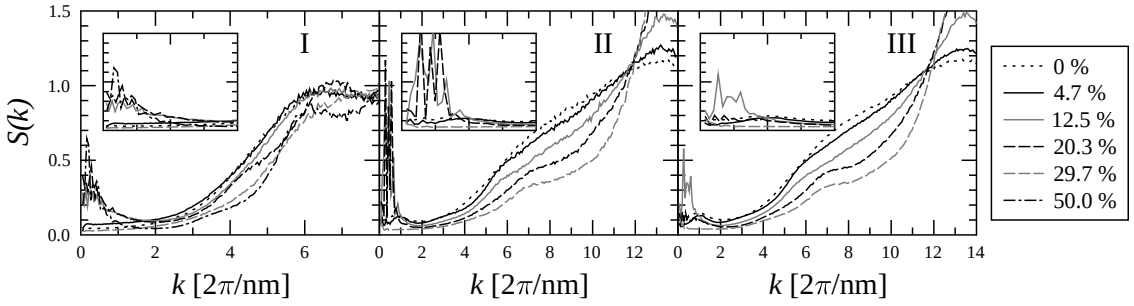

Figure 4.5: Total static structure factors calculated from different models at different cholesterol concentrations. The insets show the region $k < 2\,\mathrm{nm}^{-1}$ magnified. Left and right panels adapted from [I] and [III], respectively.

strongly suggests that the atomistic force field might also give similar results if it could be applied to a large enough system for a long enough time.

The strength of the separation varies quite strongly between the different models: including the tails separately enhances the effect strongly, but in [I] and [III] the effect has comparable strength. In fact, the effect is only very weakly visible in the 20% case in [III]. A possible explanation for these non-monotonic effects would be that since the effect of cholesterol is strongest on the individual chains, including the individual chains enhances the separation. When tail ordering is also included, the tails can better adapt to the changes in local cholesterol concentration, making the global density variation less pronounced. Finally, we note that the concentration dependence of the cholesterol–cholesterol interactions are quite similar in all the models. It is then possible that the main source of the density variation is in these interactions, and the other interactions may only play a minor role.

4.4.2 Tail Density Fluctuations

For the model in [II], the 0% and 5% cholesterol concentrations showed a small unexpected peak in the structure factor around $k \approx 1\,\mathrm{nm}^{-1}$ that stemmed purely from the tail–tail structure factor. The presence of such an inhomogeneity can be treated as an prediction of the CG model, which was confirmed from large-scale atomistic simulations in Paper [IV] (see Section 4.5). Later, similar behavior was also seen in [III], where the peak was shown to arise from segregation of ordered and disordered tails. Model [III] showed similar segregation also in higher cholesterol concentrations. However, at 13% and 20% the effect was masked by the cholesterol inhomogeneity, while at 30% the global density remained homogeneous.

Interestingly, no indication of density variation in the pure DPPC system was seen in the one-particle model in [I]. Hence, it seems that the behavior of individual tails is important for this phenomenon. This also demonstrates the profound effect that the choice of the degrees of freedom can have on a CG model.

4.4.3 Transferability and Other Issues

For each model, we also studied the transferability between the different concentrations. The results were similar for the two first models without the ordering [I, II]: qualitative

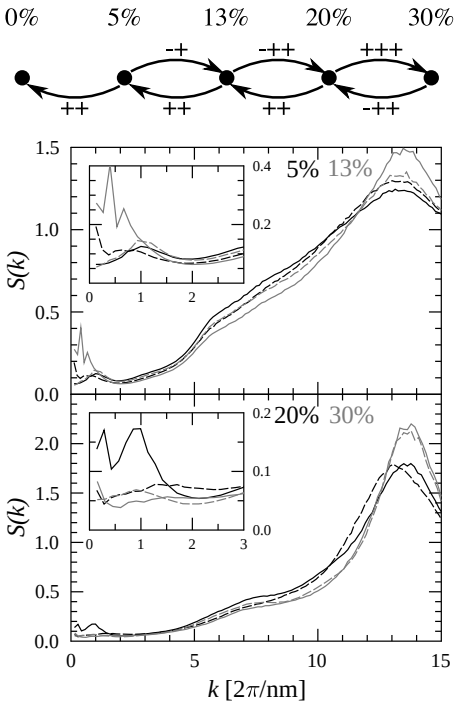

Figure 4.6: Potential transferability in [III]. The top diagram summarizes the transferability between different concentrations: the first +/- stands for (qualitative) reproduction of small k behavior of $S(k)$, the second + for qualitative reproduction of the nearest-neighbor peak in $S(k)$, and the possible third + for quantitatively nearly correct $S(k)$ away from the small k region. The figures at bottom show the transferability between two pairs of adjacent concentrations. The solid lines show the correct $S(k)$, and the dashed line the $S(k)$ given by the transferred interactions. The color of the lines shows the simulation concentration. The upper figure is also representative for the transferability in the simpler models away from the small k region. Reproduced from [III].

changes are often correct, but the magnitudes are much smaller than they should be. The cholesterol inhomogeneity seems to be determined mainly by the interactions and not the concentration: potentials determined at 13% and 20% give domains also in the nearby concentrations that should be homogeneous, while the potentials derived at homogeneous conditions fail to give domains at any concentration. For the model with ordering [III], the transferability is better, but still not perfect. The results for this case are shown in Fig. 4.6. The changes in the structure factors are also quantitatively correct for some concentrations, in particular for the nearest-neighbor peak around $k \approx 14\,\mathrm{nm}^{-1}$. Also, the potentials derived in the inhomogeneous regions now result in (nearly) homogeneous systems at the 5% and 30% concentrations, in agreement with the potentials determined in these concentrations. However, the reverse direction still fails.

Paper [II] also studied the effect of the potential cutoff on the behavior of the model for the pure DPPC system. It was shown that the quantitative $S(k)$ depends quite strongly on the cutoff in the small k region. This observation, combined with the uncertainties in selecting the best interaction in terms of the virial pressure [II] and the internal energies [III], makes it difficult to make any quantitative predictions with the CG models. This is the reason why this avenue has not been pursued in these studies. Nevertheless, the qualitative behavior seems quite robust to the above differences.

4.5 Atomistic Simulations

The strong tail density fluctuations seen in Paper [II] were somewhat surprising, and we proceeded to verify the behavior through atomistic simulations. These simulations are reported in Paper [IV]. Briefly, we performed a 40 ns simulation containing 1152 DPPC molecules. The system was three times in linear size compared to the original 128 molecule simulation used for the CG model. This should be large enough to verify or

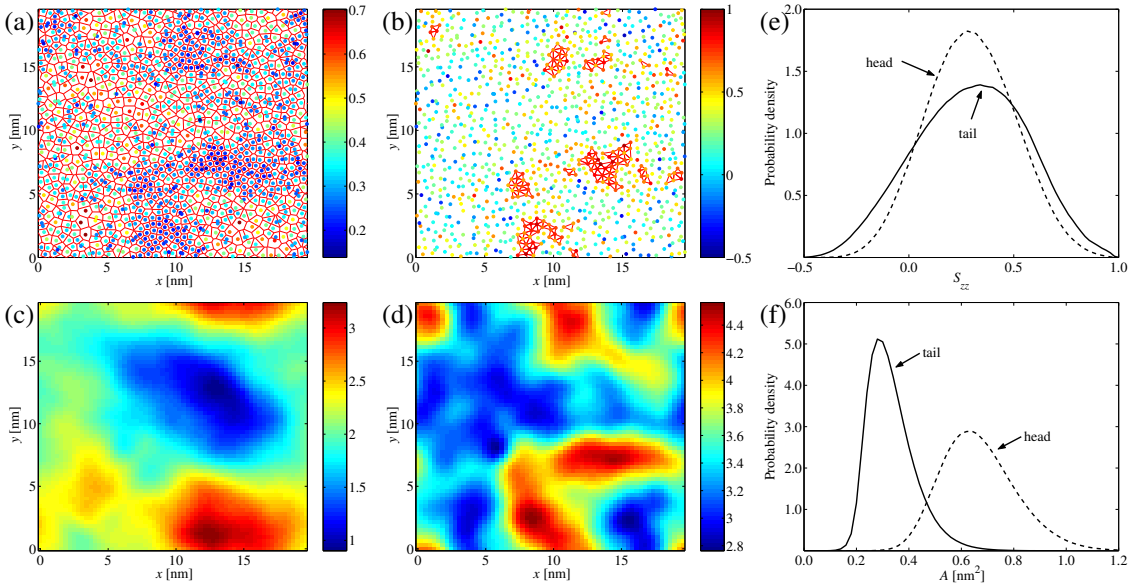

Figure 4.7: Different visualizations of a single configuration of a 1152 molecule lipid bilayer (a)–(d) together with probability distributions of tail order parameters (e) and area per lipid/tail (f). Panel (a) shows the area per tail in a monolayer. Panel (b) has the instantaneous S_{zz} values for each tail in the same monolayer. Panels (c) and (d) show the undulations and the membrane thickness, respectively. Panels (e) and (f) show the probability distributions of the S_{zz} values and the areas, calculated over the whole trajectory. The headgroup S_{zz} was defined as the average of the tails. Reproduced from [IV].

falsify the presence of such domains. However, timescale is too short to obtain accurate values for, e.g., sizes of the domains, but qualitative conclusions are possible.

The main result of Paper [IV] is that such density fluctuations do exist in the atomistic model as well. Most important results are summarized in Fig. 4.7. The figure shows snapshots from a single configuration, and the density fluctuations are clearly visible in Fig. 4.7(a). Panels (b) and (d) indicate that clusters of highly ordered chains can be present within the denser regions, and that the thickness of the bilayer is strongly correlated with the density. In contrast, membrane undulations [panel (c)] do not seem to be correlated with the density, ruling out the possibility that the 2D projection would be the cause of the density differences. Quantitative analysis of the correlations between the quantities confirmed these conclusions. It was also observed that the density fluctuations are long-lived, but the domains of high chain order had much shorter life times. These results agree with the newest CG model in Paper [III], where the main source for the density fluctuations in pure DPPC is seen to be the segregation of ordered and disordered tails. The fact that the area and order parameter distributions are single-peaked [Fig. 4.7, panels (e) and (f)] indicates that the observed domains result more likely from fluctuations than actual phase separation. However, more extensive studies would be needed, in particular at different temperatures, to address this question in detail. It might also be possible to address these issues with the MARTINI model, also in the presence of cholesterol, as demonstrated in Ref. [160] for a ternary mixture.

Chapter 5

Conformational Analysis using Self-Organizing Maps

5.1 Motivation

This chapter is based on Paper [V] and discusses the application of *self-organizing maps* (SOMs) to analysis of data produced by atomistic MD simulations, as well as possible uses of the obtained information in choosing CG degrees of freedom. Paper [V] considers the analysis of the large amounts of data produced by atomistic MD simulations: even a relatively small simulation of a lipid bilayer results in tens of thousands of snapshots of the system, each containing tens or hundreds of molecules of interest. Direct analysis of such amounts of data is impossible; instead, one has to calculate average properties of the system and interpret them. For a lipid bilayer, it is standard practice to calculate electron densities, chain order parameters, etc. [186], but such properties only give information on the global properties of the system. If molecular origin of the properties is sought based on this data, one has to resort to hypotheses based on the global properties and then proceed to verify or falsify them.

Another possible approach is to try to analyze the conformations directly, and try to link different types of conformations to the observed macroscopic behavior. To find out typical conformations occurring in the trajectory, *clustering* methods can be used [63]. The basic idea is to group the conformations into *clusters* such that conformations within one cluster are similar to each other and dissimilar to conformations in other clusters. This reduces the number of conformations to a level manageable for even visual analysis.

Clustering methods have not been very often used in analysis of lipids; this is one of the motivations for Paper [V]. Instead of "traditional" clustering methods, we decided to apply the SOM method because of several reasons. First, preliminary studies by Hyvönen *et al.* have shown promise for the method [75], but otherwise, SOM has mostly been applied to analysis on a coarser level than individual conformations. Second, SOMs are powerful in visualizing the relationships between the obtained clusters, facilitating rapid visual analysis of the results. Finally, SOMs require very little *a priori* knowledge on the system; for example, the exact number of desired clusters is not needed, in contrast to many other clustering methods.

The work on SOMs can also be loosely coupled to the coarse-graining work in other parts of the Thesis. As discussed in Section 3.2, the degrees of freedom selected for a

CG model can have a large impact on the descriptive power of the model. In principle, a systematic approach for selecting these degrees of freedom could be based on clustering approaches: in order to capture the most important features of the system, the CG model should produce conformations that are similar to those in the more detailed model. Hence, if a cluster analysis is carried out for the detailed model, a CG model can then be verified against these clusters. Knowledge from the cluster analysis could also be used for constructing the CG model and/or refining it such that it would produce the clusters with sufficient accuracy. It is also possible to provide free energy estimates based on clustering information [63], which could be used for more quantitative comparison of the models at different levels. Although this idea is currently only on a conceptual level, and has not been implemented in practice, it provides an interesting direction for future research.

A few different approaches have been proposed in the literature for selecting the CG degrees of freedom. Gohlke and Thorpe have proposed a method for identifying rigid domains in large molecules [59], the idea being that they could be treated as rigid bodies during the simulation. Arkhipov *et al.* have constructed locations for CG beads using topology-preserving maps to preserve the general shape of large molecules, and used these to simulate viral capsids [7] and a bacterial flagellum [6]. Both of these methods are based on a single configuration and do not take advantage of dynamical information that is also often available through simulations. Recently, algorithms that use the dynamics have also been developed. Gfeller and Rios have proposed an algorithm for simplifying coupled networks of oscillators while preserving the dynamics of the network [58], while Zhang *et al.* have developed a method that selects the CG positions based on the normal modes (or essential dynamics) of a molecule [202]. SOM, and clustering methods in general, are most similar to the approach by Zhang *et al.* However, the focus is on different kinds of motion: while the method of Zhang *et al.* is useful in studying slow, large-scale motions of big molecules, clustering analysis are perhaps better suited for studies of smaller molecules that have several distinct conformations.

5.2 Self-Organizing Maps

An SOM can be thought of as a non-linear mapping from a high-dimensional input space into a discrete low-dimensional output space such that two points close in the input space are mapped to the same or nearby points in the output space [96]. Because the output space typically has much fewer points than there are input points, the SOM also produces an abstraction of the data, where each point in the output space represents a typical input data point. The output space is typically one- or two-dimensional, which facilitates easy visualization of the results.

The crucial step in constructing an SOM for a set of data is the *training* of the map with the input data. In the process of training, the map "learns" to represent the input data better and better. Before discussing the training algorithm, it is useful to form an intuitive picture of how the training works. Imagine a 2D elastic sheet that lies in the high-dimensional input space, and that each input data point attracts the nearest point on the sheet. Initially the sheet is stiff and hence nearly flat. The tension is then slowly relaxed, allowing the sheet to adapt to the distribution of the data points. After the representation is good enough, the sheet is fixed, and the deformed sheet is mapped back to a 2D plane. Each input data point can then be mapped to the 2D plane by finding the nearest point on

the sheet.

Let us now formulate the SOM algorithm more quantitatively. Let d be the dimension of the map (typically one or two) and let n be the dimension of the input data vectors. Each input data vector is represented by an $\boldsymbol{x}_j \in \mathbb{R}^n$. Now, an SOM consists of a d-dimensional lattice of M *neurons*, located at points $\boldsymbol{r}_i \in \mathbb{R}^d$. With each neuron, there is also an associated model vector $\boldsymbol{m}_i \in \mathbb{R}^n$ which resides in the input space. The positions $\boldsymbol{r}_i$ are fixed, but $\boldsymbol{m}_i$ are changed during the training (see below) such that the map represents the input data. At any point during or after the training, each data vector can be mapped onto the neuron whose model vector $\boldsymbol{m}_i$ is most similar to $\boldsymbol{x}_j$. This neuron is called the *best-matching unit* (BMU) for the data vector $\boldsymbol{x}_j$. Hence, each data vector can be mapped to the position $\boldsymbol{r}_i$ of its BMU in the output space.

To train the SOM with a set of data, we first initialize the model vectors $\boldsymbol{m}_i$. This is typically done by aligning the d-dimensional lattice with the d principal components of the data, i.e., along the d-dimensional hyperplane spanned by the eigenvectors corresponding to the d largest eigenvalues of the data covariance matrix [96]. After initialization, we randomly select data points, and for each data point, we find the BMU, and then modify the map such that the BMU is more similar to the data point. The important feature of the SOM algorithm is that in addition to modifying the BMU, its neighbors in the output space are also modified, keeping neighboring neurons similar to each other. The update equation reads

$$\boldsymbol{m}_i = \boldsymbol{m}_i^0 + \alpha(t) h_{i,\mathrm{BMU}(\boldsymbol{x})}(t)[\boldsymbol{x} - \boldsymbol{m}_i^0], \quad i = 1, \ldots, M, \tag{5.1}$$

where $\boldsymbol{x}$ is the data point, $\boldsymbol{m}_i^0$ and $\boldsymbol{m}_i$ are the old and new model vectors, and $\alpha(t)$ and $h_{i,j}(t)$ determine how much the different model vectors are modified. t resembles the time elapsed since the start of the training, i.e., the number of data vectors already presented. $\alpha(t)$ is called the *learning rate* (discussed in more detail below), and $h_{i,j}(t)$ is the so-called *neighborhood function*. $h_{i,j}(t)$ is normalized such that $h_{i,i}(t) = 1$, and it should decrease as the distance between the neurons i and j increases. A typical choice is a Gaussian function

$$h_{i,j}(t) = \exp\left(-\frac{\|\boldsymbol{r}_i - \boldsymbol{r}_j\|}{2\sigma^2(t)}\right), \tag{5.2}$$

where $\sigma(t)$ (called the *neighborhood radius*) determines the radius of the update region.

In order to completely specify the training algorithm, the learning rate $\alpha(t)$ and the neighborhood radius $\sigma(t)$ need to be specified. Both of these should be decreasing functions of the training time t: this way, the map initially adjusts to rough features of the data, while later stages allow refinement of details. Typical choices for $\alpha(t)$ include linearly, exponentially, or inversely decreasing functions with an initial value $\alpha_0 = 0.1 - 1$ and a final value $0.001 - 0.01\alpha_0$, while $\sigma(t)$ is typically taken as a linearly decreasing function [96]. The effect of these choices in the present context was studied in detail in Paper [V].

Applying SOMs to different problems is made easier by a freely available software implementation, the SOM Toolbox [196]. It uses the MatLab environment, and comes with quite a complete set of training, visualization, and analysis tools. This toolbox was used also in the work reported here, modified slightly to take into account the periodic nature of the variables used. These modifications are described in detail in Ref. [97].

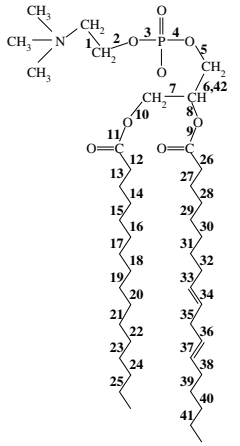

Figure 5.1: Chemical structure of PLPC. The small numbers show the indexing of the dihedral angles used in the SOM analysis. One of the glycerol bonds has two dihedrals associated with it: dihedral 6 involves all three glycerol carbons, while 42 involves the *sn*-2 and *sn*-3 oxygens. Three regions of the molecule were analyzed separately: the headgroup (dihedrals 1–11 and 42), the glycerol (dihedrals 5–13, 26–27, and 42), and the *sn*-2 tail (dihedrals 30–41). Reproduced from [V].

5.3 SOM in Conformational Analysis

In principle, SOM can be applied in conformational analysis straightforwardly: each conformation of each molecule in each frame of the trajectory is described by an n-dimensional vector, and the map is trained with these data points. The most difficult task is to choose a reasonable number of values to describe a conformation, i.e., the meaning of the components of the n-dimensional vector. Different choices are possible, with most obvious ones including the positions of atoms, distances between atoms, and/or dihedral angles. The pros and cons of different descriptions are briefly discussed in Ref. [63]. For rapid visual analysis of the results, it is advantageous to select the description (the n components of the conformation vector) such that a model conformation can be constructed from these values. This way, it is easy to visualize the averaged conformations associated with the neurons and see their major differences.

After the map has been trained, standard visualization tools developed for SOMs can be used [96]. Most important of these are a unified distance matrix (U-matrix) and component planes. In the *U-matrix*, different neurons are colored based on their similarity of the model vectors between the neuron and its neighbors. Such a visualization gives a rapid overview of possible clusters on the map. The *component planes* provide a more detailed view on the clusters: the plot consists of one figure for each of the n components, each figure showing the value of one component for each model vector.

The visualizations of SOM also provide a good starting point for further analysis: it is possible to visualize, e.g., the dynamics of the molecules [75], as well as correlations of different quantities between each other or with the conformations [132]. It is also possible to construct a smaller number of clusters based on the SOM model vectors, and visualize these clusters together with other data in the SOM output space. Overall, the main strength of SOM is the possibility to visualize different quantities related to the different conformations in the low-dimensional output space; the human analyst can then spot correlations that could otherwise get missed.

In Paper [V], we applied SOM for analysis of a 50 ns simulation of PLPC, a PC phospholipid with one saturated tail and one doubly unsaturated chain. Figure 5.1 shows the chemical structure of this lipid. Details of the simulations can be found in Ref. [98]. The system contained 128 lipids, and 36 ns of the trajectory, sampled at 10 ps intervals, was used for analysis. Hence, the input to the SOM consisted of $\sim$460 000 individual lipid conformations. Dihedral angles were used for describing the conformations, with a

single molecule containing 42 dihedrals that completely specify the conformation. The numbering of the dihedral angles is shown in Fig. 5.1. The SOM Toolbox was used for the analysis and visualization, and the periodicity of the dihedrals was taken into account by modifying the toolbox slightly. To reduce the computational cost and to make the results simpler to interpret, most of the analysis was carried out only for subsets of the dihedrals. That is, instead of the 42-component vectors, several 12 component vectors were used to describe different regions of the molecule, and separate SOMs were trained with each set. Such analysis was performed for the headgroup region (glycerol backbone and the headgroup, dihedrals 1–11 and 42), the glycerol region (including the phosphate and the first carbons of the tails, dihedrals 5-13, 26–27, and 42), and the unsaturated *sn*-2 chain (dihedrals 30–41).

5.4 Results

Paper [V] discusses three major themes in applying SOM to analysis of lipid conformations. First, the selection of the map parameters is studied in order to provide general guidance for obtaining the best possible map. Second, the resulting maps are analyzed visually and a few general conclusions about the conformational space are made. Finally, more quantitative analysis is made on the dynamics of the headgroup based on the SOM data and the underlying trajectory. The main results from each of these are summarized below.

5.4.1 Selection of Map Parameters

The effect of map size and the training parameters were studied by systematically varying them and analyzing the resulting SOMs. Six different map sizes were used, ranging from 8×12 to 48×72. A linearly decreasing neighborhood radius was used, with the initial value of 3. The final neighborhood radius σ_f was varied from 0 to 0.7. Different functional forms were tried for the learning rate $\alpha(t)$, and the initial rate α_0 was varied between 0.1 and 0.5. It was found that for the largest map size, which was used for the rest of the paper, the best combination of values was $\sigma_f = 0.7$ and $\alpha_0 = 0.3$, with the learning rate decreasing exponentially as a function of training time.

Based on the above studies, a few qualitative rules were derived for selecting the map parameters and for tuning the map towards a desired level of detail. (i) The level of detail can be tuned with the ratio of map size and the final neighborhood radius. (ii) The final neighborhood radius should be large enough to obtain a smooth map and hence good visualization properties. (iii) The training parameters should be varied slowly enough during the training to avoid local minima for the map. (iv) It is generally difficult to fully automate the process, but the exact values of the training parameters are not very important, since a rather wide range of parameters typically lead to similar maps. (v) As a general rule, the number of independent input data samples should be at least one to two orders of magnitude larger than the number of neurons on the map. The last rule avoids *overlearning*, i.e., situations where the SOM describes the data nearly perfectly, with little or no added value.

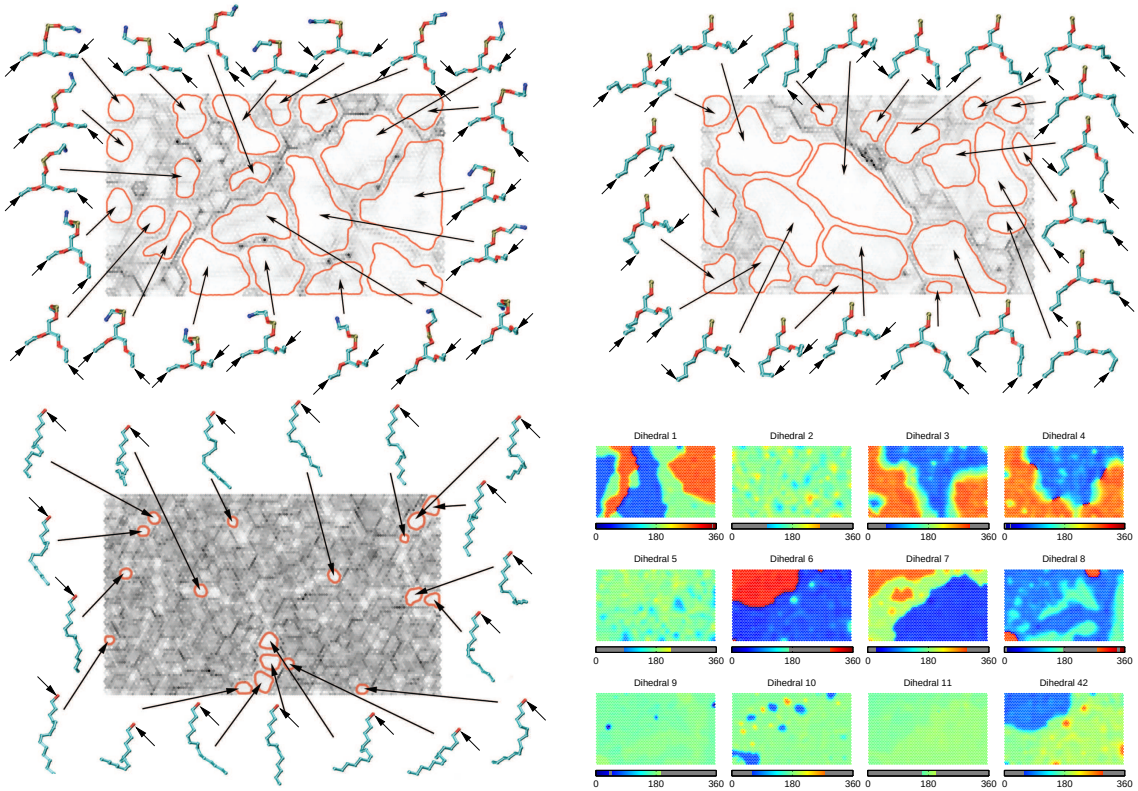

Figure 5.2: Unified distance matrices for SOMs trained with headgroup (top left), glycerol (top right), and *sn*–2 tail (bottom left) data. Neighboring neurons are similar to each other in light regions, while dark regions mark larger differences. Clusters (shown in red) have been determined manually, and a representative conformation is shown for each cluster. The arrows show the glycerol oxygens (bottom left) or the carbons where the tails start (top row). Component planes are also shown for the headgroup map (bottom right). Each small panel shows the values of a single dihedral for each model vector. The color range is the same for each figure, and the bars under each panel show the range of values present on the map. Reproduced from [V].

5.4.2 Visual Assessment of Conformations

For each of the studied regions in the PLPC molecule, a 48×72 map was trained. U-matrix and component plane visualizations were then constructed and analyzed. Based on the U-matrix, manual clustering of the neurons was also performed in regions where local similarity was high. For each such cluster, a representative conformation was visualized. The U-matrices, the manually constructed clusters, and the representative configurations are shown in Fig. 5.2 for each region. The component planes for the headgroup map are also shown. Together, these visualizations were used to identify four distinct groups of conformations for the headgroup and glycerol regions. The largest differences between these groups were associated with different conformations of the glycerol region. Within these groups, smaller clusters were observed, differing mostly in the orientation of the P–N vector and/or the first dihedrals in the tails. For the *sn*–2 tail, no clear clustering was present. Instead, the map was more or less homogeneous. Nevertheless, the distribution of different dihedral values seems to be well reproduced by the map: *trans* and *gauche*

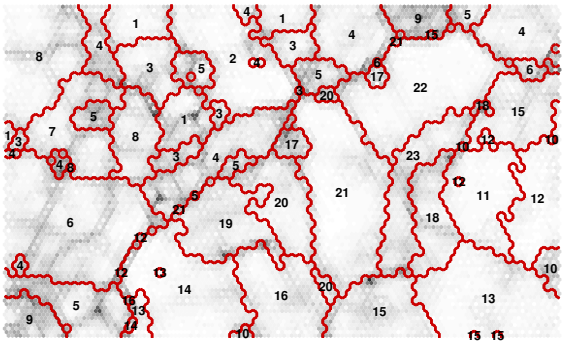

Figure 5.3: Clustering of the headgroup SOM with transition frequencies as a similarity measure. The U-matrix is shown in the background. Each cluster is identified by a distinct number (some clusters are not continuous). Reproduced from [V].

conformations are well visible for each saturated dihedral.

The U-matrix visualizations were also used to assess the correlations between the different regions of the molecule. This was done by identifying clusters within one of the maps and then finding all the lipid conformations that have their BMU in that cluster. The BMUs of these clusters can then be calculated for the other maps and the distribution visualized. Correlations should show as clustering of the BMUs in the target maps as well, while absence of correlations is characterized by a homogeneous distribution of the BMUs on the target map. Performing the calculations for all pairs of maps shows that in our case, there are some correlations between the headgroup and the glycerol regions, but the *sn*–2 region is not correlated with the other two. All of the observed correlations can be explained by the fact that the two maps share some dihedrals. The lack of correlations between the tail and the other parts also indicates that for our system, the polar and non-polar regions of the system are mostly independent on the level of single molecules.

Paper [V] also discusses briefly how information from SOMs could be used in selecting CG degrees of freedom. This discussion is expanded further in Refs. [131] and [132]. The idea is, as discussed in Section 5.1, to use knowledge gained from SOM and/or other cluster analysis to select a minimal representation that still can reproduce the most important conformational features. Currently, this has been done only qualitatively, with the main conclusion that a MARTINI-type of model should be able to reproduce the main features. An automated, more quantitative implementation would be an interesting direction for future research.

5.4.3 Analysis of Headgroup Dynamics

It is also possible to analyze dynamics using the trained map as a visualization aid. In this approach, the dynamics from the MD trajectory is used to form a set of trajectories of the input data vectors, one trajectory for each molecule. Mapping the vectors to their BMUs then results in a trajectory for each molecule on the map. These can then be either directly visualized, or can be used as a basis for further analysis.

For more quantitative analysis, the BMU trajectories can be used to calculated transition frequencies between each pair of neurons. These transition frequencies can then be used to define the similarity of the neurons. With such a similarity measure, a standard hierarchical clustering algorithm [64] can be applied to construct clusters of neurons such that most conformational transitions occur within a cluster. In the context of our PLPC system, the resulting clustering agreed very well with the visual structure of the map, with cluster boundaries coinciding with darker areas in the U-matrix. The transition frequen-

cies between each pair of clusters were also calculated, and they were used to identify transition paths between the different classes of conformations. It was seen that the most prominent boundaries on the map also result in larger transition barriers: for example, transitions across the dark boundary in the headgroup map (see Fig. 5.2, the boundary goes from bottom left to top right corner) are very rare. This analysis can also be seen as an independent verification of the quality of the map: no dynamic information was used in constructing the map, but the results from the analysis of dynamics are very similar to those obtained directly from the SOMs.

Chapter 6

Summary and Outlook

The first part of this Thesis (Papers [I]–[IV]) deal with multiscale modeling of lipid bilayers containing DPPC and cholesterol. Systematically obtained CG models were shown to predict formation of cholesterol-rich and cholesterol-poor domains at intermediate cholesterol concentrations. Also, density fluctuations were predicted to occur in the tail region at low cholesterol concentrations, an observation that was later confirmed through atomistic simulations in Paper [IV]. High chain order was seen within the denser regions in the atomistic simulations, which was later also seen in the CG model that included chain ordering [III]. The agreement between the CG and atomistic simulations in this case provides confidence in the qualitative conclusions drawn from the models, as well as in the CG approach used. However, quantitative results were shown to depend on details of the model construction, and were not studied in detail. The presence of strong density fluctuations in atomistic bilayers is also interesting in its own right, and is one possible mechanism for formation of domains in more complex bilayers as well [73].

Another point of view is that Papers [I]–[III] present an application of RDF inversion to a highly coarse-grained model. As such, they provide insight into the problems, pitfalls, and possible gains of the RDF inversion approach. The problems with the virial pressure [II] and the internal energies for multi-state particles [III] show that although in theory the RDF inversion results in well-defined interactions, this may not always be the case in practice. Paper [II] also reports technical improvements to the IMC approach that can be used to speed up the inversion, while Paper [III] extends the IMC method to systems with internal states. However, further studies are needed on simpler models with internal states, as several uncertainties remain, e.g., on whether the underlying MD simulations had sampled the phase space sufficiently.

Paper [V] approaches atomistic simulations and the structural information provided by them from another angle. It studies SOM as a tool for quickly gaining understanding of the most important features of the molecular conformations, as well as using this information in coarse-graining. It focuses on the methodology, with emphasis on the effects of the different parameters that need to be selected. As such, it provides a sound basis for subsequent studies. In addition, some applications of SOM and its visualization properties are demonstrated: the headgroup dynamics is analyzed, and the correlations between the different parts of the molecule are assessed. The paper demonstrates the possibilities that SOM has to offer in the context of conformational analysis. Further studies can then focus more on possible applications to other systems and/or in coarse-graining, using the foundation laid in the paper.

There are several interesting avenues for continuing the research. Applications of IMC coarse-graining to other systems could provide insight into the phase behavior of lipid mixtures. Of particular interest would be a ternary mixture that includes POPC (a PC lipid with one saturated and one unsaturated tail), sphingomyelin, and cholesterol. Atomistic simulations at a few selected concentrations have already been performed [138], and these could be used as the starting point for studying whether these systems tend to phase separate. This question is interesting as the mixture is thought to be a good model for *lipid rafts*, functional domains in membranes [177]. These simulations have also been analyzed using SOMs [164], with the focus on sphingomyelin–cholesterol interactions. The SOM analysis could also be extended such that the input data would consist of pairs of molecules, enabling direct visualization of the typical modes of interaction.

On a more general level, detailed comparison of the RDF-based and force-based CG methods could be fruitful. This could be first done for simple model systems to understand the fundamental differences and similarities of the approaches. The studies could then be extended to semi-atomistic models, which have already been constructed using both methods [43, 79, 81, 111]. Semi-atomistic models could also be compared in more detail to the semi-empirical models such as the MARTINI model [116, 117]. Also, a comparison on simple models such as those studied in this Thesis could be done. Combined, these comparisons could provide substantial insight into the coarse-graining process in general, as well as advantages of the different methods. Simple model systems could also be used to study in more detail the relative entropy introduced by Shell [169] for different models, as well as the problems encountered with multiple sets of interactions giving essentially the same RDFs. One main goal of such studies would be to determine and study measures for the quality of the potentials, as the RDFs themselves are not very effective in discriminating different potentials. The effect of insufficient sampling in the underlying MD simulations might also be fruitfully studied.

The use of clustering, and SOMs in particular, in coarse-graining could also be studied in more detail. A useful starting point could be to compare all-atom simulations and semi-atomistic CG models using SOM analyses of both. This could provide better understanding of the similarities and differences between the different resolutions, and might also help improve the CG models to better reproduce the atomistic conformations.

Finally, it would be interesting to combine potential matching [188] with the RDF and/or force matching methods to extract energetic and entropic interactions separately. This might prove advantageous for improving the transferability of the interactions to different temperatures. In this context, methods for determining the single-particle fields and their dependence on the thermodynamic state point could also help in constructing CG models with better transferability and wider applicability.

References

[1] R. L. C. Akkermans and W. J. Briels. 2000. Coarse-grained dynamics of one chain in a polymer melt. *J. Chem. Phys.*, 113:6409–6422.

[2] R. L. C. Akkermans and W. J. Briels. 2001. A structure-based coarse-grained model for polymer melts. *J. Chem. Phys.*, 114:1020–1031.

[3] B. Alberts, D. Bray, J. Lewis, M. Raff, K. Roberts, and J. D. Watson. 1994. *Molecular Biology of the Cell*. Garland Publishing, New York, 3rd edition.

[4] M. P. Allen and D. J. Tildesley. 1987. *Computer Simulation of Liquids*. Oxford University Press, New York.

[5] H. C. Andersen. 1983. RATTLE: A "velocity" version of the SHAKE algorithm for molecular dynamics calculations. *J. Comp. Phys.*, 52:24–34.

[6] A. Arkhipov, P. L. Freddolino, K. Imada, K. Namba, and K. Schulten. 2006. Coarse-grained molecular dynamics simulations of a rotating bacterial flagellum. *Biophys. J.*, 91:4589–4597.

[7] A. Arkhipov, P. L. Freddolino, and K. Schulten. 2006. Stability and dynamics of virus capsids described by coarse-grained modeling. *Structure*, 14:1767–1777.

[8] G. S. Ayton and G. A. Voth. 2007. Multiscale simulation of transmembrane proteins. *J. Struct. Biol.*, 157:570–578.

[9] G. S. Ayton, J. L. McWhirter, P. McMurtry, and G. A. Voth. 2005. Coupling field theory with continuum mechanics: A simulation of domain formation in giant unilamellar vesicles. *Biophys. J.*, 88:3855–3869.

[10] G. S. Ayton, J. L. McWhirter, and G. A. Voth. 2006. A second generation mesoscopic lipid bilayer model: Connections to field-theory descriptions of membranes and nonlocal hydrodynamics. *J. Chem. Phys.*, 124:064906.

[11] M. Bachar, P. Brunelle, D. P. Tieleman, and A. Rauk. 2004. Molecular dynamics simulation of a polyunsaturated lipid bilayer susceptible to lipid peroxidation. *J. Phys. Chem. B*, 108:7170–7179.

[12] Y. Barenholz. 2002. Cholesterol and other membrane active sterols: from membrane evolution to "rafts". *Prog. Lipid Res.*, 41:1–5.

[13] H. J. C. Berendsen. 2008. *Simulating the physical world*. Cambridge University Press, Cambridge.

[14] H. J. C. Berendsen, J. P. M. Postma, W. F. van Gunsteren, and J. Hermans. 1981. Interaction models for water in relation to protein hydration. In B. Pullman, editor, *Intermolecular Forces*, pages 331–342. Reidl, Dordrecht.

[15] H. J. C. Berendsen, J. P. M. Postma, A. DiNola, and J. R. Haak. 1984. Molecular dynamics with coupling to an external bath. *J. Chem. Phys.*, 81:3684–3690.

[16] H. J. C. Berendsen, D. van der Spoel, and R. van Drunen. 1995. GROMACS: A message-passing parallel molecular dynamics implementation. *Comp. Phys. Comm.*,

91:43–56.

[17] O. Berger, O. Edholm, and F. Jahnig. 1997. Molecular dynamics simulations of a fluid bilayer of dipalmitoylphosphatidylcholine at full hydration, constant pressure, and constant temperature. *Biophys. J.*, 72:2002–2013.

[18] P. G. Bolhuis, A. A. Louis, and J. P. Hansen. 2001. Many-body interactions and correlations in coarse-grained descriptions of polymer solutions. *Phys. Rev. E*, 64: 021801.

[19] P. G. Bolhuis, A. A. Louis, J. P. Hansen, and E. J. Meijer. 2001. Accurate effective pair potentials for polymer solutions. *J. Chem. Phys.*, 114:4296–4311.

[20] P. G. Bolhuis and A. A. Louis. 2002. How to derive and parameterize effective potentials in colloid–polymer mixtures. *Macromolecules*, 35:1860–1869.

[21] P. G. Bolhuis, A. A. Louis, and J. P. Hansen. 2002. Influence of polymer-excluded volume on the phase-behavior of colloid-polymer mixtures. *Phys. Rev. Lett.*, 89: 128302.

[22] P. J. Bond, J. Holyoake, A. Ivetac, S. Khalid, and M. S. Sansom. 2007. Coarse-grained molecular dynamics simulations of membrane proteins and peptides. *J. Struct. Biol.*, 157:593–605.

[23] S. D. Bond, B. J. Leimkuhler, and B. B. Laird. 1999. The Nosé-Poincaré method for constant temperature molecular dynamics. *J. Comp. Phys.*, 151:114–134.

[24] G. Brannigan, L. C.-L. Lin, and F. L. H. Brown. 2006. Implicit solvent simulation models for biomembranes. *Eur. Biophys. J.*, 35:104–124.

[25] B. R. Brooks, R. E. Bruccoleri, B. D. Olafson, D. J. States, S. Swaminathan, and M. Karplus. 1983. CHARMM: A program for macromolecular energy, minimization, and dynamics calculations. *J. Comp. Chem.*, 4:187–217.

[26] G. Bussi, D. Donadio, and M. Parrinello. 2007. Canonical sampling through velocity rescaling. *J. Chem. Phys.*, 126:014101.

[27] P. Carbone, H. A. K. Varzaneh, X. Chen, and F. Muller-Plathe. 2008. Transferability of coarse-grained force fields: The polymer case. *J. Chem. Phys.*, 128:064904.

[28] A. Catte, J. C. Patterson, D. Bashtovyy, M. K. Jones, F. Gu, L. Li, A. Rampioni, D. Sengupta, T. Vuorela, P. Niemela, M. Karttunen, S. J. Marrink, I. Vattulainen, and J. P. Segrest. 2008. Structure of spheroidal HDL particles revealed by combined atomistic and coarse-grained simulations. *Biophys. J.*, 94:2306–2319.

[29] J. T. Chayes, L. Chayes, and E. H. Lieb. 1984. The inverse problem in classical statistical mechanics. *Commun. Math. Phys.*, 93:57–121.

[30] J. T. Chayes and L. Chayes. 1984. On the validity of the inverse conjecture in classical density functional theory. *J. Stat. Phys.*, 36:471–488.

[31] L. Y. Chen, S. C. Ying, and T. Ala-Nissila. 2002. Finding transition paths and rate coefficients through accelerated langevin dynamics. *Phys. Rev. E*, 65:042101.

[32] Y.-W. Chiang, A. J. Costa-Filho, and J. H. Freed. 2007. Dynamic molecular structure and phase diagram of DPPC–cholesterol binary mixtures: A 2D-ELDOR study. *J. Phys. Chem. B*, 111:11260–11270.

[33] S. W. Chiu, M. Clark, V. Balaji, S. Subramaniam, H. L. Scott, and E. Jakobsson. 1995. Incorporation of surface tension into molecular dynamics simulation of an interface: A fluid phase lipid bilayer membrane. *Biophys. J.*, 69:1230–1245.

[34] M. Christen and W. F. van Gunsteren. 2006. Multigraining: An algorithm for simultaneous fine-grained and coarse-grained simulation of molecular systems. *J. Chem. Phys.*, 124:154106.

[35] I. R. Cooke, K. Kremer, and M. Deserno. 2005. Efficient tunable generic model for fluid bilayer membranes. *Phys. Rev. E*, 72:011506.

[36] W. D. Cornell, P. Cieplak, C. I. Bayly, I. R. Gould, K. M. Merz, D. M. Ferguson, D. C. Spellmeyer, T. Fox, J. W. Caldwell, and P. A. Kollman. 1995. A second generation force field for the simulation of proteins, nucleic acids, and organic molecules. *J. Am. Chem. Soc.*, 117:5179–5197.

[37] T. Darden, D. York, and L. Pedersen. 1993. Particle mesh Ewald: An $N \log(N)$ method for Ewald sums in large systems. *J. Chem. Phys.*, 98:10089–10092.

[38] C. Dellago and P. G. Bolhuis. 2008. Transition path sampling and other advaced simulation techniques for rare events. In C. Holm and K. Kremer, editors, *Advanced Computer Simulation Approaches for Soft Matter Sciences III*, volume 221 of *Advances in Polymer Science*, pages 167–233. Springer.

[39] S. Doniach. 1978. Thermodynamic fluctuations in phospholipid bilayers. *J. Chem. Phys.*, 68:4912–4916.

[40] B. Dunweg. 1993. Molecular dynamics algorithms and hydrodynamic screening. *J. Chem. Phys.*, 99:6977–6982.

[41] R. Durret. 1999. *Essentials of Stochastic Processes*. Springer, New York.

[42] E. Egberts, S.-J. Marrink, and H. J. C. Berendsen. 1994. Molecular dynamics simulation of a phospholipid membrane. *Eur. Biophys. J.*, 22:423–436.

[43] J. Elezgaray and M. Laguerre. 2006. A systematic method to derive force fields for coarse-grained simulations of phospholipids. *Comp. Phys. Comm.*, 175:264–268.

[44] F. Ercolessi and J. B. Adams. 1994. Interatomic potentials from 1st-principles calculations — the force-matching method. *Europhys. Lett.*, 26:583–588.

[45] A. Eriksson, M. N. Jacobi, J. Nystrom, and K. Tunstrom. 2008. Using force covariance to derive effective stochastic interactions in dissipative particle dynamics. *Phys. Rev. E*, 77:016707.

[46] A. Eriksson, M. N. Jacobi, J. Nystrom, and K. Tunstrom. 2008. Effective thermostat induced by coarse graining of simple point charge water. *J. Chem. Phys.*, 129:024106.

[47] D. L. Ermak and H. Buckholtz. 1980. Numerical integration of the Langevin equation: Monte Carlo simulation. *J. Comp. Phys.*, 35:169–182.

[48] P. Español and P. Warren. 1995. Statistical mechanics of dissipative particle dynamics. *Europhys. Lett.*, 30:191–196.

[49] P. Español. 1995. Hydrodynamics from dissipative particle dynamics. *Phys. Rev. Lett.*, 52:1734–1742.

[50] U. Essmann, L. Perera, M. L. Berkowitz, H. L. T. Darden, and L. G. Pedersen. 1995. A smooth particle mesh Ewald method. *J. Chem. Phys.*, 103:8577–8592.

[51] E. Falck, M. Patra, M. Karttunen, M. T. Hyvönen, and I. Vattulainen. 2004. Lessons of slicing membranes: Interplay of packing, free area, and lateral diffusion in phospholipid/cholesterol bilayers. *Biophys. J.*, 87:1076–1091.

[52] R. Faller. 2004. Automatic coarse graining of polymers. *Polymer*, 45:3869–3876.

[53] J. Fan, M. Sammalkorpi, and M. Haataja. 2008. Domain formation in the plasma membrane: Roles of nonequilibrium lipid transport and membrane proteins. *Phys. Rev. Lett.*, 100:178102.

[54] G. W. Feigenson. 2009. Phase diagrams and lipid domains in multicomponent lipid bilayer mixtures. *Biochim. Biophys. Acta*, 1788:47–52.

[55] S. Feller and A. MacKerell, Jr. 2000. An improved empirical potential energy function for molecular simulations of phospholipids. *J. Phys. Chem. B*, 104:7510–

7515.

[56] A. L. Fetter and J. D. Walecka. 2003. *Theoretical Mechanics of Particles and Continua*. Dover.

[57] N. Foloppe and A. D. MacKerell, Jr. 2000. All-atom empirical force field for nucleic acids: 1) Parameter optimization based on small molecule and condensed phase macromolecular target data. *J. Comp. Chem.*, 21:86–104.

[58] D. Gfeller and P. D. L. Rios. 2008. Spectral coarse graining and synchronization in oscillator networks. *Phys. Rev. Lett.*, 100:174104.

[59] H. Gohlke and M. F. Thorpe. 2006. A natural coarse graining for simulating large biomolecular motion. *Biophys. J.*, 91:2115–2120.

[60] E. I. Goksu, J. M. Vanegas, C. D. Blanchette, W.-C. Lin, and M. L. Longo. 2009. AFM for structure and dynamics of biomembranes. *Biochim. Biophys. Acta*, 1788: 254–266.

[61] R. D. Groot and P. B. Warren. 1997. Dissipative particle dynamics: Bridging the gap between atomistic and mesoscopic simulation. *J. Chem. Phys.*, 107:4423–4435.

[62] B. Guillot. 2002. A reappraisal of what we have learnt during three decades of computer simulations on water. *J. Mol. Liq.*, 101:219–260.

[63] F. A. Hamprecht, C. Peter, X. Daura, W. Thiel, and W. F. van Gunsteren. 2001. A strategy for analysis of (molecular) equilibrium simulations: Configuration space density estimation, clustering, and visualization. *J. Chem. Phys.*, 114:2079–2089.

[64] D. Hand, H. Mannila, and P. Smyth. 2001. *Principles of Data Mining*. MIT Press, Cambridge.

[65] J.-P. Hansen and I. R. McDonald. 1986. *Theory of Simple Liquids*. Academic Press, London, 2nd edition.

[66] S. W. Hell. 2007. Far-field optical nanoscopy. *Science*, 316:1153–1158.

[67] R. L. Henderson. 1974. A uniqueness theorem for fluid pair correlation functions. *Phys. Lett. A*, 49:197–198.

[68] B. Hess, H. Bekker, H. J. C. Berendsen, and J. G. E. M. Fraaije. 1997. LINCS: A linear constraint solver for molecular simulations. *J. Comp. Chem.*, 18:1463–1472.

[69] B. Hess. 2008. P-LINCS: A parallel linear constraint solver for molecular simulation. *J. Chem. Theory Comput.*, 4:116–122.

[70] B. Hess, C. Kutzner, D. van der Spoel, and E. Lindahl. 2008. GROMACS 4: Algorithms for highly efficient, load-balanced, and scalable molecular simulation. *J. Chem. Theory Comput.*, 4:435–447.

[71] M. Höltje, T. Förster, B. Brandt, T. Engels, W. von Rybinski, and H.-D. Höltje. 2001. Molecular dynamics simulations of stratum corneum lipid models: fatty acids and cholesterol. *Biochim. Biophys. Acta*, 1511:156–167.

[72] A. R. Honerkamp-Smith, P. Cicuta, M. D. Collins, S. L. Veatch, M. den Nijs, M. Schick, and S. L. Keller. 2008. Line tensions, correlation lengths, and critical exponents in lipid membranes near critical points. *Biophys. J.*, 95:236–246.

[73] A. R. Honerkamp-Smith, S. L. Veatch, and S. L. Keller. 2008. An introduction to critical points for biophysicists; observations of compositional heterogeneity in lipid membranes. *Biochim. Biophys. Acta*, 1788:53–63.

[74] W. G. Hoover. 1985. Canonical dynamics: equilibrium phase-space distribution. *Phys. Rev. A*, 31:1695–1697.

[75] M. T. Hyvönen, Y. Hiltunen, W. El-Deredy, T. Ojala, J. Vaara, P. T. Kovanen, and M. Ala-Korpela. 2001. Application of self-organizing maps in conformational anal-

ysis of lipids. *J. Am. Chem. Soc.*, 123:810–816.

[76] J. H. Ipsen, G. Karlström, O. G. Mouritsen, H. Wennerström, and M. J. Zuckermann. 1987. Phase equilibria in phosphatidylcholine-cholesterol system. *Biochim. Biophys. Acta*, 905:162–172.

[77] J. N. Israelachvili. 1992. *Intermolecular and Surface Forces*. Academic Press.

[78] S. Iuchi, S. Izvekov, and G. A. Voth. 2007. Are many-body electronic polarization effects important in liquid water? *J. Chem. Phys.*, 126:124505.

[79] S. Izvekov and G. A. Voth. 2005. A multiscale coarse-graining method for biomolecular systems. *J. Phys. Chem. B*, 109:2469–2473.

[80] S. Izvekov and G. A. Voth. 2005. Multiscale coarse graining of liquid-state systems. *J. Chem. Phys.*, 123:134105.

[81] S. Izvekov and G. A. Voth. 2006. Multiscale coarse-graining of mixed phospholipid/cholesterol bilayers. *J. Chem. Theory Comput.*, 2:637–648.

[82] S. Izvekov and G. A. Voth. 2006. Modeling real dynamics in the coarse-grained representation of condensed phase systems. *J. Chem. Phys.*, 125:151101.

[83] S. Izvekov, M. Parrinello, C. J. Burnham, and G. A. Voth. 2004. Effective force fields for condesed phase systems from ab initio molecular dynamics simulation: A new method for force-matching. *J. Chem. Phys.*, 120:10896–10913.

[84] S. Izvekov, J. Swanson, and G. Voth. 2008. Coarse-graining in interaction space: A systematic approach for replacing long-range electrostatics with short-range potentials. *J. Phys. Chem. B*, 112:4711–4724.

[85] S. Jain, S. Garde, and S. K. Kumar. 2006. Do inverse Monte Carlo algorithms yield thermodynamically consistent interaction potentials? *Ind. Eng. Chem. Res.*, 45: 5614–5618.

[86] P. Jedlovszky, I. Bako, G. Palinkas, T. Radnai, and A. K. Soper. 1996. Investigation of the uniqueness of the reverse Monte Carlo method: Studies on liquid water. *J. Chem. Phys.*, 105:245–254.

[87] R. A. L. Jones. 2002. *Soft Condensed Matter*. Oxford University Press, New York.

[88] W. L. Jorgensen, J. Chandrasekhar, J. D. Madura, R. W. Impey, and M. L. Klein. 1983. Comparison of simple potential functions for simulation liquid water. *J. Chem. Phys.*, 79:926–935.

[89] W. Jorgensen, D. Maxwell, and J. Tirado-Rives. 1996. Development and testing of the OPLS all-atom force field on conformational energetics and properties of organic liquids. *J. Am. Chem. Soc.*, 118:11225–11236.

[90] W. L. Jorgensen and J. Tirado-Rives. 1988. The OPLS [optimized potentials for liquid simulations] potential functions for proteins, energy minimizations for crystals of cyclic peptides and crambin. *J. Am. Chem. Soc.*, 110:1657–1666.

[91] C. Junghans, M. Praprotnik, and K. Kremer. 2008. Transport properties controlled by a thermostat: An extended dissipative particle dynamics thermostat. *Soft Matter*, 4:156–161.

[92] H. A. Karimi-Varzaneh, P. Carbone, and F. Muller-Plathe. 2008. Fast dynamics in coarse-grained polymer models: The effect of the hydrogen bonds. *J. Chem. Phys.*, 129:154904.

[93] G. A. Khelashvili, S. A. Pandit, and H. L. Scott. 2005. Self-consistent mean-field model based on molecular dynamics: Application to lipid-cholesterol bilayers. *J. Chem. Phys.*, 123:034910.

[94] S. H. L. Klapp, D. J. Diestler, and M. Schoen. 2004. Why are effective potentials

"soft"? *J. Phys.: Condens. Matter*, 16:7331–7352.

[95] D. A. Kofke. 2005. Free energy methods in molecular simulation. *Fluid Phase Equilibria*, 228-229:41–48.

[96] T. Kohonen. 2001. *Self-organizing maps*, volume 30 of *Springer series in information science*. Springer, Berlin, 3rd edition.

[97] M. Kupiainen. 2006. Structural analysis of lipid molecules in cell membranes by self-organizing maps. Master's thesis, Helsinki University of Technology.

[98] M. Kupiainen, E. Falck, S. Ollila, P. Niemelä, A. A. Gurtovenko, M. T. Hyvönen, M. Patra, M. Karttunen, and I. Vattulainen. 2005. Free volume properties of sphingomyelin, DMPC, DPPC, and PLPC bilayers. *J. Comput. Theor. Nanoscience*, 2: 401–413.

[99] E. Lindahl, B. Hess, and D. van der Spoel. 2001. GROMACS 3.0: A package for molecular simulation and trajectory analysis. *J. Mol. Mod.*, 7:306–317.

[100] G. Lindblom and G. Orädd. 2009. Lipid lateral diffusion and membrane heterogeneity. *Biochim. Biophys. Acta*, 1788:234–244.

[101] P. Liu, S. Izvekov, and G. Voth. 2007. Multiscale coarse-graining of monosaccharides. *J. Phys. Chem. B*, 111:11566–11575.

[102] A. A. Louis. 2002. Beware of density dependent pair potentials. *J. Phys.: Condens. Matter*, 14:9187–9206.

[103] E. Lyman, F. M. Ytreberg, and D. M. Zuckerman. 2006. Resolution exchange simulation. *Phys. Rev. Lett.*, 96:028105.

[104] E. Lyman and D. M. Zuckerman. 2006. Resolution exchange simulation with incremental coarsening. *J. Chem. Theory Comput.*, 2:656–666.

[105] A. P. Lyubartsev and A. Laaksonen. 1995. Calculation of effective interaction potentials from radial distribution functions: A reverse Monte Carlo approach. *Phys. Rev. E*, 52:3730–3737.

[106] A. P. Lyubartsev and A. Laaksonen. 1997. Osmotic and activity coefficients from effective potentials for hydrated ions. *Phys. Rev. E*, 55:5689–5696.

[107] A. P. Lyubartsev and A. Laaksonen. 1999. Effective potentials for ion–DNA interactions. *J. Chem. Phys.*, 111:11207–11215.

[108] A. P. Lyubartsev and A. Laaksonen. 2000. Determination of effective pair potentials from ab initio simulations: Application to liquid water. *Chem. Phys. Lett.*, 325: 15–21.

[109] A. P. Lyubartsev and S. Marčelja. 2002. Evaluation of effective ion-ion potentials in aqueous electrolytes. *Phys. Rev. E*, 65:041202.

[110] A. P. Lyubartsev, M. Karttunen, I. Vattulainen, and A. Laaksonen. 2003. On coarse-graining by the Inverse Monte Carlo method: Dissipative Particle Dynamics simulations made to a precise tool in soft matter modeling. *Soft Materials*, 1:121–137.

[111] A. P. Lyubartsev. 2005. Multiscale modeling of lipids and lipid bilayers. *Eur. Biophys. J.*, 35:53–61.

[112] A. MacKerell, Jr., D. Bashford, M. Bellott, R. Dunbrack, J. Evanseck, M. Field, S. Fischer, J. Gao, H. Guo, S. Ha, D. Joseph-McCarthy, L. Kuchnir, K. Kuczera, F. Lau, C. Mattos, S. Michnick, T. Ngo, D. Nguyen, B. Prodhom, W. Reiher, B. Roux, M. Schlenkrich, J. Smith, R. Stote, J. Straub, M. Watanabe, J. Wiórkiewicz-Kuczera, D. Yin, and M. Karplus. 1998. All-atom empirical potential for molecular modeling and dynamics studies of proteins. *J. Phys. Chem. B*, 102:3586–3616.

[113] A. D. MacKerell, Jr., M. Feig, and C. L. Brooks, III. 2004. Extending the treatment of backbone energetics in protein force fields: limitations of gas-phase quantum mechanics in reproducing protein conformational distributions in molecular dynamics simulations. *J. Comp. Chem.*, 25:1400–1415.

[114] A. Malevanets and R. Kapral. 1999. Mesoscopic model for solvent dynamics. *J. Chem. Phys.*, 110:8605–8613.

[115] A. Malevanets and R. Kapral. 2000. Solute molecular dynamics in a mesoscale solvent. *J. Chem. Phys.*, 112:7260–7269.

[116] S. J. Marrink, A. H. de Vries, and A. E. Mark. 2004. Coarse grained model for semi-quantitative lipid simulations. *J. Phys. Chem. B*, 108:750–760.

[117] S. J. Marrink, H. J. Risselada, S. Yefimov, D. P. Tieleman, and A. H. de Vries. 2007. The MARTINI force field: Coarse grained model for biomolecular simulations. *J. Phys. Chem. B*, 111:7812–7824.

[118] S. J. Marrink, A. H. de Vries, and D. P. Tieleman. 2008. Lipids on the move: Simulations of membrane pores, domains, stalks and curves. *Biochim. Biophys. Acta*, 1788:149–168.

[119] G. J. Martyna, M. L. Klein, and M. Tuckerman. 1992. Nosé–Hoover chains: The canonical ensemble via continuous dynamics. *J. Chem. Phys.*, 97:2635–2643.

[120] M. Matsumoto and T. Nishimura. 1998. Mersenne Twister: A 623-dimensionally equidistributed uniform pseudorandom number generator. *ACM Trans. Model. Comput. Simul.*, 8:3–30.

[121] S. Matysiak, C. Clementi, M. Praprotnik, K. Kremer, and L. Delle Site. 2008. Modeling diffusive dynamics in adaptive resolution simulation of liquid water. *J. Chem. Phys.*, 128:024503.

[122] N. Metropolis, A. W. Rosenbluth, M. N. Rosenbluth, and A. H. Teller. 1953. Equation of state calculations by fast computing machines. *J. Chem. Phys.*, 21:1087–1092.

[123] L. Miao, M. Nielsen, J. Thewalt, J. H. Ipsen, M. Bloom, M. J. Zuckermann, and O. G. Mouritsen. 2002. From lanosterol to cholesterol: Structural evolution and differential effects on lipid bilayers. *Biophys. J.*, 82:1429–1444.

[124] S. Miyamoto and P. A. Kollman. 1992. SETTLE: An analytical version of the SHAKE and RATTLE algorithm for rigid water models. *J. Comp. Chem.*, 13:952–962.

[125] L. Monticelli, S. K. Kandasamy, X. Periole, R. G. Larson, D. P. Tieleman, and S.-J. Marrink. 2008. The MARTINI coarse-grained force field: Extension to proteins. *J. Chem. Theory Comput.*, 4:819–834.

[126] H. Mori. 1965. Transport, collective motion, and Brownian motion. *Prog. Theor. Phys.*, 33:423–455.

[127] O. G. Mouritsen. 2005. *Life — as a matter of fat*. The Frontiers Collection. Springer, Berlin.

[128] O. G. Mouritsen. 1991. Theoretical models of phospholipid phase transitions. *Chem. Phys. Lipids*, 57:179–194.

[129] O. G. Mouritsen, B. Dammann, H. C. Fogedby, J. H. Ipsen, C. Jeppesen, K. Jørgensen, J. Risbo, M. C. Sabra, M. M. Sperotto, and M. J. Zuckermann. 1995. The computer as a laboratory for the physical chemistry of membranes. *Biophys. Chem.*, 55:55–68.

[130] F. Müller-Plathe. 2002. Scale-hopping in computer simulations of polymers. *Soft*

Materials, 1:1–31.

[131] T. Murtola, I. Vattulainen, and M. Karttunen. 2008. Systematic approach to coarse-graining of molecular descriptions and interactions with applications to lipid membranes. In G. A. Voth, editor, *Coarse-Graining of Condensed Phase and Biomolecular Systems*. CRC Press, Boca Raton, FL.

[132] T. Murtola, A. Bunker, I. Vattulainen, M. Deserno, and M. Karttunen. 2009. Multiscale modeling of emergent materials: biological and soft matter. *Phys. Chem. Chem. Phys.*, 11:1869–1892.

[133] J. F. Nagle and S. Tristam-Nagle. 2000. Structure of lipid bilayers. *Biochim. Biophys. Acta*, 1469:159–195.

[134] M. Nielsen, L. Miao, J. H. Ipsen, O. G. Mouritsen, and M. J. Zuckermann. 1996. Random-lattice models and simulation algorithms for the phase equilibria in two-dimensional condensed systems of particles with coupled internal and translational degrees of freedom. *Phys. Rev. E*, 54:6889–6905.

[135] M. Nielsen, L. Miao, J. H. Ipsen, M. J. Zuckermann, and O. G. Mouritsen. 1999. Off-lattice model for the phase behavior of lipid-cholesterol bilayers. *Phys. Rev. E*, 59:5790–5802.

[136] M. Nielsen, J. Thewalt, L. Miao, J. H. Ipsen, M. Bloom, M. J. Zuckermann, and O. G. Mouritsen. 2000. Sterol evolution and the physics of membranes. *Europhys. Lett.*, 52:368–374.

[137] S. O. Nielsen, C. F. Lopez, G. Srinivas, and M. L. Klein. 2004. Coarse grain models and the computer simulations of soft materials. *J. Phys.: Condens. Matter*, 16:R481–R512.

[138] P. Niemelä, S. Ollila, M. T. Hyvönen, M. Karttunen, and I. Vattulainen. 2007. Assessing the nature of lipid raft membranes: From atomic-scale structure to lateral pressure profiles. *PLoS Comput. Biol.*, 3:304–312.

[139] H. Noguchi and G. Gompper. 2004. Fluid vesicles with viscous membranes in shear flow. *Phys. Rev. Lett.*, 93:258102.

[140] W. Noid, J.-W. Chu, G. Ayton, and G. Voth. 2007. Multiscale coarse-graining and structural correlations: Connections to liquid-state theory. *J. Phys. Chem. B*, 111: 4116–4127.

[141] W. G. Noid, J.-W. Chu, G. S. Ayton, V. Krishna, S. Izvekov, G. A. Voth, A. Das, and H. C. Andersen. 2008. The multiscale coarse-graining method. I. A rigorous bridge between atomistic and coarse-grained models. *J. Chem. Phys.*, 128:244114.

[142] S. Nosé. 1984. A unified formulation of constant temperature molecular-dynamics methods. *J. Chem. Phys.*, 81:511–519.

[143] H. Ohvo-Rekilä, B. Ramstedt, P. Leppimäki, and J. P. Slotte. 2002. Cholesterol interactions with phospholipids in membranes. *Prog. Lipid Res.*, 41:66–97.

[144] L. Onsager. 1936. Electric moments of molecules in liquids. *J. Am. Chem. Soc.*, 58:1486–1493.

[145] C. Oostenbrink, A. Villa, A. E. Mark, and W. F. V. Gunsteren. 2004. A biomolecular force field based on the free enthalpy of hydration and solvation: The GROMOS force-field parameter sets 53A5 and 53A6. *J. Comp. Chem.*, 25:1656–1676.

[146] M. Orsi, D. Haubertin, W. Sanderson, and J. Essex. 2008. A quantitative coarse-grain model for lipid bilayers. *J. Phys. Chem. B*, 112:802–815.

[147] S. A. Pandit and H. L. Scott. 2009. Multiscale simulations of heterogeneous model membranes. *Biochim. Biophys. Acta*, 1788:136–148.

[148] S. A. Pandit, S.-W. Chiu, E. Jakobsson, A. Grama, and H. L. Scott. 2007. Cholesterol surrogates: A comparison of cholesterol and 16:0 ceramide in POPC bilayers. *Biophys. J.*, 92:920–927.

[149] S. A. Pandit, G. Khelashvili, E. Jakobsson, A. Grama, and H. L. Scott. 2007. Lateral organization in lipid-cholesterol mixed bilayers. *Biophys. J.*, 92:440–447.

[150] M. Parrinello and A. Rahman. 1981. Polymorphic transitions in single crystals: A new molecular dynamics method. *J. Appl. Phys.*, 52:7182–7190.

[151] R. K. Pathria. 1996. *Statistical Mechanics*. Butterworth-Heinemann, Oxford, 2nd edition.

[152] X. Periole, T. Huber, S. J. Marrink, and T. P. Sakram. 2007. G protein-coupled receptors self-assemble in dynamics simulations of model bilayers. *J. Am. Chem. Soc.*, 129:10126–10132.

[153] J. C. Phillips, R. Braun, W. Wang, J. Gumbart, E. Tajkhorshid, E. Villa, C. Chipot, R. D. Skeel, L. Kale, and K. Schulten. 2005. Scalable molecular dynamics with NAMD. *J. Comp. Chem.*, 26:1781–1802.

[154] D. A. Pink, T. J. Green, and D. Chapman. 1980. Raman scattering in bilayers of saturated phosphatidylcholines. Experiment and theory. *Biochemistry*, 19:349–356.

[155] B. Polyak. 2006. Newton-Kantorovich method and its global convergence. *J. Math. Sci.*, 133:1513–1523.

[156] M. Praprotnik, L. Delle Site, and K. Kremer. 2005. Adaptive resolution molecular-dynamics simulation: Changing the degrees of freedom on the fly. *J. Chem. Phys.*, 123:224106.

[157] M. Praprotnik, L. Delle Site, and K. Kremer. 2007. A macromolecule in a solvent: Adaptive resolution molecular dynamics simulation. *J. Chem. Phys.*, 126:134902.

[158] M. Praprotnik, L. Delle Site, and K. Kremer. 2008. Multiscale simulation of soft matter: From scale bridging to adaptive resolution. *Annu. Rev. Phys. Chem.*, 59: 545–571.

[159] D. Reith, M. Pütz, and F. Müller-Plathe. 2003. Deriving effective mesoscale potentials from atomistic simulations. *J. Comp. Chem.*, 24:1624–1636.

[160] H. J. Risselada and S. J. Marrink. 2008. The molecular face of lipid rafts in model membranes. *Proc. Natl. Acad. Sci. USA*, 105:17367–17372.

[161] L. J. Root and R. Lovett. 1991. On the interpretation of radial distribution functions determined from integral equations. *J. Chem. Phys.*, 95:8390–8397.

[162] J.-P. Ryckaert and A. Bellemans. 1978. Molecular dynamics of liquid alkanes. *Faraday Discuss. Chem. Soc.*, 66:95–106.

[163] J.-P. Ryckaert, G. Ciccotti, and H. J. C. Berendsen. 1977. Numerical integration of the cartesian equations of motion of a system with constraints: Molecular dynamics of n-alkanes. *J. Comp. Phys.*, 23:327–341.

[164] A. Salonen. 2009. Conformational analysis of sphingolipids with self-organizing maps. Master's thesis, Tampere University of Technology.

[165] W. Schommers. 1973. A pair potential for liquid rubidium from the pair correlation function. *Phys. Lett. A*, 43:157–158.

[166] W. Schommers. 1983. Pair potentials in disordered many-particle systems: A study for liquid gallium. *Phys. Rev. A*, 28:3599–3605.

[167] L. D. Schuler, X. Daura, and W. F. van Gunsteren. 2001. An improved GROMOS96 force field for aliphatic hydrocarbons in the condensed phase. *J. Comp. Chem.*, 22:1205–1218.

[168] J. Seelig and A. Seelig. 1980. Lipid conformation in model membranes and biological systems. *Q. Rev. Biophys.*, 13:19–61.

[169] M. S. Shell. 2008. The relative entropy is fundamental to multiscale and inverse thermodynamic problems. *J. Chem. Phys.*, 129:144108.

[170] J. C. Shelley, M. Y. Shelley, R. C. Reeder, S. Bandyopadhyay, and M. L. Klein. 2001. A coarse grain model for phospholipid simulations. *J. Phys. Chem. B*, 105: 4464–4470.

[171] J. C. Shelley, M. Y. Shelley, R. C. Reeder, S. Bandyopadhyay, P. B. Moore, and M. L. Klein. 2001. Simulations of phospholipids using a coarse grain model. *J. Phys. Chem. B*, 105:9785–9792.

[172] P. Sherwood, B. R. Brooks, and M. S. Sansom. 2008. Multiscale methods for macromolecular simulations. *Curr. Opin. Struct. Biol.*, 18:630 – 640.

[173] Q. Shi and G. A. Voth. 2005. Multi-scale modeling of phase separation in mixed lipid bilayers. *Biophys. J.*, 89:2385–2394.

[174] Q. Shi, S. Izvekov, and G. A. Voth. 2006. Mixed atomistic and coarse-grained molecular dynamics: Simulation of a membrane-bound ion channel. *J. Phys. Chem. B*, 110:1545–1548.

[175] A. Y. Shih, A. Arkhipov, P. L. Freddolino, and K. Schulten. 2006. Coarse grained protein-lipid model with application to lipoprotein particles. *J. Phys. Chem. B*, 110: 3674–3684.

[176] J. R. Silbermann, S. H. L. Klapp, M. Schoen, N. Chennamsetty, H. Bock, and K. E. Gubbins. 2006. Mesoscale modeling of complex binary fluid mixtures: Towards an atomistic foundation of effective potentials. *J. Chem. Phys.*, 124:074105.

[177] K. Simons and E. Ikonen. 1997. Functional rafts in cell membranes. *Nature*, 387: 569–572.

[178] T. Soddemann, B. Dünweg, and K. Kremer. 2003. Dissipative particle dynamics: A useful thermostat for equilibrium and nonequilibrium molecular dynamics simulations. *Phys. Rev. E*, 68:046702.

[179] A. K. Soper. 1996. Empirical potential Monte Carlo simulation of fluid structure. *Comp. Phys.*, 202:295–306.

[180] F. H. Stillinger. 1970. Effective pair interactions in liquids. Water. *J. Phys. Chem.*, 74:3677–3687.

[181] F. H. Stillinger, H. Sakai, and S. Torquato. 2002. Statistical mechanical models with effective potentials: Definitions, applications, and thermodynamic consequences. *J. Chem. Phys.*, 117:288–296.

[182] B. J. Thijsse, M. A. Hollanders, and J. Hendrikse. 1998. A practical algorithm for least-squares spline approximation of data containing noise. *Computers In Physics*, 12:393–399.

[183] J. M. Thijssen. 1999. *Computational Physics*. Cambridge University Press, Cambridge.

[184] L. Thogersen, B. Schiott, T. Vosegaard, N. C. Nielsen, and E. Tajkhorshid. 2008. Peptide aggregation and pore formation in a lipid bilayer: A combined coarse-grained and all atom molecular dynamics study. *Biophys. J.*, 95:4337–4347.

[185] I. F. Thorpe, J. Zhou, and G. A. Voth. 2008. Peptide folding using multiscale coarse-grained models. *J. Phys. Chem. B*, 112:13079–13090.

[186] D. P. Tieleman, S. J. Marrink, and H. J. C. Berendsen. 1997. A computer perspective of membranes: Molecular dynamics studies of lipid bilayer systems. *Biochim.*

Biophys. Acta, 1331:235–270.

[187] D. P. Tieleman, J. L. MacCallum, W. L. Ash, C. Kandt, Z. Xu, and L. Monticelli. 2006. Membrane protein simulations with a united-atom lipid and all-atom protein model: Lipid–protein interactions, side chain transfer free energies and model proteins. *J. Phys.: Condens. Matter*, 18:S1221–S1234.

[188] G. Tóth. 2007. Effective potentials from complex simulations: A potential-matching algorithm and remarks on coarse-grained potentials. *J. Phys.: Condens. Matter*, 19:335222.

[189] G. Tóth. 2007. Interactions from diffraction data: Historical and comprehensive overview of simulation assisted methods. *J. Phys.: Condens. Matter*, 19:335220.

[190] G. Tóth and A. Baranyai. 2000. Direct determination of two-body potentials from measured pair structures. *J. Mol. Liq.*, 85:3–9.

[191] W. Treptow, S.-J. Marrink, and M. Tarek. 2008. Gating motions in voltage-gated potassium channels revealed by coarse-grained molecular dynamics simulations. *J. Phys. Chem. B*, 112:3277–3282.

[192] D. van der Spoel, , E. Lindahl, B. Hess, A. R. van Buuren, E. Apol, P.-J. Meulenhoff, D. P. Tielemann, A. L. T. M. Sijbers, K. A. Feenstra, R. van Drunen, and H. J. C. Berendsen. 2005. *Gromacs User Manual version 3.3*. http://www.gromacs.org.

[193] D. van der Spoel, E. Lindahl, B. Hess, G. Groenhof, A. E. Mark, and H. J. C. Berendsen. 2005. GROMACS: Fast, flexible and free. *J. Comp. Chem.*, 26:1701–1719.

[194] W. F. van Gunsteren, X. Daura, and A. E. Mark. 2002. Computation of free energy. *Helvetica Chimica Acta*, 85:3113–3129.

[195] C. Vega, J. L. F. Abascal, M. M. Conde, and J. L. Aragones. 2009. What ice can teach us about water interactions: a critical comparison of the performance of different water models. *Faraday Discuss.*, 141:251–276.

[196] J. Vesanto, J. Himberg, E. Alhoniemi, and J. Parhankangas. 1999. Self-organizing maps in Matlab: the SOM Toolbox. In *Proceedings of the Matlab DSP Conference 1999*, pages 35–40, Espoo, Finland, 1999.

[197] M. R. Vist and J. H. Davis. 1990. Phase equilibria of cholesterol/dipalmitoylphosphatidylcholine mixtures: ^{2}H nuclear magnetic resonance and differential scanning calorimetry. *Biochemistry*, 29:451–464.

[198] G. A. Voth, editor. 2008. *Coarse-Graining of Condensed Phase and Biomolecular Systems*. CRC Press, Boca Raton, FL.

[199] J. Wang, R. M. Wolf, J. W. Caldwell, P. A. Kollman, and D. A. Case. 2004. Development and testing of a general Amber force field. *J. Comp. Chem.*, 25:1157–1174.

[200] S. J. Weiner, P. A. Kollman, D. A. Case, U. C. Singh, C. Ghio, G. Alagona, S. Profeta, and P. Weiner. 1984. A new force field for molecular mechanical simulation of nucleic acids and proteins. *J. Am. Chem. Soc.*, 106:765–784.

[201] S. Yefimov, E. van der Giessen, P. R. Onck, and S. J. Marrink. 2008. Mechanosensitive membrane channels in action. *Biophys. J.*, 94:2994–3002.

[202] Z. Zhang, L. Lu, W. G. Noid, V. Krishna, J. Pfaendtner, and G. A. Voth. 2008. A systematic methodology for defining coarse-grained sites in large biomolecules. *Biophys. J.*, 95:5073–5083.

[203] J. Zhou, I. F. Thorpe, S. Izvekov, and G. A. Voth. 2007. Coarse-grained peptide modeling using a systematic multiscale approach. *Biophys. J.*, 92:4289–4303.

[204] R. Zwanzig. 1960. Ensemble method in the theory of irreversibility. *J. Chem. Phys.*, 33:1338–1341.

[205] J. Zwicker and R. Lovett. 1990. When does a pair correlation function fix the state of an equilibrium system? *J. Chem. Phys.*, 93:6752–6755.

ISBN 978-951-22-9854-9
ISBN 978-951-22-9855-6 (PDF)
ISSN 1795-2239
ISSN 1795-4584 (PDF)